Neutron Production with Thorium Fuel in Accelerator Driven Subcritical Reactors

By

David Sangcheol Lee

A thesis submitted to the University of Huddersfield
in partial fulfilment of the requirements for
the degree of Doctor of Philosophy

School of Computing and Engineering
International Institute for Accelerator Applications

April 2018

Abstract

ADSRs (Accelerator-Driven Subcritical Reactors) incorporate a spallation technique which is an efficient way to produce high neutron flux by externally supplying neutrons into the reactor.

In this thesis, a review of spallation is given explaining the spallation reaction process, describing spallation reactions in dense metal and analysing the resulting neutron energy spectra. The thesis also discusses current spallation sources around the world. Studies involving proton-induced neutron production in spallation target are demonstrated. Spallation reactions on a lead target have been simulated using a Monte Carlo transport code called GEANT4, and the benchmarking of these simulations against experimental neutron spectra produced from a thick lead target bombarded with 0.5 and 1.5 GeV protons is discussed. This is followed by discussion of the angular distribution of neutrons of different energies in order to understand the emission of neutrons from a spallation target.

Lead and Lead Bismuth Eutectic (LBE) are both widely utilised to produce neutrons; this is due to the fact that lead is a high Z, heavy metal element which is relatively cheap to use. This thesis provides a comparison between lead and LBE in terms of their effect on neutron energy spectra at various projecting angles.

Given the confidence in the GEANT4 simulation provided by the benchmarking studies, the thesis goes on to discuss neutron production and behaviour in the environment of thorium-fuelled ADSRs. With a spallation target composed of LBE, the design of the MYRRHA reactor developed by SCKCEN has been configured to explore neutron production created from each layer filled with thorium fuel. This is then followed by a focus on neutrons escaping from the LBE-composed reflector, and the thesis provides an analysis of the effect of several different materials used for inner and outer shielding in the reactor core.

By using the latest nuclear data library and numerical techniques provided in the GEANT4 code, the author has been able to simulate the actual usage of thorium in an ADSR reactor set-up which has not yet been fully demonstrated. The thesis concludes with the idea that thorium could well be utilised as an actual fuel source in an ADSR for the purpose of transmutation, and possibly for energy production as well.

Copyright statement

Acknowledgements

I would like to express my sincere gratitude to the following people:

- Professor Robert Cywinski for his guidance throughout the PhD project and invaluable advice about knowledge of physics, thorium, spallation and ADSR. I would like to thank him personally for helping me in every way.
- Professor Rebecca Seviour for her guidance during my PhD studies and kind advice, both on technical aspects of physics and on personal matters. I would also like to thank her personally for helping me in every way.
- Professor Roger Barlow for his guidance and helpful advice on technical knowledge of thorium and spallation.
- Dr Cristian & Adriana Bungau for help regarding the GEANT4 code and technical advice on spallation and ADSR. I would like to thank them personally for giving me support in every way.
- Mrs Roxanna Rata for being my best friend and colleague. I would like to express my grateful thanks for her support when I was experiencing some personal issues.
- Mr James Scotson for being my good friend. I would like to express my grateful thanks for his support with my English language.
- My family who constantly pray for me and support me, even though they are far away from the UK.
- All colleagues in IIAA for their support and advice.
- High Performance Grid, University of Huddersfield for allowing me to use their resources
- All those whom praying for me and supporting me
- I thank God for strengthen me and guiding me

Science is a way of life. Science is a perspective. Science is the process that takes us from confusion to understanding in a manner that's precise, predictive and reliable - a transformation, for those lucky enough to experience it, that is empowering and emotional.
Brian Greene

Do not be anxious about anything, but in everything, by prayer and petition, with thanksgiving, present your requests to God. And the peace of God, which transcends all understanding, will guard your hearts and your minds in Christ Jesus. (Philippians 4:6-7)

Contents

List of Figures

List of Tables

Chapter 1. Introduction

1.1 Introduction

Since the industrial revolution, energy consumption has been growing exponentially due to the increase in electrical applications and industrial demands; indeed, the global demand for energy is expected to have increased another 60 % by 2050 [1]. It has been of great concern to many that power generation through fossil fuel has caused numerous issues, such as air pollution, global warming and shortage of the fossil fuel itself. Currently, fossil fuels such as coal, oil and gas are supplying the world's minimum energy requirements. However, due to the increasing quantity of greenhouse gases produced during the energy generation process, there is a trend for many countries to seek alternative renewable or sustainable energy sources. Various renewable sources have been proposed, such as wind power, tidal energy generation and geothermal power. However, energy production through such sources is limited by several conditions, such as the shortage of suitable locations, limited periods of activity and, most importantly, the insufficient quantities of energy produced.

Nuclear fission power generation, using enriched uranium as a fuel source, is regarded as the only nuclear power option that can provide enough energy to support the demand of the current civilisation without producing greenhouse gases. However, there are some risks involved with nuclear energy production using fission reactions, such as the potential proliferation risk and the problem of managing nuclear waste [2]. The most recognised and dangerous problem is that it produces unwanted and harmful material during the reaction process, such as radioactive ^{239}Pu. This product could have a huge impact on mankind for a very long time, since the duration of their half-life is lengthy.

The world has seen the seriousness of incidents in Fukushima and Chernobyl, where radioactive waste materials have caused the affected areas to become non-living territories for more than 100 years. Following the events in Fukushima, Germany

stopped producing energy through nuclear power and Japan had to re-activate its nuclear power stations after halting their operation for a long time [3]. Although many countries are trying to use fewer nuclear power stations, it is acknowledged that they will face potential problems in supplying sufficient energy to meet society's demand, especially during the summer season when energy demand is extremely high.

Nevertheless, nuclear fission provides sufficient amounts of energy. Currently, it uses uranium as a fuel source. However, thorium has several properties that make it highly suitable for replacing uranium as a reaction source. Thorium is a fertile material which can be used to breed fissile fuel and then undergo fission.

Using ^{232}Th, it is difficult to achieve weapon grade ^{233}U or ^{239}Pu, a factor which provides comforting protection from the danger of nuclear weapons [4]. Another advantage is that the thorium produces fewer waste products than the amounts produced by uranium, which helps to reduce the economic cost of dealing with nuclear waste [3-5]. However, natural thorium does not contain fissile materials, unlike natural uranium which contains ~0.7% of ^{235}U. This disadvantage can be overcome by using thorium and thorium based fuel in combination with ^{235}U or ^{239}Pu for the conversion of ^{232}Th to fissile ^{233}U[4].

Since thorium can be turned into fissionable ^{233}U, producing fewer radioactive materials as waste products and being more abundant than ^{238}U, it is a source that is of great potential interest for future energy generation. Thorium does not sustain its chain reaction without the source of neutrons being continuously supplied. The fission reaction stops by default if it is no longer primed, which makes a runaway chain reaction accident improbable [6]. Furthermore, a thorium fuel-based fission reactor could potentially contribute to reducing the world's current carbon emissions, since no greenhouse gases are produced during the process. Additionally, a thorium-based fuel reactor could increase employment within the sector, which would boost any economy that invested in it.

Awareness of the potential of thorium as a nuclear fuel has raised an interest in using it in a new type of reactor. Accelerator-Driven Subcritical Reactors (ADSRs), with a thorium fuel cycle, could provide a way to incinerate heavy actinides safely with low waste, and this would offer the possibility of a proliferation-resistant nuclear power technology. The two main envisioned improvements that could be made to the ADSR are the spallation design and running the reactor with a thorium fuel cycle. The spallation process plays an important role in Accelerator Driven Systems (ADS), which is to supply neutrons in which fission reactions take place inside the nuclear fuel. The ADS is equipped with a sub-critical assembly driven by an accelerator which delivers a proton beam onto a target to produce neutrons by spallation [7]. It is suggested that the optimal beam energy in terms of proton energy cost per neutron is about 1 GeV which the value chosen by the Spallation Neutron Source [8]. It is also known that at least 20 neutrons are produced for each incident 1 GeV proton in a typical spallation target, i.e. 1 neutron per 50 MeV of beam energy [2]. According to [2], each neutron requires approximately 150 MeV incident energy (i.e. wall-plug energy) considering the fact that modern accelerator technology having a typical efficiency of 30 % (i.e. approximately 30 % of 150 MeV would be supplied to produce 1 neutron from the spallation target). Hence, it is very important to increase this efficiency in order to use ADSRs as a commercially-adaptable source of energy production. Furthermore, beam power losses during the process must be kept to the lowest level possible. The typical proton loss rate of 1W/m is relatively high, which raises the concern that this needs to be improved.

This thesis is primarily focused on neutron production involved in the spallation process, which is a major contributing source of neutrons in the ADSR system. Firstly, the thesis provides a thorough discussion of the spallation process in Chapter 2, which also includes an explanation of how spallation technology has evolved. The chapter then further discusses how the spallation process works from an atomic point of view. After that, the chapter discusses the relationship between spallation neutron yield and the heavy metal which has become a popular choice of spallation target material. It concludes by providing an overview of existing spallation sources around the world.

In order to provide as detailed an understanding as possible of neutron production through the spallation process, this research has used a Monte-Carlo transport code to analyse neutronic behaviour; this code is called GEANT4, which stands for 'GEometry ANd Tracking version 4'. Chapter 3 describes the benchmarking of published results from KEK, Japan, for neutron energy spectra produced from a lead target [9]. This benchmarking was processed using GEANT4 in order to validate the program's capability in terms of predicting neutron production, and to determine whether this program can be used for further spallation studies. The study was able to confirm the reliability of the results produced by the GEANT4 program and its capabilities. Hence, it was determined that GEANT4 could continue to be used throughout the projects discussed in this thesis.

Neutron yield is very much dependent on proton beam energy and the spallation target material. Lead is commonly used as spallation material. However, there has been an interest in the usage of lead bismuth eutectic lately, such as in MYRRHA [10]. Chapter 4 offers a comparison between lead and Lead Bismuth Eutectic (LBE) in terms of neutron production. Neutron spectra at different angles were compared for both materials using 0.5 and 1.5 GeV proton beams set up in the same way as described in Chapter 3. This has enabled the effects of mixing lead with bismuth to be identified.

The remainder of the thesis is primarily focused on research regarding the use of thorium as a main source of fuel in an ADSR. Thorium is an attractive alternative fuel source to uranium in nuclear fission power generation [2]. The research was driven by the consideration that the potential of thorium fuel and the benefits of ADSR could be combined. Hence, an in-depth discussion of neutron production in a thorium-fuelled ADSR is provided in Chapter 5, which also describes a series of neutron production studies using MYRRHA's core design [11]. The chapter firstly describes the neutron spectra in each of the regions, which are composed of various materials, in order to identify which region contributes most significantly to neutron production. Then, having understood the neutron production contributed by each region, the chapter goes on to discuss the energy spectra of neutrons escaping from the fuel region and the impact of

further regions consisting of reflectors and shielding. The idea was to understand and analyse the changes in energy spectra of neutrons which had escaped from the fuel region as they passed through different materials. This would enable the reflection and moderation of those neutrons to be clearly understood. For the reflector, LBE was used, which is the same material as the spallation target used in MYRRHA [9, 11]. After the reflector region, there were multiple candidates for inner and outer shielding materials. For inner shielding, three materials were chosen in order to assess their effects in terms of neutron blocking. These materials were Y_2O_3, ZrO_2 and Zr_2O_3. Finally, the chapter discusses the combined effect of both inner and outer shielding on those neutrons which have escaped from the central fuel region. This enables the study to suggest the best combination of materials to sufficiently shield the core vessel.

This thesis contains two appendices, comprising contributions to the proceedings of the 2016 IPAC and ADST conferences, in which the research described here was published.

Thorium has gained much attention around the world as an alternative source of energy for nuclear power generation. In fact, thorium has been used around the world for many years. The last two reactors that used thorium were THTR, Germany, and Fort St Vrain, USA, which used it until 1989 [4]. It was proven that thorium and its fuel cycle could be operational as a major power source.

Thorium is a fertile material, which means it can convert to ^{233}U by capturing one neutron from ^{232}Th [13]. Thorium can itself be fissionable with sufficiently fast neutrons [14]. However, the fertile-fissile conversion and subsequent fission of ^{233}U is preferable because thorium has a higher cross section of thermal neutron absorption than ^{238}U. Hence, there is a higher chance of fertile to fissile conversion for ^{232}Th than for ^{238}U [4]. According to [4], the number of neutrons produced per neutron absorption(η) is greater than 2.0 for a wide range of neutron spectra, a feature which neither ^{235}U nor ^{239}Pu possesses (see Figure 1.1).

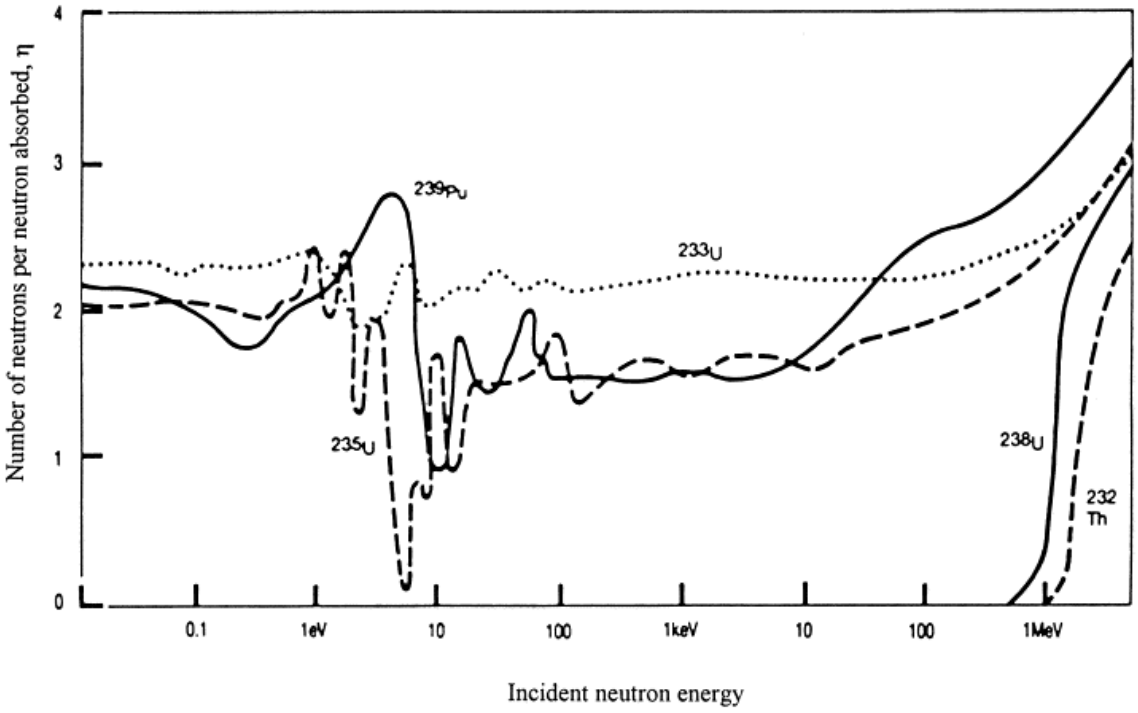

Figure 1.1 Neutron yield per neutron absorbed (taken from [15] **which is sourced from** [16]**)**

While the ^{238}U – ^{239}Pu fuel cycle operates best in fast neutron spectra only, the ^{232}Th – ^{233}U fuel cycle can be operated with fast, epithermal or thermal spectra [3, 14].

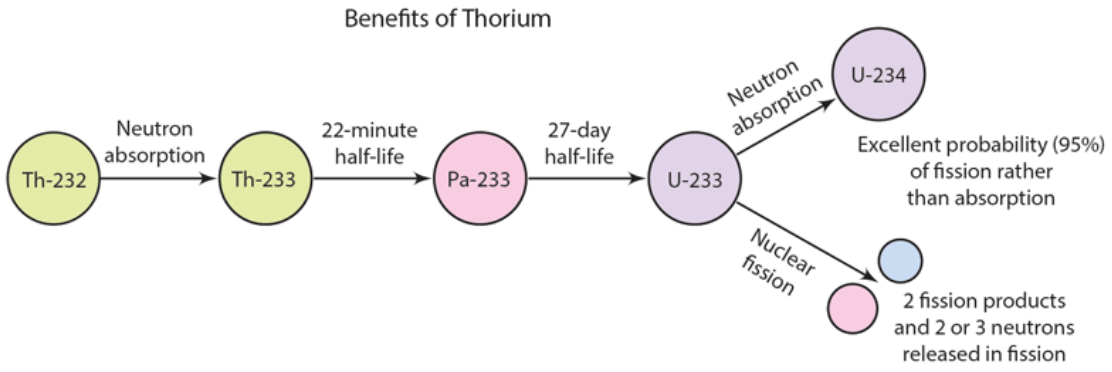

Figure 1.2: Overview of ^{232}Th to ^{233}U conversion, taken from [18]

As shown in Figure 1.2, ^{232}Th goes through several stages to transmute into fissionable ^{233}U, with a period of 27 days taken for conversion from ^{233}Pa. In the thorium fuel

cycle, this step is the most time-consuming stage. Hence, improvements to time-dependent thorium fuel conversion could be the key to boosting the thorium fuel cycle.

In terms of nuclear waste, the ^{232}Th – ^{233}U fuel cycle offers advantages over the ^{238}U – ^{239}Pu fuel cycle. It is noted in [4] that ^{232}Th – ^{233}U fuel cycle produces a much lower quantity of plutonium and long-lived minor actinides such as neptunium, americium and curium compared with the ^{238}U – ^{239}Pu fuel cycle. The ^{232}Th – ^{233}U fuel cycle has the potential to mitigate the toxicity and decay heat problems [4]. However, the ^{232}Th – ^{233}U fuel cycle produces other radionuclides such as ^{231}Pa, ^{229}Th and ^{230}U which could cause long-term radiological impact [4]. In additions, there are also fission products produced from the fission of ^{233}U such as ^{129}I and ^{135}Cs with half-lives of millions of years. ^{59}Ni and ^{94}Nb have half-lives of tens of thousands of years [4]. There are also other isotopes such as ^{135}Xe and ^{85}Kr which have approximately 9 hours and 10 years half-lives. In general, the fission products are likely to have shorter half-lives than the minor actinides.

The ^{232}Th – ^{233}U fuel cycle has better nuclear characteristics than the conventional ^{238}U – ^{239}Pu fuel cycle. The capture cross section of thermal neutron for ^{233}U is much smaller than that for ^{235}U and ^{239}Pu (i.e. ^{233}U = 46 barns, ^{235}U = 101 barns and ^{239}Pu = 271 barns) [4]. However, the ^{233}U is that its fission cross section is only slightly lower than those for ^{235}U and ^{239}Pu (fission cross section for ^{233}U = 525 barns while ^{235}U and ^{239}Pu = 577 and 742 barns respectively) [4]. Hence, the chance that ^{233}U not giving fission but absorbing a neutron to become ^{234}U is less probable compared with the chance that ^{235}U to ^{236}U or ^{239}Pu to ^{240}Pu [4].

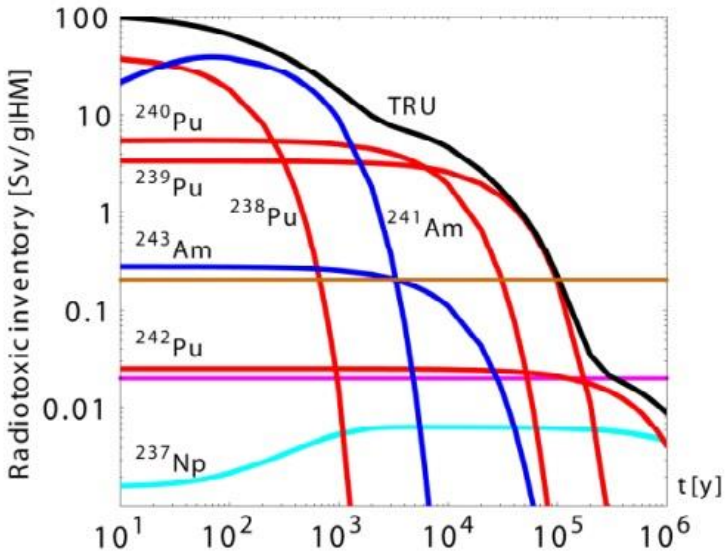

Figure 1.3: Radiotoxic inventory of the main transuranic isotopes in spent nuclear fuel (3.7% ^{235}U, 42MWd.lgIHM) taken from [19]

The nuclear wastes have different radiotoxicities and half-lives that could have severe effects for both human beings and the environment. Figure 1.3 shows how individual elements contribute to the total transuranic waste (TRU) radiotoxicity. It can be seen from the figure that ^{241}Am dominates the total TRU radiotoxicity during 50 and 2000 years [19]. After that, ^{239}Pu and ^{240}Pu are leading elements for the radiotoxicity. The minor actinides shown in have a long half-life. For example, ^{241}Am has a half-life of 430 years whereas, ^{239}Pu has a half-life of 24100 years. It is therefore, important to understand process through which the radiotoxicity would be increased such as the formation of ^{241}Am through beta decay from ^{241}Pu. Overall, it is significant that the elimination of transuranic elements would reduce the long-term radio hazards which supports the need of transmutation.

1.2 Overview of Accelerator-Driven Systems

The Accelerator-Driven Subcritical Reactor (ADSR) is a new concept in nuclear reactor technology which brings much potential. With the energy amplifier developed by Carlo Rubbia [20], the ADSR offers a new breeding reactor in a closed system [4]. An ADSR consists of three major parts; an accelerator, a spallation target and a fuel reactor. The accelerator acts as an external controller of the production of fast neutrons, as it controls the proton beam which collides with the spallation target and emits the neutrons (see Figure 1.4 for an overview of the system).

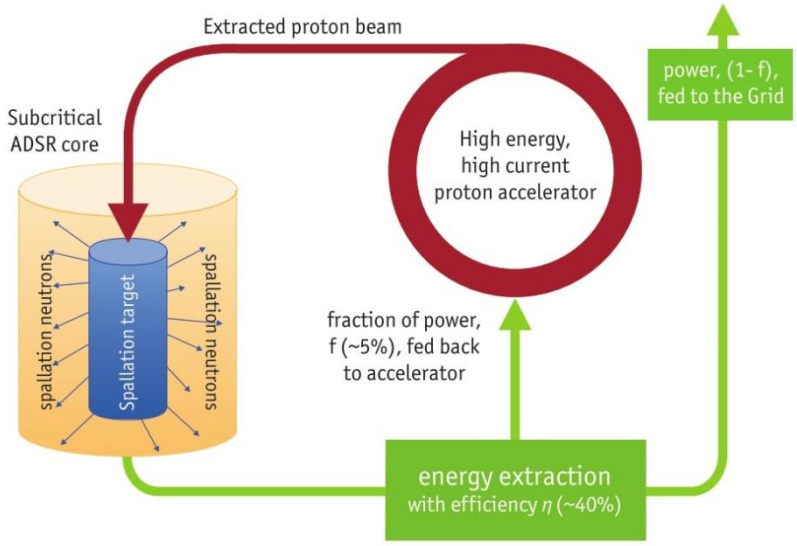

Figure 1.4 Schematic of accelerator-driven subcritical reactor, taken from [13]

For the operation of an ADSR run in subcritical mode, the criticality needs to be maintained at less than 1. Due to the subcritical operation, neutrons have to be continually supplied to keep the fission reaction running in the core. Hence, the spallation target, which is positioned inside the subcritical core, acts as an external source of neutrons [13]. By putting thorium in the core and breeding it, the fuel cycle eventually leads to the creation of ^{233}U, with the possibility of mixing an additive to the thorium fuel such as plutonium and other fissionable materials as a fission driver [3, 12]. This makes the ADSR a unique reactor which can burn plutonium by incorporating

a thorium fuel cycle. As previously mentioned, the thorium fuel cycle gives a low concentration of nuclear waste, leading to a reduction in radiotoxicity [13].

According to [2], in order to operate an ADSR sufficiently, the proton beam requires certain conditions, i.e.,

$$I = e\frac{(1-k)P}{nfE_f} \tag{1.1}$$

where I is the beam current; k is the criticality which is maintained at less than 1, P is the reactor power, n is the number of neutrons produced per incident proton, f is the fraction of the neutrons produced that give a fission reaction and E_f is the mean energy release per fission. It is suggested that a typical 1550 MW_{th} powered reactor requires an average current of 10 mA with a beam power of 10 MW. This translates into 1 GeV proton beam energy. Taking into consideration the efficiency factor for thermal conversion, the ADSR system might be able to generate 600 MW_e with the criticality as low as 0.985 [13].

At this stage, ADSR technology is currently being developed by several institutes and companies. Examples of these include MYRRHA by SCKCEN [21], a 200 MW_e PHWR ADS system designed by the Indian Atomic Energy Commission [22], and a 600 MWe ADTR™ designed by the Jacobs Engineering Group Inc. [23].

1.3 Bibliography

[1] International Energy Agency:, *"World Energy Outlook" (2006),"Key World Energy Statistics" (2010)*. OECD Publishing.

[2] S. Peggs, W. Horak, T. Roser, and et.al, "Thorium energy futures," in *In: Proceedings of the International Particle Accelerator Conference IPAC 2012. JACoW, New Orleans, Louisiana, USA*, 2012.

[3] World Nuclear Association, "Nuclear Power in Japan," 2016. [Online]. Available: http://www.world-nuclear.org/information-library/country-profiles/countries-g-n/japan-nuclear-power.aspx. [Accessed: 10-Nov-2016].

[4] International Atomic Energy Agency, "Thorium fuel cycle-Potential benefits and challenges," IAEA, Vienna,Rep. IAEA-TECDOC-1450, May 2005.

[5] S. K. Jain, "Nuclear Power-an alternative." NPCIL Retrieved 27, 2012. [Online]. Available: http://npcil.nic.in/pdf/nuclear%20power-%20an%20alternative.pdf. [Accessed: 25-Sep-2013]

[6] A. Demirbas, "Introduction," in *Biohydrogen: For Future Engine Fuel Demands*, Springer London, 2009, pp. 1–42.

[7] S. S. T. Mongelli, *et.al*, "Spallation physics and the ADS target design," *Brazilian J. Phys.*, vol. 35, no. 3B, pp. 894–897, 2005.

[8] T. E. Mason and et.al, "Spallation Neutron Source Project Completion Report,", Oak Ridge National Laboratory., US, Rep. SNS 100000000-BL0005-R00, June., 2006.

[9] S. Meigo *et al.*, "Measurements of neutron spectra produced from a thick lead target bombarded with 0.5- and 1.5-GeV protons," *Nucl. Instruments Methods*

Phys. Res. Sect. A Accel. Spectrometers, Detect. Assoc. Equip., vol. 431, no. 3, pp. 521–530, Jul. 1999.

[10] P. Baeten, M. Schyns, *R. Fernandez, D. De Bruynet.al*, and G. Van den Eynde, "MYRRHA: A multipurpose nuclear research facility," *EPJ Web Conf.*, vol. 79, no. 3001, p. 3001, Dec. 2014.

[11] M. Sarotto, "MYRRHA-FASTEF FA / core design," in *Int Workshop on Innovative Nuclear Reactors cooled by HLM: Status & Perspectives, ENEA-MSE & EU FP7 EC SEARCH., Pisa (Italy)., April 17-20* , 2012

[12] H. Aït Abderrahim, "MYRRHA An innovative and unique irradiation research facility," in *Tenth International Topical Meeting on Nuclear Applications of Accelerators (AccApp'11)*, Tennessee, USA, April 3-7., 2011.

[13] R. Cywinski, A. Herrera-Martínez, G. Hodgson, and *et.al*, "Towards an Alternative Nuclear Future," The Thorium Energy Amplifier Association (ThorEA), 2009.

[14] Atomic Energy Board Canada, "Fundamentals of Power Reactors; Module One Science & Engineering fundamentals," IEEE, Jul. 1993.[Online] Available: https://canteach.candu.org/Content%20Library/19930201.pdf [Accessed: 30-Jul-2017]Atomic Energy Board Canada, "Fundamentals of Power Reactors Module One Science & Engineering Fundamentals," IEEE, Jul. 2012.

[15] M. Lung and O. Gremm, "Perspectives of the thorium fuel cycle," *Nucl. Eng. Des.*, vol. 180, no. 2, pp. 133–146, Mar. 1998.

[16] OECD/NEA, "Plutonium An assessment," in *Excavation response in geological repositories for radioactive waste. Proc. NEA Workshop, 26–28 April 1988, Winnipeg, OECD, Paris*, 1989.

[17] D. Mathers, “The Thorium Fuel Cycle,” presented in *Thorium Energy Conference 2013*,CERN,Geneva, October.27-31., 2013. [Online] Available: http://www.thoriumenergyworld.com/uploads/6/9/8/7/69878937/the_thorium_fuel_cycle_-_daniel_p._mathers_-_nnl_-_thec13.pdf .[Accessed: 03-11-2016].

[18] Kirk Sorensen, “What’s the Difference Between Thorium and Uranium Nuclear Reactors? | What’s the Difference Between... content from Machine Design,” *Machine Design*, 2016. [Online]. Available: http://machinedesign.com/whats-difference-between/whats-difference-between-thorium-and-uranium-nuclear-reactors. [Accessed: 03-Nov-2016].

[19] M. Eriksson, “Accelerator-driven Systems : Safety and Kinetics Marcus Eriksson Doctoral Thesis Department of Nuclear and Reactor Physics Royal Institute of Technology Stockholm 2005,” Royal Institute of Technology Stockholm, 2005.

[20] C. Rubbia, J. A. Rubio, S. Buono, *et.al*, “Conceptual design of a fast neutron operated high power energy amplifier,” European Organization for Nuclear Research, Rep. CERN/AT/95-44 (ET),1995.C. Rubbia, J. A. Rubio, S. Buono, and et.al, “Conceptual design of a fast neutron operated high power energy amplifier,” European Organization for Nuclear Research, 1995.

[21] D. De Bruyn, H. A. Abderrahim, P. Baeten, *et.al*, “The MYRRHA ADS Project in Belgium Enters the Front End Engineering Phase,” *Phys. Procedia*, vol. 66, no. April 2014, pp. 75–84, 2015.

[22] S. Banerjee, “Towards a Sustainable Nuclear Energy Future,” in *WNA Symposium*, 2010.

[23] V. Ashley and R. Ashworth, “The Technically Viable ADTR^{TM} Power Station,” *Nuclear Future Volume 7 issue 3* . 2011.pp.41-46.

Chapter 2. Spallation

2.1 Introduction

Spallation is the process of producing neutrons by causing particles from an accelerator to impact a heavy metal target [1]. The reaction takes place when light particles (for example, protons, neutrons or light nuclei) with kinetic energies from several hundreds of MeV to several GeV interact with a heavy nucleus such as lead, mercury or uranium and cause the emission of a large number of hadrons, which are principally neutrons or nuclear fragments. Accelerator-driven spallation neutron sources are presently used to produce intense neutron beams for the investigation of condensed matter, but are also of interest as a potential method for transmutation of long-lived actinides and nuclear waste [2].

Until spallation neutron sources were introduced, intense neutron fluxes were obtained from nuclear reactors. However, the nuclear non-proliferation treaty prohibits the use of highly enriched uranium which is necessary for compact cores in research reactors. Chou [3] notes that, in order to produce high rates of neutron intensity, the reactor-based neutron source would require 93% of ^{235}U, which is the reason why the original proposal of a uranium-based Advanced Neutron Source at Oak Ridge National Laboratory in the US was rejected, and subsequently replaced with the SNS project.

The neutron is a subatomic particle which carries no charge and which is stable while the particle is bound within a nucleus. The neutron remains a free particle for an approximate mean lifetime of 900 seconds, after which it then decays through weak interaction into a proton, an electron and an antineutrino [4].

Since the end of the Second World War, many researchers have exploited nuclear reactors for energy production with high rates of neutron flux [4]. The idea of neutron

production through controlled nuclear reactions was first introduced by Enrico Fermi in 1942. He showed that neutron production was possible via a controlled chain reaction from the fission of uranium nuclei.

Currently, there are several research reactors in the world designed to produce high thermal neutron fluxes for research rather than for energy production; examples of these are ILL in France and OPAL in Australia. The range of neutron flux is between 10^{14} to 10^{15} $cm^{-2}s^{-1}$. This parameter is recommended by the IAEA for the essential flux level of research reactors, in which neutron-scattering instruments can be run successfully for the purpose of material structure studies [5]. However, many research reactors are nearing the end of their useful lifetime (indeed two were built between 1950 and 1960), but due to the legal restrictions on building new high flux reactors employing highly enriched uranium in a compact core, the ageing reactors are not being replaced and the future of reactor-based intense neutron sources is uncertain.

On the other hand, the development of pulsed spallation sources over the past forty years has enabled higher peak fluxes to be obtained. With the advancement of both accelerator and target technologies, several powerful spallation sources have been built around the world. In 1985, the 160kW ISIS spallation source at the Rutherford Appleton Laboratory in Oxfordshire commenced operation, and at the turn of this century the 1MW SNS at Oak Ridge in the US and J-PARC at Tokai in Japan were commissioned. Currently the 5MW European Spallation Source, with a projected peak thermal neutron flux of $2 \times 10^{17} ncm^{-2}s^{-1}$, 30 times that of ISIS, is under construction [4].

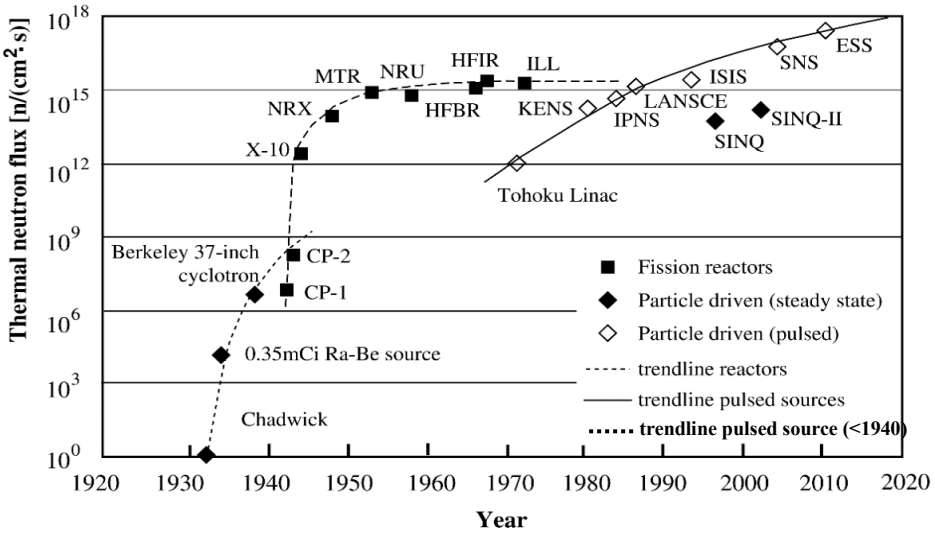

Figure 2.1: Evolution of the performance of reactors and pulsed spallation sources, taken from [4]

Figure 2.1 shows the evolution with time of performance measured by peak thermal neutron flux obtained from reactors and other neutron sources. The most significant aspect shown in this figure is that the thermal neutron flux for research-based reactors has levelled off, whereas the level of accelerator-based neutron sources is increasing and will continue to increase further with ongoing developments in accelerator technology. Despite the fact that accelerator-based neutron sources are both effective and allow for significant further development, their performance and reliability are highly dependent on the performance of increasingly complex and advanced accelerators, and upon the geometry, material and material properties of the spallation targets. With respect to the latter, there is consequently a significant need for detailed simulation studies on the optimisation of spallation targets.

2.2 Evolution of Spallation Research

The phenomenon of spallation for neutron production was first observed in cosmic ray interactions in the 1930s [6]. Subsequently, the first accelerator-driven spallation reactions were discovered by Cunningham [7] at Berkeley in 1947. In practical terms, the idea of exploiting spallation was first conceived as a part of the MTA project in the

United States[8], which was designed to convert ^{238}U to ^{239}Pu with intense neutron fluxes in order to produce weapons-grade plutonium for the US nuclear weapon programme. This early spallation-induced transmutation programme faltered [9], as it was found that plutonium production through fast breeding in fission reactors was more suitable as the technology was already well established. However, the interest in spallation-based neutron production was kept alive due to the following two reasons [9]:

1. Fission reactors are effectively neutron-poor because relatively few excess neutrons are available either for fertile-fissile conversion or for nuclear transmutation for nuclear waste burn-up.

2. As already shown in the previous section, nuclear reactors designed for the production of high neutron fluxes have almost reached their limits in terms of the thermal and fast neutron fluxes that can be generated with existing fuel technology, particularly because of power density problems in the core.

   On the other hand, there is scope for considerable progress in spallation neutron production for the following reasons:

   - Significantly lower heat is released per neutron (e.g. the 160kW ISIS is largely equivalent to the 56MW ILL reactor), and the increased flexibility in target material choices might help to push time average fluxes to higher values than in fission reactors;
   - A spallation source allows significantly greater control over the time structure, output level and geometry of neutron production;
   - There is continuing development of accelerator technology, which allows significant gains in accelerated particle beam energies and intensities, which in turn result in increased neutron fluxes.

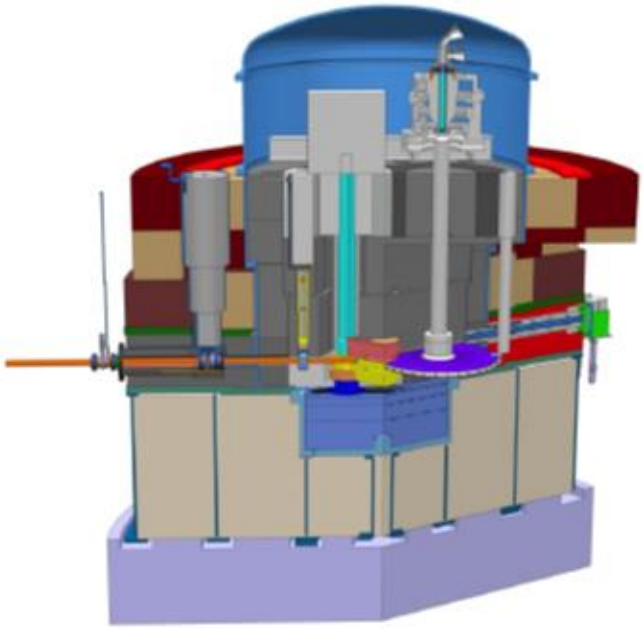

Figure 2.2: Principal arrangement of target wheel, moderators and reflector in a spallation neutron source for ESS, taken from [10]

Developments in spallation neutron sources have been focused on two aspects. The first aspect is increasing the proton beam energy. This needs to be sufficiently high for nuclear energy losses to exceed the electronic energy losses. The other aspect is the target material and geometry configuration in relation to enhancement of the neutron production process. In the past, the proton beam power of spallation sources was in the range of 10–200 kW, but with advanced developments in accelerator technology, much higher proton beam power can be achieved. For example, SNS's beam power is 1MW, and ESS is even expected to achieve 5 MW beam power [11].

Figure 2.2 shows a schematic of spallation target station and the entrance of protons into the target to produce fast neutrons. Moderators are placed into this design in order to slow down the spalled neutrons from fast (1-10 MeV) to epithermal (0.025-0.4 eV) and thermal (below 0.025 eV) energies. Reflectors are also placed around the target to increase the neutronic coupling between the moderator and the target assembly by reflecting as many neutrons as possible back into the moderator [9].

2.3 Spallation Process

As described in the previous chapter, a spallation reaction is known to be effective in the production of a large number of neutrons. It is important to understand the particle interactions taking place in the target nucleus.

At the moment of interaction between the incident particle and the target nucleus, the reactions occur in three stages: intra-nuclear cascade, pre-equilibrium stage and evaporation or fission (refer to Figure 2.3 and Figure 2.4).

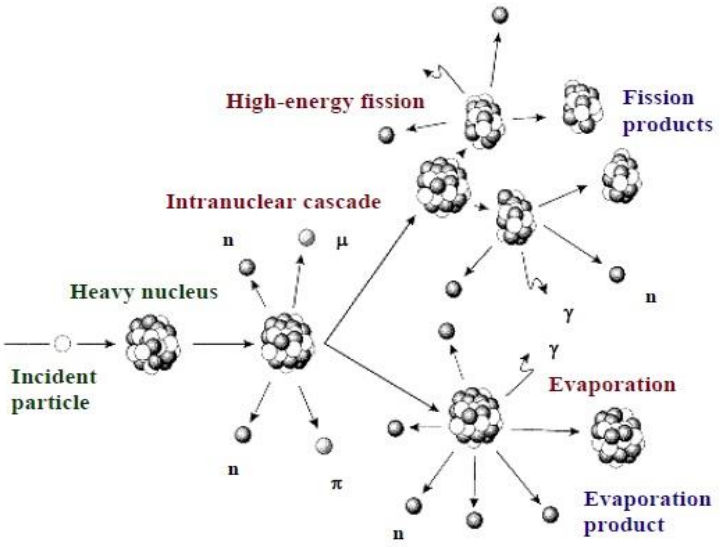

Figure 2.3: Scheme of a spallation reaction, taken from [12]

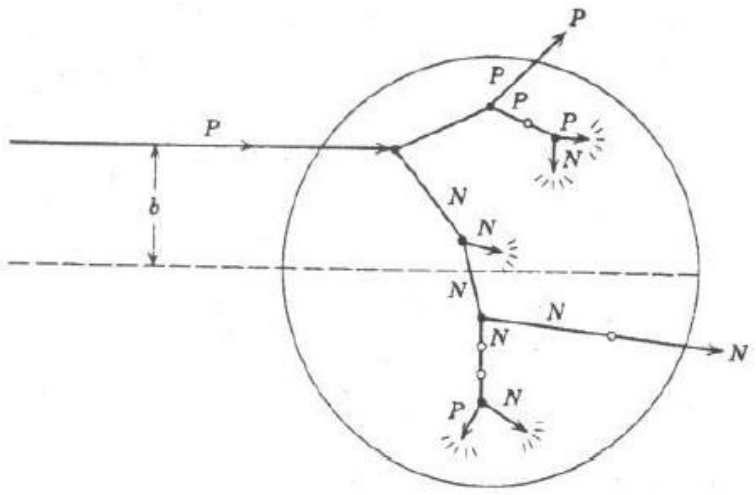

Figure 2.4: Scheme of an intra-nuclear cascade generated by a proton in a heavy nucleus with the impact parameter b. The solid circles represent the positions of collisions; the open circles represent the positions forbidden by the Pauli Exclusion Principle. The short arrows indicate 'captured' nucleons, which contribute to the excitation of the nucleus, taken from [13]

The intra-nuclear cascade is the first stage to take place, in which a series of interactions between protons and individual nucleons occur inside the nucleus (refer to Figure 2.4) at a very fast rate (~10^{-22} seconds). The de Broglie wavelength of the proton $\lambda = h/\sqrt{2mE}$ for a 1 GeV proton beam is approximately 0.1 fm [12]. This value indicates that a series of interactions can occur between proton and nucleus because the proton has a smaller wavelength than the diameter of a heavy nucleus, which explains the nuclear interaction as a series of collisions with individual nucleons inside the nucleus of the target [9],[14]. As described in Figure 2.4, the collisions leading the final transition stage in phase space are forbidden due to the blocking effect by the Pauli Exclusion Principle [12]. This is also known as Pauli blocking. Pauli blocking occurs when the final particle states are already occupied. Hence, the incoming particles can no longer do the transition which makes collision forbidden. The threshold energies for particle production are affected by the increase of incident proton energy. During the course of the interaction, pions come up at energies of a few hundred MeV initially, but heavier hadrons are also produced at energies of around 2 to 10 GeV [15]. These hadrons can also participate in intra-nuclear cascade or interact between each other, which is known

as the hadron cascade [12],[14]. The particles created from this stage are emitted with high energy from the target nucleus and the direction of the particles being emitted is almost the same as the direction in which the incident protons travel. The energy of the incident particles is equally distributed among the nucleons in the nucleus, which causes the nucleus to be in a highly excited state.

The second stage of the spallation reaction is the pre-equilibrium stage, which is also known as the pre-compound stage. This stage involves an interaction whereby the incident particles, which are the protons in this case, transfer kinetic energy to the target nucleons through elastic collisions. After the energy transfer is complete, a cascade of nucleon-nucleon collision follows, which happens in 10^{-18} seconds [12]. The products during this stage are mainly high energy particles or fragments. The energies of particles produced in the pre-equilibrium stage are greater than the energies of particles emitted during the equilibrium decay stage.

Finally, the equilibrium stage takes place over 10^{-16} seconds. The energies from the remaining particles are equally distributed to the nucleus, and the nucleus remains in a highly excited state with a small angular momentum. The evaporation of neutrons is then followed by a loss of energy in the nucleus. The evaporations of neutrons or light fragments such as deuteron or alpha-particles carry energies of up to 40 MeV (nuclear potential well depth) and the trajectories of these emitted particles are isotropic.

In addition, a fission process may occur when the nucleus is de-excited and the fission products also undergo a further evaporation process. When the nucleus does not have sufficient energy to emit neutrons (the excitation energy from the nucleus becomes smaller than the binding energy), the nucleus de-excites through beta and gamma transitions which cause the nucleus to become beta-radioactive and to undergo decay until it becomes stable.

In order to achieve high rates of neutron production in the spallation process, the power deposited on the target needs to be sufficiently high. Proton energies of between 1 and 5

GeV have proved to be the optimal range for neutron production using the spallation process.

According to [3], the relationship between beam power *P*, proton energy, *E*, proton intensity *N* and repetition rate *f* can be described by this formula:

$$P(MW) = 1.6 \times 10^{-16} \times E(GeV) \times N \times f(Hz) \quad (2.2)$$

The typical parameters applicable to a modern high power spallation source are:

$$P \sim 1\ MW, E \sim 1\ GeV, N \sim 1 \times 10^{14} \text{ and } f \sim 10\text{-}60\ Hz$$

In the process of producing neutrons from an accelerator-based spallation neutron source, the accelerator plays an important part in the facility to achieve the maximum number of neutrons. There are three types of accelerators that can be applied: a linac, synchrotron and cyclotron

Goldenbaum [4] explains that a linac-based neutron source has the capability of producing a high power proton beam from the H^- beam injection, which has pulses of ~ 1 ms length to energies of up to several GeV. An accumulator is placed in the accelerator to strip electrons from the H^- particles, leaving protons behind in the ring. The protons produced from this process are then extracted from the ring in a single turn onto the target material. However, European Spallation Source (ESS) does not have a ring before the beam travels to the target.

On the other hand, a cyclotron-based spallation neutron source uses a continuous beam. Beams with variable currents are delivered onto the target. By allowing the beams to pass through a thin 'stripping' foil, electrons are taken from the ion, which is left as a positive ion. The ion beam is then extracted and undergoes further processing to meet the energy density requirements of the target [16].

The synchrotron-based neutron source works similarly to linac-based sources, using intense H^- beams. However, a synchrotron-based neutron source uses a linac to accelerate H^- initially, then these H^- particles are injected into a synchrotron where the charge exchange process occurs as mentioned above. The injection process takes several hundreds of turns. The electrons are stripped from the hydrogen on injection to the synchrotron and the H^+ beam is then accelerated in the synchrotron to 1 GeV or higher, then extracted onto a target [4].

It is not possible to determine which type is best. A synchrotron-based source has the potential advantages of lower cost and the fact that it is easy to replace the stripping foil, since the linac, which only plays an initial role in supplying the particle, operates at lower beam energy in the synchrotron source. However, the synchrotron-based source uses an AC machine, rather than the DC machines used by linac-based accumulators. AC machines are more difficult to build, due to the large aperture of AC magnets, their rapid cycling power supply systems, and the need for a high-powered tuneable RF system, etc. Furthermore, AC machines are also more difficult to operate than DC machines, which can cause reliability issues during operation [3].

2.4 Characteristics of Spallation Neutrons

In order to achieve the highest rate of neutron production, the target material of the spallation process has to be composed of an element which has a high atomic number along with a reasonable thickness.

It is widely understood that the reaction between heavy nuclei and highly energised incident protons can produce a large number of neutrons with a wide spectrum of neutron energy, which makes this method ideal for transmutation of nuclear wastes.

Furthermore, it is also considered that the neutron yield increases as the mass of the target nucleus increases. Therefore, uranium, which has a high atomic mass, can be used as a spallation target material and yields about twice as many neutrons as lead [9].

However, due to the significant fission fraction of uranium, and the metallurgical problems of a uranium target, this does not represent a favourable choice for a spallation source [9].

2.4.1 Neutron angular distribution

When the highly energised protons hit a thick metal target, neutrons are produced at different energies and at different angles.

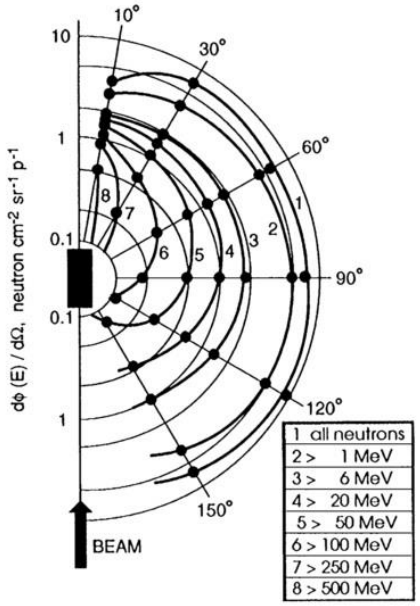

Figure 2.5: Measured angular distribution of neutrons in different energy groups for a 20 cm diameter lead target bombarded by proton beam of 2 GeV, taken from [9] **with original reference** [17]

Figure 2.5 shows the angular distribution of neutrons produced by a proton beam generated from an accelerator fired into the target. According to Bauer [9], the average neutron energies at 30°, 90° and 150°, at 2.55 GeV proton beam energy, were found to be 21.6, 7.31 and 4.38 MeV. This shows that the neutrons produced at higher energies were projected from the target in the same direction respect to the direction of beam travelled. It is important to consider this phenomenon in relation to the formation of a shield surrounding the target if neutrons at high energies need to be moderated before

they penetrate the outer structure. The neutrons expelled in the angular range between 90° and 150° have less energy than those expelled at 10 to 90 degrees. This effect is caused by cascade neutrons in a forward hemisphere relative to the proton beam.

2.4.2 Neutron energy spectrum

Figure 2.6 shows the significant differences in energy distribution between spallation and fission neutrons. Krasa [15] explains that the spallation neutron spectrum can extend from the proton beam energy, which is 1 GeV in this figure, down to tenths of keV, with a maximum around 2 MeV. This differs from the fission neutron spectrum, which reaches energies with a mean of around 2 MeV. This shows that the spallation spectrum is more advantageous in producing high energy neutrons compared with the fission spectrum under the same conditions. Spallation neutron production is initiated by a high-powered proton beam, and the fractions of incident particle beam energies are transferred to the neutrons produced from the spallation target. Thereby, spallation neutrons potentially have higher energy than fission neutrons, which are produced from chain reactions within the particle structure.

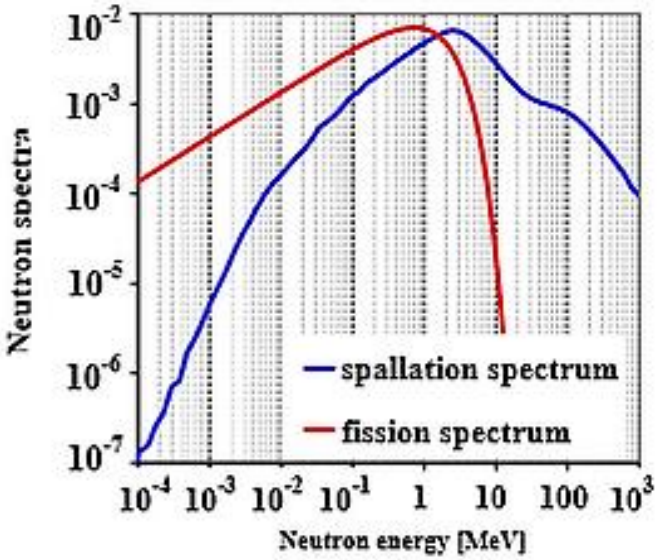

Figure 2.6: Spallation neutron spectrum (MCNPX simulation of neutron production in p+Pb at 1 GeV; an arbitrary normalisation and fission spectrum), taken from [12]

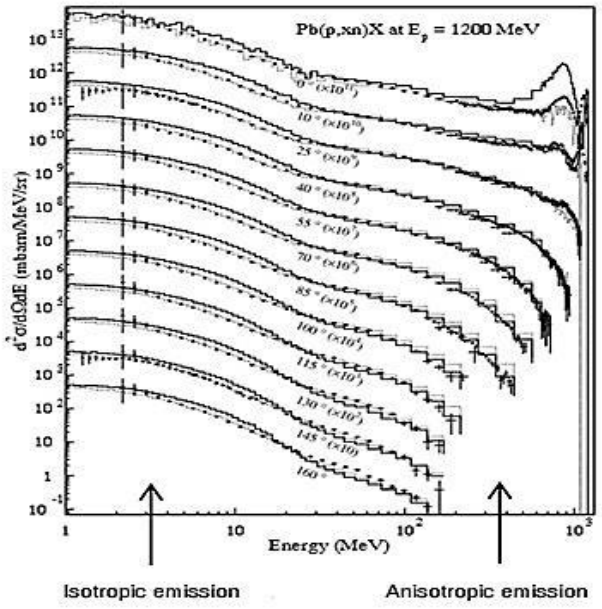

Figure 2.7 : Energy spectra of neutrons emitted at different angles, following interaction of 1.2 GeV protons with Pb target [18]**. The histogram represents TIERCE simulations** [19] **using the Bertini (solid line) or Cugnon (dotted line) cascade model, taken from** [20]

According to Nifenecker [20], the SATURNE group studied small angle neutron spectra before the closure of the Saclay synchrotron SATURNE facility in France. The study aimed to provide an energy spectrum of neutrons emitted in the experimental set-up. Figure 2.7 represents the small angle neutron energy spectrum for various target materials where 1.2 GeV proton beam energy was used in the experiment. The experimental data were then compared with Bertini INC and Cugnon INC models. Comparison between the two different cascade models shows that Cugnon INC describes the experimental data in better detail than Bertini INC. The figure also shows that the higher angles have lower energies compared with the neutron energies at lower angles. This phenomenon is likely to be caused by the neutrons produced from the pre-equilibrium stage, in which the energy of the incident particles is transferred.

2.4.3 Neutron multiplicity

Neutron multiplicity is defined as the number of neutrons per incident particle (n/p). This parameter is crucial for showing the performance of applications on an accelerator-

driven neutron source. Neutron multiplicity is a function of beam energy and target materials, and is linearly dependent on the target mass number (in the range $12 < A < 238$) and "slow increase with incident proton energy (in the range $0.2 < E < 2$ GeV)" [15].

The average number of neutrons is approximately given by

$$\langle n \rangle = (0.0803 + 0.0336\, ln\, E)A \tag{2.3}$$

where E is the incident proton energy in GeV and A is the target mass number. This formula provides 10 % accuracy or better for $A \geq 40$ [21].

There are two kinds of process contributing to neutron yield: the cascade and the evaporation process, both of which are dependent on incident beam energy. Both Figure 2.8 and Figure 2.9 show that the contribution of the evaporation process to neutron production is roughly more than that of the cascade at energies higher than 1 GeV. The rate of cascade production increases with the target mass number and proton energy.

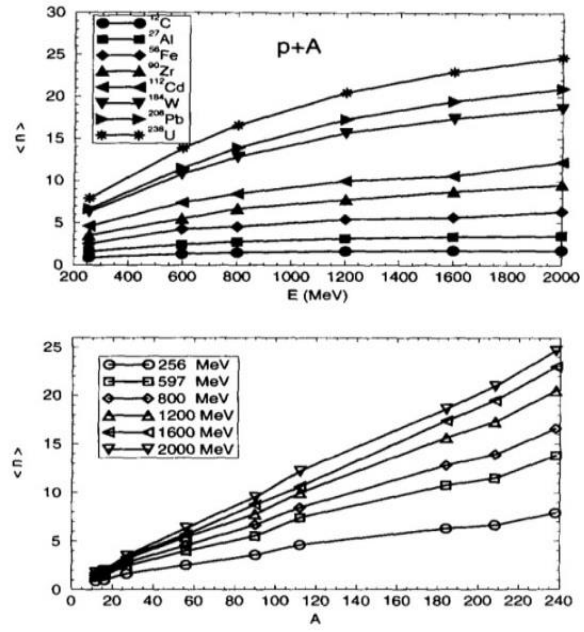

Figure 2.8: Neutron multiplicity per incident proton as a function of beam energy (upper part) and thin target material (lower part). Results of INCL+Dresner simulation, taken from [20]

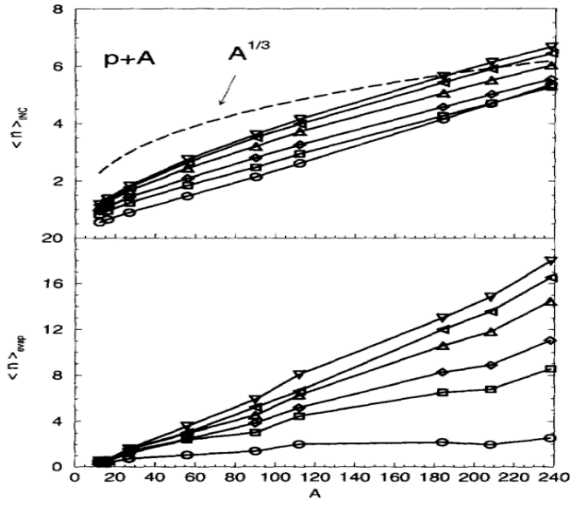

Figure 2.9: Neutron multiplicity as a function of the (thin) target material. Split into cascade (upper part) and evaporation components (lower part). The symbols refer to the incident energies which are the same values as in Figure 2.8, taken from [21]

However, the evaporation components show a strong correlation between neutron multiplicity and the target mass number and even more for the proton energies. Therefore, in order to achieve the highest rate of neutron multiplicity, both target mass and proton energy need to be set taking the optimal output into consideration.

2.5 Spallation Reactions on Thick Metal Targets

As previously mentioned in section 2.3, spallation reactions occur in three stages, INC, pre-equilibrium and evaporation, and these stages create neutrons with different energies (refer to section 2.3, Spallation Process). The neutrons created can increase the rate of neutron production by the interaction of (n,xn) reactions in other nuclei, in an inter-nuclear cascade [12].

The key figure for measuring neutron production in an experimental observation is the number of neutrons produced per proton-nucleus reaction, which can also be described as neutron yield.

Regarding the nuclear physics properties, a number of studies have extensively explored high-Z targets at an incident proton energy of larger than 800 MeV [22]. In order to achieve the highest rate of neutron fluxes from thick target materials for applications in scientific and industrial fields, two types of spallation target materials have been considered. One type are materials made of solids, among which tantalum (Ta), tungsten (W), lead (Pb) and uranium (U) are favourable, whilst the other type are liquid-based materials, among which those made of lead (Pb) or lead-bismuth eutectic (Pb-Bi) and mercury (Hg) [23] are commonly used. The heavy metal targets provide many neutrons as the highly energised proton beam impacts on the material; thus, it is important that the thickness of the metal target is selected carefully. For the purpose of obtaining the maximum number of neutrons, the most attractive candidate for spallation target material would be lead bismuth eutectic (45% lead and 55% bismuth). This material offers not only high rates of neutron yield and a low cross-section for re-absorption of

thermalized neutrons, but it also has a high rate of heat transfer which makes it ideal as a coolant [22].

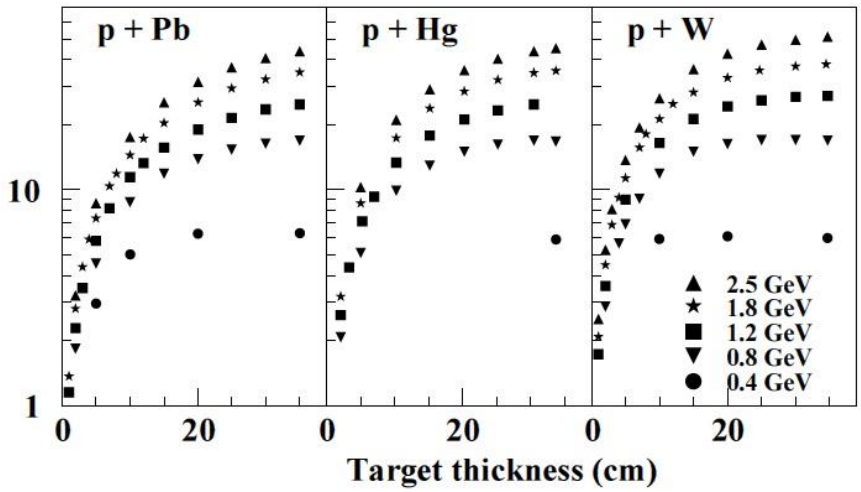

Figure 2.10: Neutron multiplicity as a function of target thickness and beam energy for Pb, Hg, W target materials. All targets were 15 cm in diameter, taken from [24]

Figure 2.10 shows the influence of target thickness of heavy metal targets on neutron multiplicity. All three graphs show that neutron multiplicity depends on the projectile-target combination [12]. The figure also shows that multiplicity levels off at a maximum thickness of 30 cm. This result suggests that there is a limitation to the thickness parameter in each material. Krasa [12] suggests a cylinder target with a typical size of 10 cm in diameter and a thickness of tens of cm. For the tungsten target, the thickness is about 30 cm, and for the lead target about 55 cm (this finding will be verified in the author's simulation in Chapter 4). Heavy metal targets provide many neutrons with a wide range of neutron energies. However, there are risks involved, such as radiotoxicity induced in the spallation target, thermal conductivity, receptivity, and melting and boiling points. Hence, the incident beam energy cannot be increased without considering these risks, not to mention the capability of generating a high energy beam in an accelerator.

Many institutes have chosen different materials based on their specifications, and their spallation neutron sources provide intense neutron beams for scientific research and

industrial development. Such institutes include SNS at Oak Ridge National Laboratory; LANSCE at Los Alamos National Laboratory; ISIS at Rutherford Appleton Laboratory; SINQ at PSI (Switzerland); IPNS at Argonne National Laboratory; and KENS at KEK (Japan). All these facilities use proton beams impacting onto a target for the production of spallation neutrons.

The target materials chosen by these facilities are liquid mercury (SNS), tungsten or tungsten alloy (ISIS, LANSCE), depleted uranium (IPNS), tantalum (KENS) or lead (SINQ). There are plans to build a European Spallation Source (ESS) in Lund (Sweden) and according to its design, ESS is expected to become about 30 times more powerful than facilities in the US and Japan. The spallation target of ESS will be composed of tungsten with a rotating wheel providing efficient heat distribution.

2.6 Spallation Sources

2.6.1 Overview of spallation sources

Table 2.1: Specifications of spallation sources (comprised from [25]- [33] and [11])

	ESS Sweden	ISIS RAL UK	KEK Japan	SINQ PSI Switzerland	LANSCE, Los Alamos National Laboratory, US
Accelerator	linac	70 MeV linac and synchrotron	40 MeV linac and synchrotron	72 MeV cyclotron and cyclotron	linac
Proton energy (GeV)	2.5	0.8	0.5	0.590	0.800
Beam current (mA)	50	0.2	14.9	1.3	0.100
Beam power (kW)	5000	160	2.3	1000	100
Target	Tungsten (rotational)	Tantalum mixed tungsten target	Tantalum-clad tungsten target	Zircaloy	Tungsten
Peak neutron flux($cm^{-2}s^{-1}$)	4×10^{16}	6×10^{15}	7×10^{13}	1.5×10^{14} (cm^{-2})[1]	3×10^{15}

[1] The flux for SINQ, PSI has an integrated flux only with the unit of cm^{-2}

As stated previously, spallation technique is effective of producing neutrons and the technique has been used widely for neutron science community such ESS, KEK and ISIS. Table 2.1 shows the main specifications of existing spallation neutron sources around the world.

The European Spallation Source (ESS) was set to start construction in 2014, aiming to become the world's leading neutron source [25]. The ESS project was conceived 20 years ago, and 17 countries are now signatories to the MOU for its construction [1].

The most unique feature of ESS is that the facility is specially designed to operate for long pulses. This specific set-up requires the instrument design to be intermediate between those of continuous flux sources, such as reactor sources, and short-pulsed spallation sources like those of SNS, ISIS and JPARC [27], [28].

KEK is the Japanese high energy accelerator research organisation which provides a strong neutron source. KEK's neutron source facility, which is named KENS, is a pulse-based neutron facility located at the national laboratory for high energy physics, Tsukuba, Japan. KENS started operation in 1980 dedicated to condensed matter science and neutron physics [29], [30]. KENS' advanced research in neutron physics and other areas led to the creation of a new facility called the Japan Hadron Facility (JHF) project, which has contributed hugely to the construction of the Japanese Proton Accelerator Complex (J-PARC).

ISIS is a spallation neutron source in which a synchrotron is based. The facility is located at the Rutherford Appleton Laboratory (RAL) in Oxfordshire, UK. This facility is designed for a short-pulse-based neutron source, because it is capable of handling some imaging experiments by "freezing the motion of molecules" [31], and it has the additional advantage of being able to measure and determine the kinetic energy of individual neutrons using the time-of-flight method [9].

Los Alamos Neutron Science Center (LANSCE) has been hosting unique equipment to conduct various science and technology experiments. According to LANSCE's operational status paper [26], there are four experiment areas within the LANSCE facility, and two of those four areas are directly related to neutron production. The facility involved in neutron production is the Weapons Neutron Research (WNR) facility, which provides an intense source of high energy neutrons intended for nuclear neutron science.

2.6.2 MEGAPIE at SINQ - Paul Scherrer Institute, Switzerland

SINQ, the Swiss spallation neutron source, is driven by PSI's 590 MeV proton accelerator and has been demonstrated to be one of the most powerful accelerator-driven facilities in the world. The beam operates at 1MW power and is designed to apply various ADS transmutation concepts [32]. Its spallation target is also unique in that the target material is liquefied lead-bismuth metal. The project dedicated to this target station is named MEGAPIE, which stands for MEGAwatt Pilot Experiment. The project is under consideration for the application of "various concepts of Accelerator Driven Systems (ADS) to be used in the transmutation of nuclear waste and other applications" [11]. The neutron efficiency of this facility has shown an improvement of about 80% compared with a lead-cannelloni based target station.

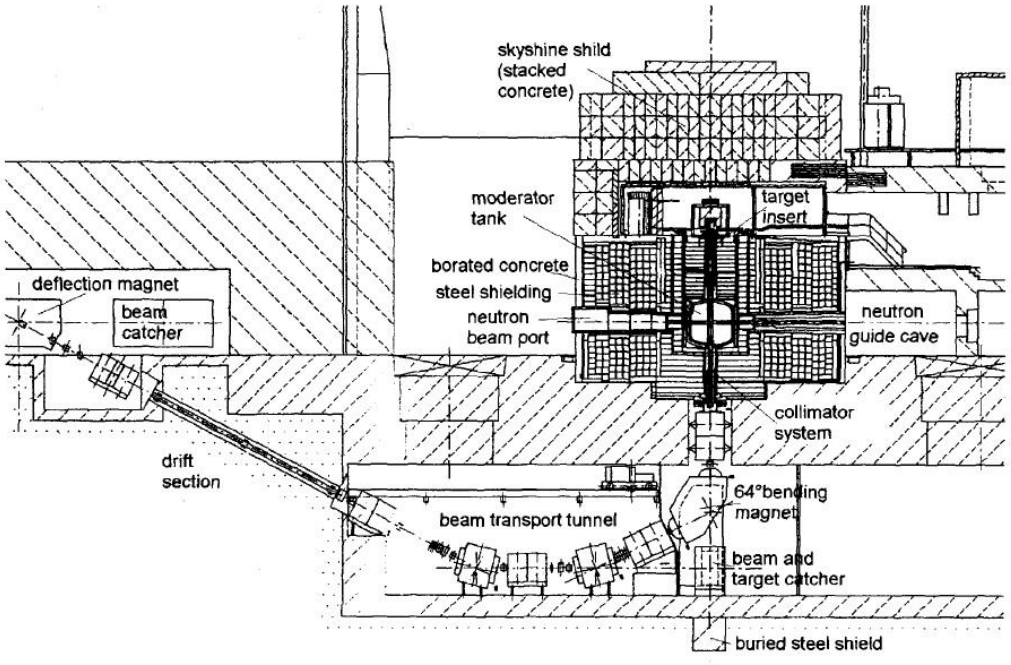

Figure 2.11: Vertical cross-section of the target block and part of the proton beam transport line of SINQ (taken from [33]**)**

The MEGAPIE target shielding house layer is filled with 1 tonne of liquid lead bismuth eutectic (LBE) in a steel container. By using LBE as coolant in a spallation target area, the energy deposition caused by high powered beams can be removed effectively while keeping the target temperature stable. The experiment shows the outstanding performance of the target and its dedicated ancillary system. The facility has achieved a good rate of neutron delivery, producing about 80% more neutrons than the previous record with a lead-cannelloni target [32].

2.7 Bibliography

[1] European Spallation Source, “Spallation | ESS,” *European Spallation Source*. [Online]. Available: http://europeanspallationsource.se/spallation.[Accessed: 30-10-2016]

[2] C. Bungau, R. Cywinski, and R. Barlow, “Neutron Spallation Studies in Thick Lead Targets for an Accelerator Driven Subcritical Reactor (submitted),” *Nucl.*

Instruments Methods Phys. Res. Sect. A Accel. Spectrometers, Detect. Assoc. Equip., 2013.

[3] W. Chou, "Spallation Neutron Source and Other High Intensity Proton Sources," *arXiv Prepr. physics/0301025*, 2003. [Online] Available: https://arxiv.org/abs/physics/0301025., [Accessed: 30-09-2016]

[4] F. Goldenbaum, "The Physics of Spallation Processes," Bergische Universität Wuppertal, 2003. [Online] Available: http://elpub.bib.uni-wuppertal.de/servlets/DerivateServlet/Derivate-1018/hc0301.pdf., [Accessed: 30-09-2016]

[5] International Atomic Energy Agency, "Applications of Research Reactors,", Vienna., Rep. IAEA NUCLEAR SERIES No NP-T-5.3., 2014.

[6] B. Rossi, "About properties of penetrating, corpuscular radiation at sea level," *Zeitschrift fur Phys. 82*, vol. 151, 1933.

[7] B. B. Cunningham *et al.*, "Transmutations with High-Energy Deuterons in the 184-Inch Cyclotron," in *Physical Review*, 1947, vol. 72, no. 8, pp. 739–740.

[8] C. R. Gould, G. Greene, F. Plasil *et al.,* "Fundamental Physics with Pulsed Neutron Beams (FPPNB-2000 - Research Triangle Park, North Carolina, USA 1-3 June 2000)," World Scientific, p. 260.

[9] G. S. Bauer, "Physics and technology of spallation neutron sources," *Nucl. Instruments Methods Phys. Res. Sect. A Accel. Spectrometers, Detect. Assoc. Equip.*, vol. 463, no. 3, pp. 505–543, May 2001.

[10] J. R. Haines, "ESS Target Facility Design," *in presented at the 6th International Particle Accelerator Conference, Richmond, VA, USA, paper THXB3, not published,* 2015.

[11] I. S. K. Gardner, "A review of spallation neutron source accelerators," in *Particle accelerator. Proceedings, 6th European conference, EPAC'98,* Stockholm, Sweden, June 22-26, 1998., pp. 98–102.

[12] A. Krasa, “Neutron Emission in Spallation Reactions of 0.7 – 2.0 GeV Protons on Thick, Lead Target Surrounded by Uranium Blanket,” Ph.D. dissertation, Czech Technical Univeristy, 2008.

[13] G. Friedlander, *Nuclear and radiochemistry*. New York: J. Wiley & Sons., 1955.

[14] C. Bungau, R. Cywinski, and R. Barlow, “Neutron spallation studies for an accelerator driven subcritical reactor,” in *Particle Accelerator Conference*, Vancouver, Canada, May 4-8 2009.

[15] A. Krása, “Spallation Reaction Physics.” Czech Technical Univeristy Lecture, 2010. [Online] Available: http://ojs.ujf.cas.cz/~krasa/ZNTT/SpallationReactions-text.pdf. [Accessed : 30-10-2016]

[16] A. W. Chao and W. Chou, *Reviews of accelerator science and technology - volume 4: accelerator applications in industry and the environment:* World Scientific Pub Co Pte, 2012.

[17] V. Yurevitch, “Review and analysis of the experimental data on neutron production in lead targets obtained at p/d-beam of the dubna synchrophasotron during 1986-1992;preprint.”

[18] X. Ledoux, F. Borne, A. Boudard, and et.al, “Spallation Neutron Production by 0.8, 1.2, and 1.6 GeV Protons on Pb Targets,” *Phys. Rev. Lett.*, vol. 82, no. 22, pp. 4412–4415, May 1999.

[19] O Bersillon, in *2nd Int. Conf. on Accelerator Driven Transmutation Technologies*, Kalmar, Sweden, 3–7 June, 1996., p 520

[20] H. Nifenecker, O. Meplan, and S. David, *Accelerator Driven Subcritical Reactors (Series in Fundamental and Applied Nuclear Physics)*. London, IOP Publishing Ltd, 2003.

[21] J. Cugnon, C. Volant, and S. Vuillier, “Nucleon and deuteron induced spallation reactions,” *Nucl. Phys. A*, vol. 625, no. 4, pp. 729–757, Nov. 1997.

[22] K. van der Meer and et al, “Spallation yields of neutrons produced in thick lead/bismuth targets by protons at incident energies of 420 and 590 MeV,” *Nucl. Instruments Methods Phys. Res. Sect. B Beam Interact. with Mater. Atoms*, vol. 217, no. 2, pp. 202–220, Apr. 2004.

[23] Y. Malyshkin and et al, “Neutron production and energy deposition in fissile spallation targets studied with Geant4 toolkit,” *Nucl. Instruments Methods Phys. Res. Sect. B Beam Interact. with Mater. Atoms*, vol. 289, pp. 79–90, Oct. 2012.

[24] A. Letourneau, J. Galin, F. Goldenbaum, and et.al, “Neutron production in bombardments of thin and thick W, Hg, Pb, targets by 0.4, 0.8, 1.2, 1.8 and 2.5 GeV protons,” *Nucl. Instruments Methods Phys. Res. Res. Sect. B Beam Interact. with Mater. Atoms*, vol. 170, pp. 299–322, 2000.

[25] R. Hall-Wilton and C. Theroine, “Status of the European Spallation Source ESS AB, the Instrument Selection Process, and a Fundamental Physics Beamline at the ESS,” *Phys. Procedia*, vol. 51, no. February 2012, pp. 8–12, 2014.

[26] S. Peggs and et al, “ESS Conceptual Design Report”, European Spallation Source, Lund, Rep. ESS-2012-001,2012.

[27] S. Peggs and et al, “ESS technical design report”, European Spallation Source, Lund, Rep. ESS-doc-274, 2013.

[28] K. Suzuki and E. Al, “Review of the neutron science laboratory KENS in the high energy accelerator research organization KEK , JAPAN Summary and Recommendations of the KENS Review Committee,” 2004.

[29] T. Nakamura, T. Nunomiya, H. Yashima, and S. Yonai, “Overview of recent experimental works on high energy neutron shielding,” *Prog. Nucl. Energy*, vol. 44, no. 2, pp. 85–187, 2004.

[30] S. C. T. Tygier, “High Current Proton Fixed-Field Alternating-Gradient Accelerator Designs,” Ph.D. dissertation, The University of Manchester, Manchester, UK, 2012.

[31] K. W. Jones and K. F. Schoenberg, “Operation status and future plans for the Los Alamos Neutron Science Center (LANSCE),” in *Proceedings of LINAC08*, Victoria, British Columbia, Canada, 29 September – 3 October, 2008.

[32] W. Wagner, F. Gröschel, K. Thomsen, and H. Heyck, “MEGAPIE at SINQ – The first liquid metal target driven by a megawatt class proton beam,” *J. Nucl. Mater.*, vol. 377, no. 1, pp. 12–16, Jun. 2008.

[33] G. S. Bauer, M. Salvatores, and G. Heusener, “MEGAPIE, a 1 MW pilot experiment for a liquid metal spallation target,” *J. Nucl. Mater.*, vol. 296, no. 1–3, pp. 17–33, 2001.

Chapter 3. Benchmarking GEANT4 Simulation with Experimental Data

3.1 Introduction

As noted in Chapter 2, the spallation process is a safe, controllable and efficient means of producing an intense flux of neutrons. Additionally, the spallation technique is a major method of implementing an ADSR for both energy production and the transmutation of nuclear waste.

In general, a neutron can undergo different reactions in the spallation target such as inelastic, elastic, capture and fission reactions. Each material has different cross sections indicating the most probable reactions in the range of neutron energies. For example, the isotope ^{207}Pb, which is a large constituent of natural lead has following cross sections.

Table 3.1: the neutron cross-section of ^{207}Pb taken from [1], [2]

	Thermal cross section (barn)	Fast cross section (barn)
Elastic	10.82	4.88
Inelastic	0.002	0.548
Capture	0.699	0.00147

These cross-section values show that both thermal and fast neutrons are likely undergo elastic scattering reactions. They indicate that there would be a low chance of a neutron captured by the lead nucleus. This suggests lead as a favourable material for a spallation target because the material would not be likely to capture neutrons and thus to decrease the number of neutrons which is crucial for ADSR operation.

In order to facilitate this study, it was necessary to ensure that our chosen simulation codes accurately reproduce the spallation process and associated neutron production.

Monte Carlo-based transport simulation codes such as GEANT4 [3] and MCNPX [4] are commonly used to describe neutron spectra and yields. In this study of spallation reactions, an attempt was made to benchmark GEANT4 against published experiment results. The published data [5], contain the measured neutron spectra from spallation reactions at 0.5 and 1.5 GeV proton beam energies. The experiments were performed at KEK, Japan, and the authors used MCNP-4A simulation code to compare with the experiment results.

GEANT4, which is a Monte Carlo-based transport code developed by CERN, provides an extensive set of hadronic physics models for energies up to 10-15 GeV, both for the intra-nuclear cascade region and for modelling evaporation [6]. Hence, the GEANT4 simulation code has the capability to describe neutron spectra and spallation interactions.

In this study, an attempt was made to examine the neutron spectra created by GEANT4 by comparing them with the neutron flux (n/MeV/sr/proton) of experimental data from KEK. If they agree GEANT4 simulations would be suitable for simulating the spallation processes in a full simulation of a model ADSR.

GEANT4 offers three hadron physics models for simulating secondary particle production. Initially comparisons were made between the results produced by these models in order to determine the most suitable physics models for such an application. Following this further extensive simulations were performed in which the size of the spallation target utilized in the benchmarking process was varied in order to evaluate the neutron yield produced by various target sizes to find the optimal conditions for achieving a maximum rate of neutron production.

3.2 Experiment setup

The KEK experiment was originally intended to study the discrepancy between calculate and experimental for the reaction rate for lead and tungsten targets bombarded with 500 MeV and 1.5 GeV protons. Time-of-flight and unfolding techniques were used in this experiment to measure the neutron energy. In the KEK study, a 12 GeV proton synchrotron supplied a stream of protons onto the spallation target after passing through a bending magnet. This process configured the beams with a unique momentum suitable for the thick spallation target. The beam supplied to the target had the following specifications:

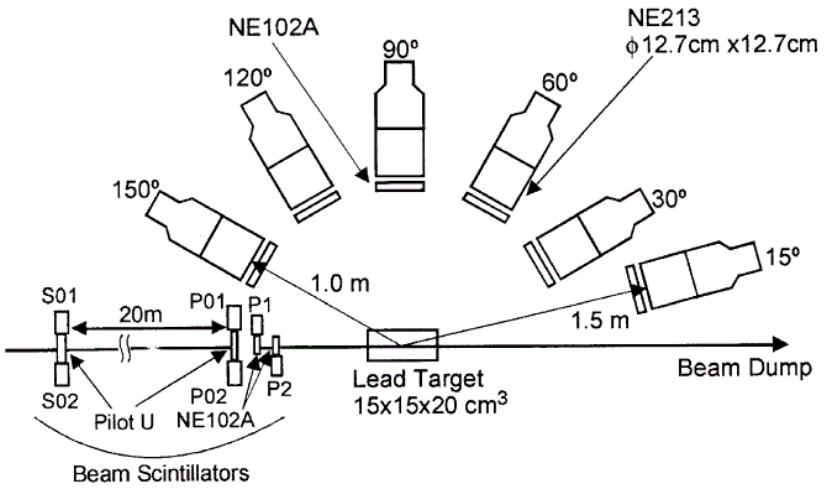

Figure 3.1: Illustration of experimental arrangement (taken from [5]**)**

Table 3.2: Beam specifications used in the experiment

Proton pulses	
Interval times (seconds)	4
Duration times (seconds)	2.5
Intensity of incident particles (particle/pulse)	
$\leq 10^5$	
Size and shape of the target	
$15 \times 15 \times 20$ cm^3 rectangular shaped beam (lead target with 99.95 % [5])	
Beam dump	
Material	Carbon block pile
Size	0.5×0.5 m^2 with 1 metre length
Location	8.5 metres from Pb target

3.3 Characteristics of GEANT4 hadronic physics list

GEANT4, which stands for GEometry ANd Tracking, is a Monte-Carlo transport code program. This program is capable of simulating the interactions of particles and ions in matter within an energy range between 35 keV and a few TeV. GEANT4 is designed to build a virtual environment for a complete experiment with all the detectors, scintillators and other objects required to model particle propagation in a simulation [7].

The program defines the course of particle interaction through the step length for particle propagation. This value is pre-defined internally by the program by taking into account the particle energy, the material traversed and the possible particle interactions that may take place [8].

GEANT4 has many libraries governing interactions of particles with any material. In studies of spallation and neutron production, the most commonly used libraries are

G4hIonisation, G4nprocess, G4nInelastic and G4MultipleScattering. G4hIonisation creates a simulation of the energy loss of hadrons during any interactions taking place.

The physics encoded inside GEANT4 is compiled into many classes called 'physics lists'. A physics list is a complete set of the physics deployed in the simulation of a particle's path through an experimental setup.

It is noted in [8] that in GEANT4, the energy loss process must be calculated, especially the continuous and discrete loss of energy in a material.

$$\frac{d\sigma(Z,E,T)}{dT} \tag{3.1}$$

The differential cross-section per atom (atomic number Z) described in the above equation (3.1) is calculated for the ejection of a secondary particle with kinetic energy T by an incident particle of total energy E moving in a material of density ρ. This equation then leads into the calculation of mean rate of energy loss. The kinetic energy cut-off is denoted by T_{cut}. This threshold value determines whether the secondary particles ejected are simulated as continuous energy loss by the incident particle, or as explicit production of secondary particles such as gamma, electron and positron particles. The calculation is described in the following equation (3.2):

$$\frac{dE}{dx}(E, T_{cut}) = n_{at} \int_0^{T_{cut}} \frac{d\sigma}{dT}(Z, E, T) T dT \tag{3.2}$$

where n_{at} is the number of atoms per volume in the material.

Due to the wide energy range of particles involved in modelling hadronic interactions, the physics list is created by combining suitable physics models in order to be able to describe physical interactions covering an energy range from a few keV to the TeV scale [5, 7].

The following three main cascade models (Bertini, Binary and INCL) explained in this chapter are used in many applications of GEANT4. These are applicable within the energy range 20 MeV – 3 GeV [10].

3.3.1 QGSP_BERT_HP

QGSP_BERT_HP is a physics list made up of a combination of three different models; these are the Quark Gluon Secondary Particle (QGSP) model, the Bertini model and the neutron high precision model.

The Quark Gluon Secondary Particle model is derived from the Quark Gluon String (QGS) model, which covers particle energies above 20 GeV. The Bertini-style cascade model (BERT) covers up to 10 GeV, while the energy range between 10 and 20 GeV is covered by the Low Energy Parameterized (LEP) model [7].

Since the ATLAS, CMS and LHCb experiments use a configured QGSP_BERT physics list for their detector simulations [7], these models have been frequently validated for extensive use in many experiments. Hence, each update of the GEANT4 program contains improvements and bug fixes resulting from such experiments, which causes significant changes to the models.

The GEANT4 Bertini-style model is a classical intra-nuclear cascade based on the re-configured INUCL code [11]. The physics list includes a Bertini intra-nuclear cascade model with excitons, a pre-equilibrium model, a simple nuclear explosion model, a fission model and an evaporation model. Since the Bertini model includes the Intra-

Nuclear Cascade model (INC) [12], there is a necessary condition of validity imposed on this model, which is

$$\frac{\lambda_B}{v} \ll \tau_C \ll \Delta t \tag{3.3}$$

where λ_B is the de-Broglie wavelength of the nucleons, v is the average relative nucleon-nucleon velocity and Δt is the time interval between collisions. This means that the physical foundation is approximate at energies less than about 200 MeV, and this is where a supplemented pre-equilibrium model needs to be enforced to describe the particle interaction [13].

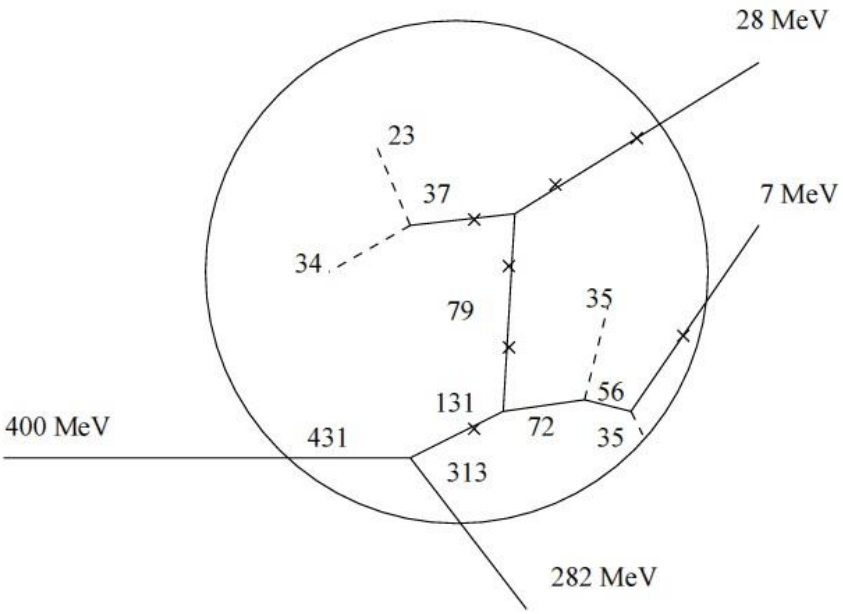

Figure 3.2: Schematic representation of the intra-nuclear cascade. A hadron with 400 MeV energy is forming an INC history. Crosses represent the Pauli exclusion principle in action. The numbers represent the neutron energy in each step taken (Figure is taken from [13]**, reproduced from an original version by Bertini** [14]**)**

As shown in Figure 3.2, if Pauli's exclusion principle allows and $E_{Particle} > E_{cutoff}$ = 2 MeV, transportation of produced particles is performed based on the path length of projectile particles. This path length is determined from free particle-particle cross-sections and region-dependent nucleon densities [13]. After the INC stage, a pre-equilibrium model is then applied to simulate particle interactions. The pre-equilibrium model consists of the Griffin exciton model [15], a simple nucleus explosion model and a fission model [10]. The pre-equilibrium model uses target excitation data and exciton configurations for neutrons and protons to produce the non-equilibrium evaporation [13]. In some cases, the Fermi break-up stage is applied when there are light nuclei (A < 12 and 3(A-Z) < Z<6) and if the excitation energy is greater than 3 times the binding energy. Finally, an evaporation model is used to simulate emission of particles until the excitation energy falls below 0.1 MeV. As a result of the major updates to GEANT4, the Bertini model has improved significantly in CPU performance in terms of speed and memory handling during simulations [7].

On the other hand, the Quark-Gluon String model (QGS) is the first handling model in the QGSP_BERT_HP physics list. QGS governs the calculation of the highest energy interactions in GEANT4 hadronics. The model simulates hadron-nucleon interactions which arise from exchanging quarks. The exchange forms strings which become hadronised. The process is then led into its final stage by the production of multiple particles. Improvements to the QGS model are regularly updated through comparison with ATLAS calorimeter data [7].

3.3.2 QGSP_BIC_HP

The QGSP_BIC_HP physics list couples the above QGS model with the neutron HP cascade. However, while these models are essential components within this physics list, the GEANT4 Binary Intranuclear Cascade (BIC) is the main physics model contributing to the calculation of neutron production. The BIC model is a time-dependent model of the intra-nuclear cascade and has the ability to re-scatter hadrons using either the QGS or the Fritiof Fragmentation (FTF) high energy models [7]. Hence, there is a more

physical path for combining the cascade and string models than the random sampling used in other cascades. The binary cascade model is a theory-driven model that is an alternative to the Bertini cascade model. This model has the capability of producing results for an energy range up to 2 GeV [7].

3.3.3 QGSP_INCLXX_HP

QGSP_INCLXX_HP is a recently developed physics list that includes the INCL/ABLA cascade model. The Liege Intranuclear Cascade model (INCL), is a 'parameter-free time-like' Monte-Carlo cascade model [16]. The model can be applied to nucleon-, pion- and light ion-induced reactions in a kinetic energy range of up to 3 GeV per nucleon. This model is still experimental but significant improvements have recently been made, such as the modelling of de-excitation, amendments to the underlying physics and improved interpretation of pre-equilibrium emission of light particles (up to A = 8) using "a dynamical phase-space coalescence algorithm and the transition to the fusion model for covering lower energy range of ~ 100 MeV" [9].

3.4 GEANT4 simulation setup for the benchmarking study

As a part of our benchmarking procedure we have compared the experimental results from KEK with the results produced by our own GEANT4 simulations ensuring that the simulation geometry reproduces as closely as possible the configurations used in the experiment. The spallation target in the simulation was placed at the centre of a simulated space. The target was composed of natural lead which is automatically constructed by GEANT4 simulation as the default [3]. Geant4 simulation defines the natural composition derived from the NIST database of elements and isotope compositions [1]. Detectors were placed at 15, 30, 60, 90, 120 and 150 degrees with respect to the target; in most cases these were at a distance of 1 metre, though the detector at 15 degrees was placed at 1.5 metres due to the higher neutron energy (see

Figure 3.3). In order to achieve an accurate prediction using GEANT4, three physics models were chosen to compare with the experimental data. These models were QGSP_Bertini_HP, QGSP_BIC_HP and QGSP_INCLXX_HP. All three physics models were coupled with a high precision (HP) neutron model which uses evaluated neutron data libraries for neutron cross-sections below 20 MeV [17]. These physics models were chosen due to the fact that they are capable of predicting neutron production with a precise range of neutron energies, and because they are the recommended physics models for secondary particle production.

The detecting media placed in the simulation were composed of vacuum. This enabled the media to avoid any interaction with the neutrons. The code used to design these media was also configured to count neutrons at the moment when the neutrons were in contact with the surface of the detectors. The area of the detecting media was 12.7×12.7 cm. This is the same as the NE213 scintillator used in the KEK experiment. In the simulation, a proton beam was set to travel from the left-hand side of the target towards the right. The proton beam energy was set for 0.5 GeV and 1.5 GeV, as in the experiments, whilst the number of protons impacting on the target was set for 10^8 particles in order to establish a statistically reliable result.

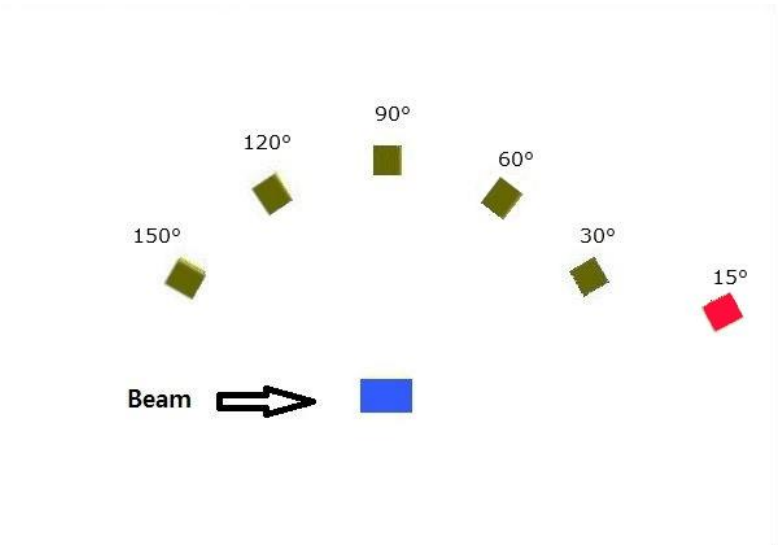

Figure 3.3: Configuration of detectors and target in the simulation (target is coloured blue and detectors are coloured green, except the 15° detector, which is coloured red)

3.5 Validation results

The simulations run by GEANT4 were successful, and several analyses were performed upon the neutron spectra for both experimental and simulation-based results. Figure 3.4 and Figure 3.5 represents the results of neutron flux measured in KEK along with the MCNP-4A simulation results by the author of [5].

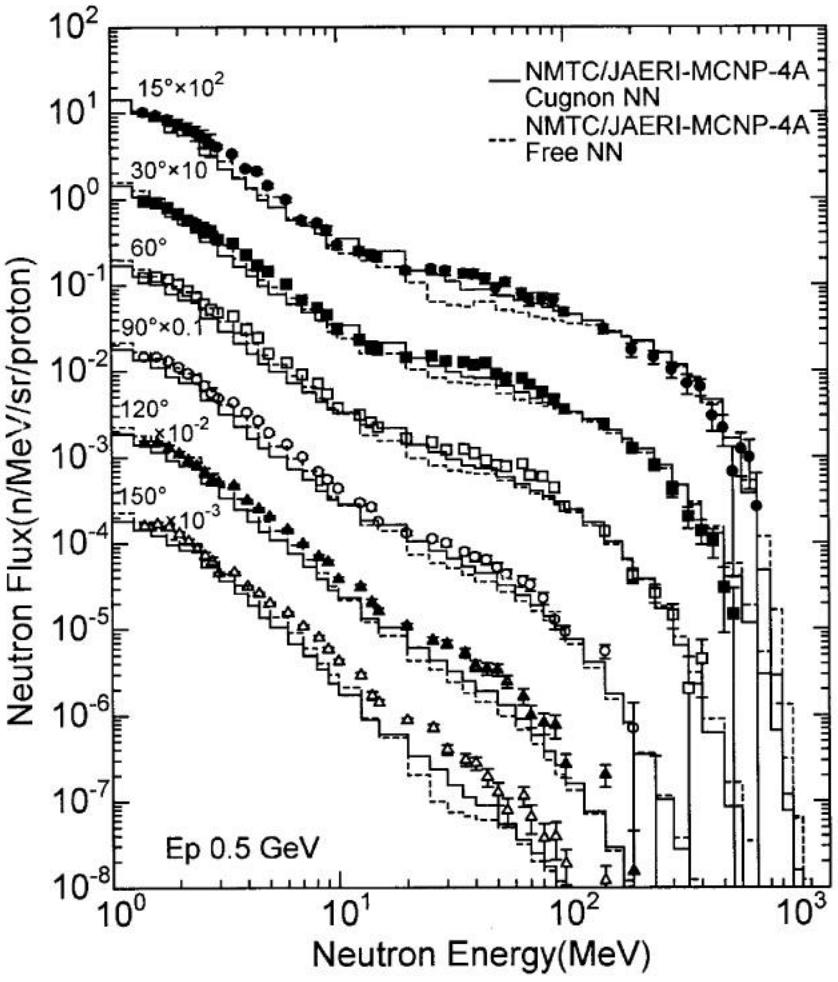

Figure 3.4: Neutron flux at 0.5 GeV proton beam energy using MCNP-4A, with the experimental results shown as dots (taken from [5]**)**

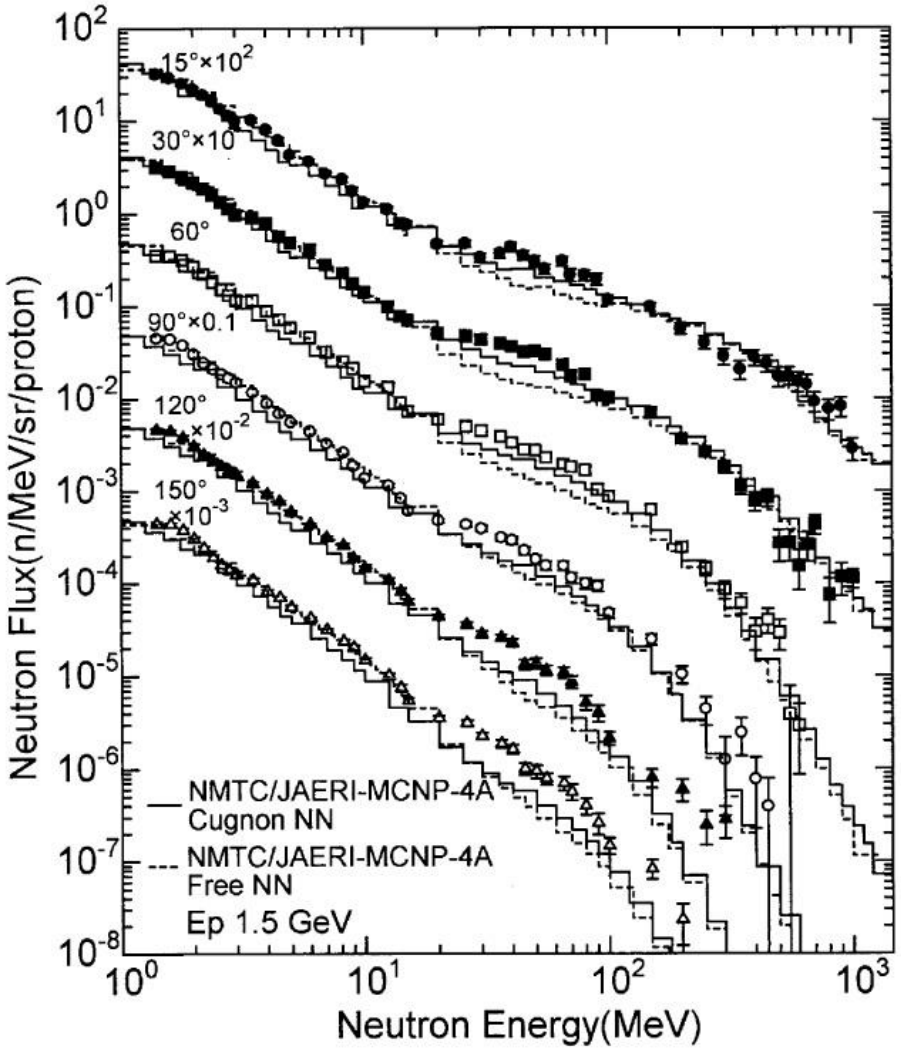

Figure 3.5: Neutron flux at 1.5 GeV proton beam energy using MCNP-4A, with the experimental results shown as dots (taken from [5]**)**

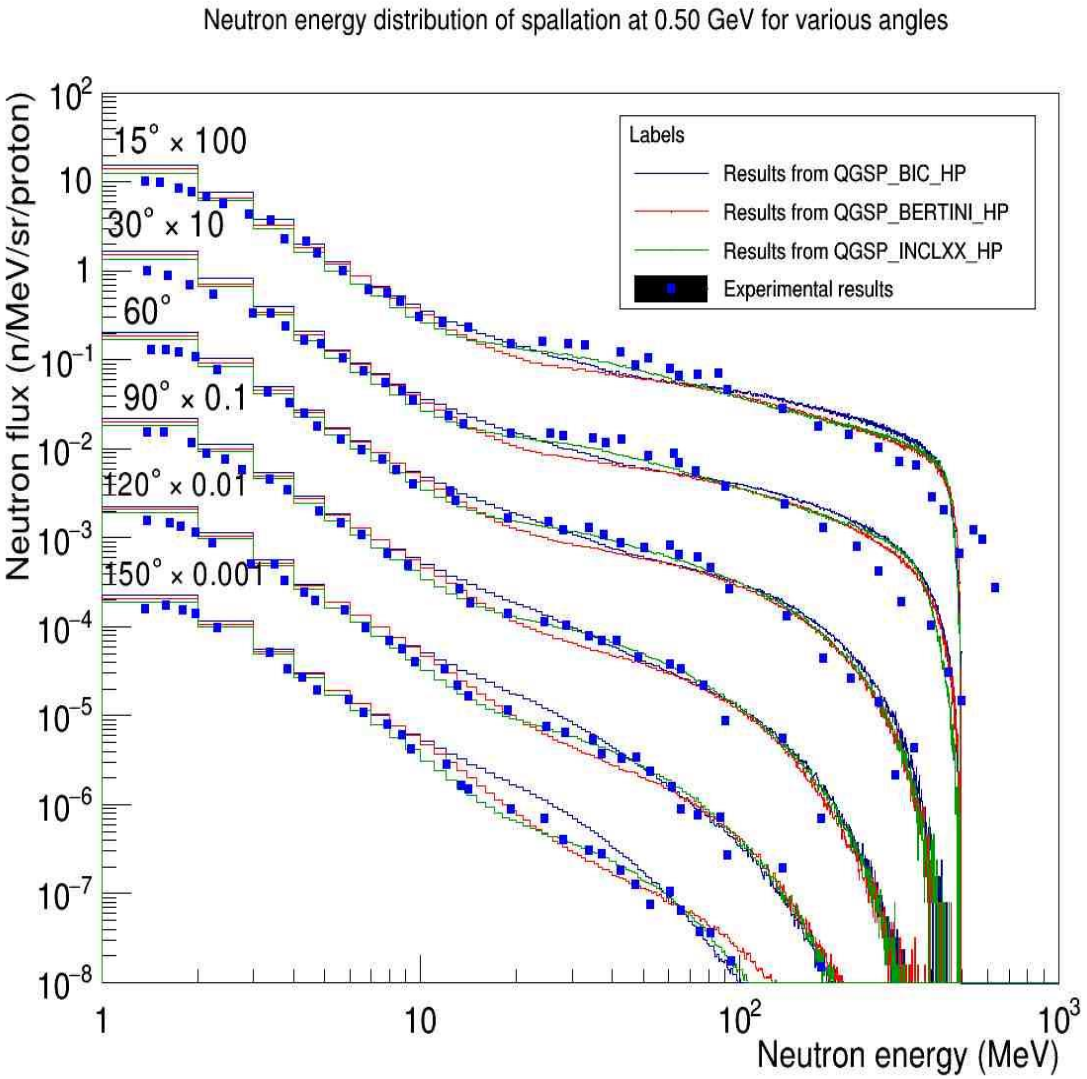

Figure 3.6: Neutron flux at 0.5 GeV proton beam energy using GEANT4, with the experimental data [5] **shown as dots**

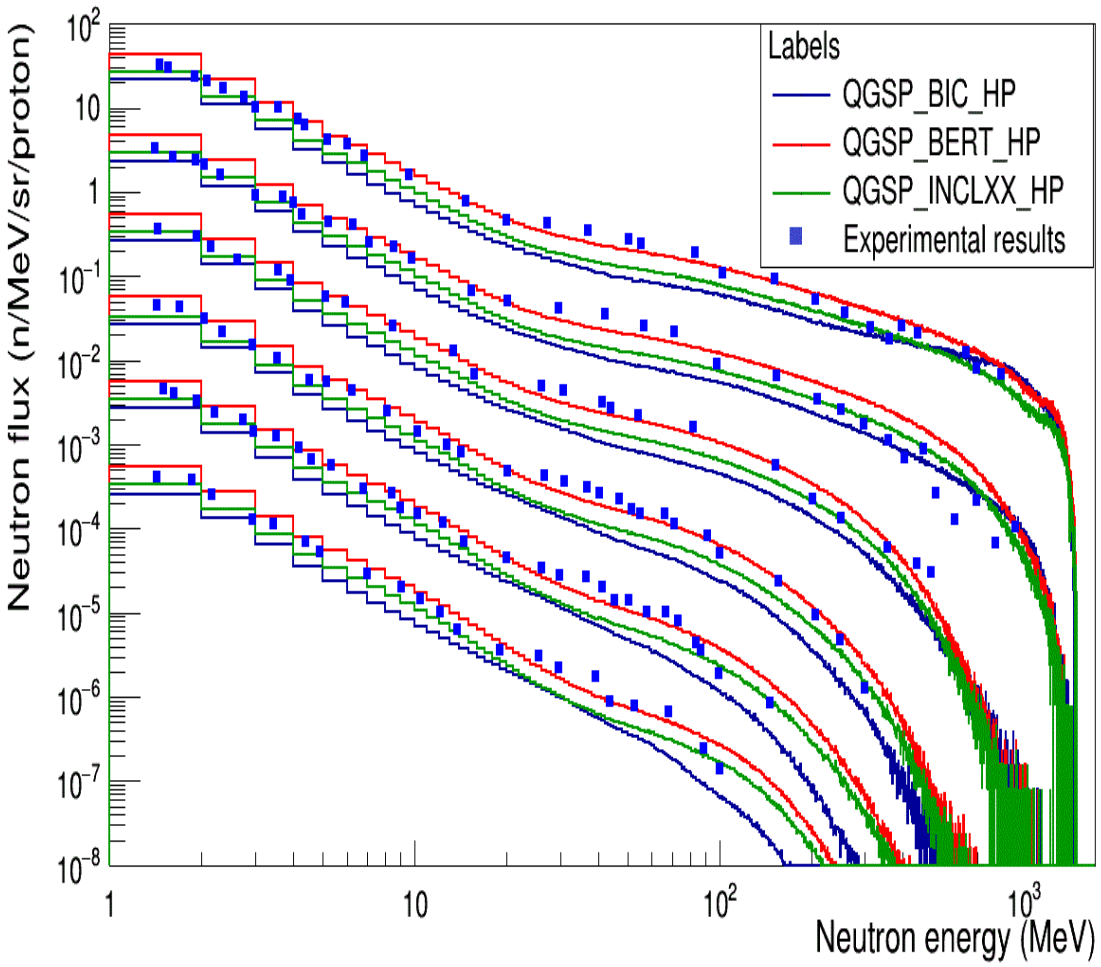

Figure 3.7: Neutron flux at 1.5 GeV proton beam energy using GEANT4, with the experimental results [5] **shown as dots**

As shown in the figures, it was clear from visual inspection that GEANT4 produced a very convincing outcome in describing the actual experiment results. Furthermore, whilst the spectra created by GEANT4 are similar in form to those created by the MCNP-4A code, GEANT4 more closely reproduces the experimental results than does MCNP-4A, especially at higher neutron energies and higher angles. In terms of the accuracy of the physics models, the QGSP_INCLXX_HP physics model produced the closest outcome to the experimental results, followed by the Bertini model. The BIC model proved to be the least accurate physics model in predicting the experimental

results. When examined more closely, the results from INCL at 0.5 GeV proton beam energy almost matched the experimental results at every angle. The Bertini model also produced fairly accurate results at between 0 and 10 MeV of neutron energy, but with increases in neutron energy gave a wider prediction than the experimental results. At 1.5 GeV, INCL also produced the most accurate outcome in relation to the experimental results at neutron energy ranges between 0-10 MeV and 100-1000 MeV. However, the Bertini model produced better predictions than the INCL model at the range between 10-100 MeV, which was unexpected. Nevertheless, the overall performance of GEANT4 at 1.5 GeV did give as accurate an estimation as MCNP-4A's prediction. It was significant that the INCL model was the most accurate in predicting neutron spectra close to those of the experimental results. The INCL model is a newly-developed physics model and is designed for an energy range of 0-3 GeV. The INCL model is combined with a precise calculation of cascade and nuclear de-excitation to enhance the description of spallation interactions [7].

The data collected from all GEANT4 simulations detailed in this thesis involve some degree of uncertainty. This uncertainty can be expressed by using standard Poisson statistics for a random counting process as described below [18]:

$$\Delta N = \sqrt{N} \tag{3.4}$$

where N in this context is the neutron count.

In most cases, the error bars were so small as to be invisible, and so graphical representation of any errors in the results has been omitted. For the experimental results at high energy, however, either the error bar was not visible due to the low resolution of the original graph or the size of the error bars was so large that they merged with the author's simulation results. Hence, it was necessary to extract the data based on the actual points represented in the graphs.

In order to confirm the visual inspection of the results plotted on the graph, a chi squared analysis was performed. Chi squared statistics uses a comparison between the observed value and expected value to show a numerical indication of the closeness between two sets of data [19].

$$\chi^2 = \sum \frac{(obs-exp)^2}{(E_{exp})^2+(E_{obs})^2} \tag{3.5}$$

Chi squared formula (taken from [20]**)**

where *obs* in this context is observed value, *exp* as expected value, E_{exp} is error of expected value and E_{obs} is the error of observed value.

As shown in Table 3.3 and Table 3.4, the INCL model showed the lowest values, which meant that INCL created the closest outcome to the experimental results. This was usually followed by the Bertini and BIC models in that order. These values support the earlier statement that INCL produced the most accurate predictions. They also support the observation that the Bertini model produced a reasonable level of prediction. In the case of BIC, the values are higher than the other two models, which suggest that the BIC prediction was not sufficiently accurate in describing the neutron energy spectra in this case.

In order to calculate the probability that these predictions are accurate, the results were further evaluated through the calculation of p-value. The p-value is the probability that a chi squared this large could arise if the model is completely correct [21]. To calculate this value, the degrees of freedom were used shown in Table 3.5. The number of degrees of freedom is the number data points minus the number of adjustable parameters.

Table 3.3: A table showing chi squared values for 0.5 GeV results using GEANT4 physics models

0.5 GeV proton beam energy			
	Chi squared value		
Degree	BIC	BERT	INCL
15	7046.776019	4520.223313	5584.579373
30	10492.71057	5740.011463	5286.30835
60	4911.0023	3706.112731	2145.397506
90	2821.504426	2805.972555	1591.957641
120	4601.954412	2804.126894	1588.654364
150	10056.36285	3892.686162	3024.390525

Table 3.4: A table showing chi squared values for 1.5 GeV results using GEANT4 physics models

1.5 GeV proton beam energy			
	Chi-square value		
Degree	BIC	BERT	INCL
15	1847.823402	1489.645127	1102.68291
30	4454.283639	26179.8059	8077.011483
60	2278.293197	1226.898247	1207.920095
90	3146.041641	1505.365961	1613.205006
120	2551.324855	2172.720691	1250.458012
150	1647.578631	1725.400387	810.3514905

Table 3.5. The degree of freedom of dataset used in the GEANT4 benchmarking simulation

0.5 GeV		
Degree of dataset in the simulation	Degree of freedom	P- value
15	24	<0.00001 (all three physics models)
30	26	
60	13	
90	13	
120	13	
150	19	
1.5 GeV		
Degree of dataset in the simulation	Degree of freedom	P- value
15	22	<0.00001 (all three physics models)
30	24	
60	17	
90	23	
120	23	
150	17	

The calculation of P-value was processed by using the calculator available in [22] and the chi-square distribution table available from [23]. Following from the calculation, all of the p-values were small. This result indicates that the GEANT4 models cannot describe the experimental result exactly. However, it can be seen that the chi-square values that the values from INCL were lower than other two physics model. Hence, the INCL describes the experimental results measurably better than other physics lists.

Despite the fact that the INCL model produced outstanding results, the computation time taken to generate the results was almost three times longer than for the other two models. In fact, the Bertini physics model was the fastest physics model in producing the results. Therefore, for conditions requiring high energy incident particles with a high number of particles involved, INCL would take an extremely long time to produce a useful results.

3.6 Conclusion on benchmarking process

The benchmarking study comparing GEANT4-simulated neutron spectra with experimental data collected by KEK showed good agreement between GEANT4 and the experimental results. The comparison between the results of GEANT4 and MCNP-4A also showed good agreement in the spectral form. This study proved the potential capability of the GEANT4 simulation code to produce reliable results in terms of neutron spectra and yields when applied to spallation-based neutron production. It was conclusive that the QGSP_INCLXX_HP physics model produced the most accurate outcome in predicting the experimental results. The QGSP_Bertini_HP physics model also produced fairly accurate results at higher angles. The QGSP_BIC_HP physics model was the least accurate model in predicting neutron spectra.

In terms of the time taken for generating results, the Bertini model produced results most quickly, followed by the BIC and then the INCL model. The INCL model took a very long time to complete the simulations. Therefore, in order to simulate neutron interaction in a condition such as spallation reaction coupled with ADSR, which would require a high energy incident beam and a high number of particles involved in the interaction, the most efficient model would be the Bertini physics model. It would be ineffective to choose the INCL model to run this type of study, due to time consumption and unaffordable computational resources.

3.7 Target size variation

An extensive study to determine the effect on neutron yield caused by varying the size of a lead-composed target was then performed. In order to facilitate this study, an incident proton beam was set to 0.5 GeV, which was the same energy as that used in the benchmarking study so that only the changes caused by variation in size could be monitored. This study gave useful information about natural lead targets with the composition derived from Geant4 program in relation to the MYRRHA studies

described in the next chapter. The MYRRHA facility uses 600 MeV proton beam energy, which is only 100 MeV higher than that used in this study. Their target material is also a variant of lead (i.e. lead bismuth eutectic).

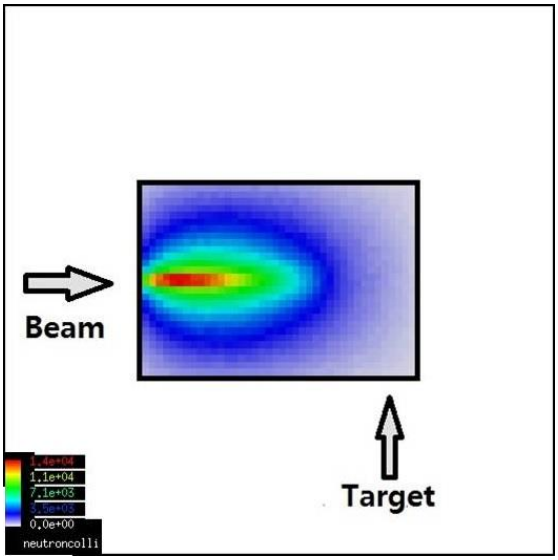

Figure 3.8: Neutron collision at 0.5 GeV proton beam energy at various lengths (30 to 60 cm)

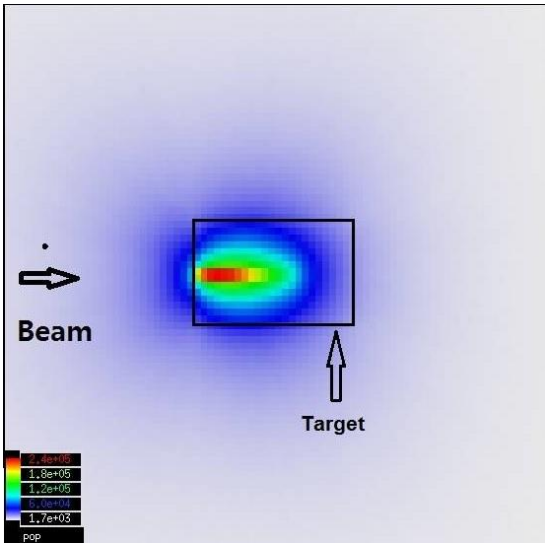

Figure 3.9: Population of neutron at 0.5 GeV proton beam energy at various length (30 to 60 cm)

Whilst the simulation was running, neutron collision and population were also monitored; Figure 3.8 and Figure 3.9 provide information about neutron interactions

within the target material, which in turn can facilitate the optimisation of the spallation target design.

Figure 3.8 shows that many interactions occur close to the area where the proton beam impacts the target and along the beam inside the target. This suggests that target shape can be optimised to maximise the rate of neutron production, as well as to avoid material stress from associated heat deposition. Figure 3.9 shows that the highest neutron density was along the proton beam from the primary neutrons produced from the interaction between incident protons and the nuclei of the target material.

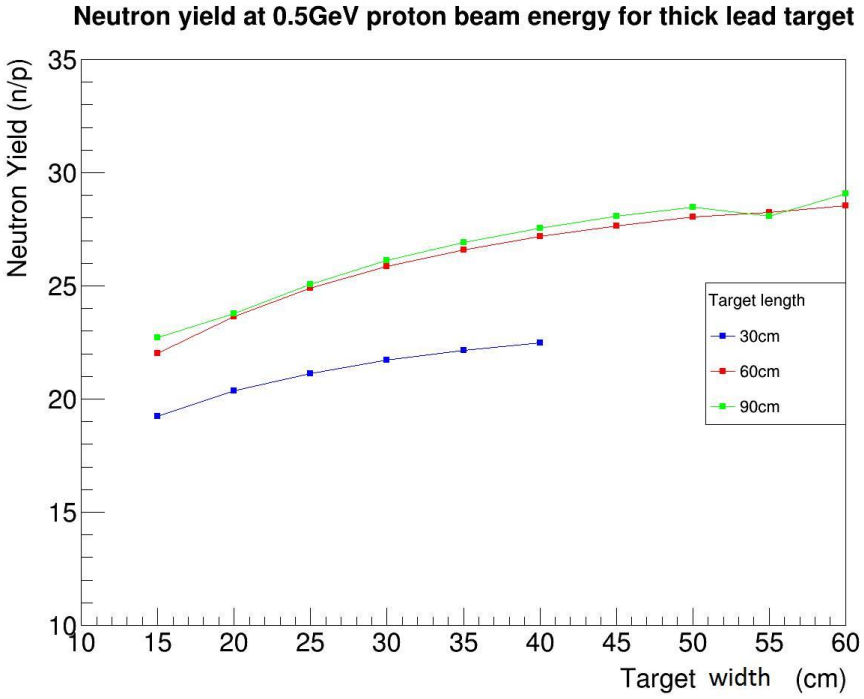

Figure 3.10: Neutron yields at 0.5 GeV proton beam energy for 30cm, 60cm and 90cm target lengths and various target widths

Figure 3.10 shows the effects when changes in the size of the target were applied. As the results in the figure demonstrate, the neutron yield increased with the target length. However, there was no real gain when the target length was increased from 60 cm to 90 cm. This means that there was no significant effect on neutron production for a target length greater than 60cm. Hence, it is suggested that the maximum rate of neutron

production in lead is at a cylindrical target length of 60 cm. Moreover, neutron production rate begins to plateau at target diameters beyond approximately 30-40cm. This finding is similar to the rate described in Figure 2.8 in chapter 2. For example, in Figure 2.8, the neutron yield at the lead target with the thickness of 20cm shows as 15 neutrons/proton at 0.6 GeV proton beam. In Figure 3.10, the neutron yield at 20 cm of target thickness is 20 neutrons/proton with the diameter of 30 cm. Although the neutron yields seem to be slightly different, Figure 2.8 does not consider the target thickness. Furthermore, Figure 2.10 also shows extensively that there is no significant increase in the neutron yield after a certain thickness which is similar to the result shown in Figure 3.10.

3.8 Neutron production from lead spallation target as a function of proton beam energy

3.8.1 Introduction

The spallation process plays an important role in Accelerator Driven Systems (ADS), which is to supply neutrons in which fission reactions take place inside the nuclear fuel. The ADS is equipped with a sub-critical assembly driven by an accelerator delivering a proton beam onto a target to produce neutrons by spallation [24]. The spallation process has been of specific interest in many other areas. It is also used in the transmutation of long-lived actinides from nuclear power plants and weapon-grade radioactive substances. The incident protons transfer their kinetic energy to the nucleons of the target through elastic collisions. Subsequently, a cascade of nucleon-nucleon collisions follows [25]. The nucleon collisions lead to the ejection of light particles such as protons, neutrons, alpha particles and pions. The further stage involves the excitation of the nucleus followed by de-excitation and the evaporation process. The evaporation process is known to release large amounts of low energy (a few MeV) neutrons. Hence, the yield of neutrons from the spallation process depends on the initial energy of the incident particle and the atomic number of the target nucleus.

In this study, simulations were carried out to determine the effect of proton beam energies on neutron production in a lead based spallation target, particularly for neutron yield and the angular trajectories of spalled neutrons.

3.8.2 GEANT4 computation detail

In the study of neutron spallation, a natural lead target was used. GEANT4 provides a set of hadronic physics models for energies of up to 10 GeV, both for the intranuclear cascade region and for modelling of evaporation, which makes the program suitable for this kind of research [3]. The Quark Gluon Secondary Particle Binary Inter-nuclear Cascade High Precision (QGSP_BIC_HP) physics list was chosen for the simulation of interactions between incident protons and the target nuclei. The BIC model passes the information to the pre-compound model to simulate nuclear de-excitation following these interactions. Previous validation studies in collaboration with GEANT4 [5] have shown that the QGSP_BIC_HP physics list can accurately describe the production of secondary particles in the interactions of incident protons and neutrons with nuclei. In this physics model, the interaction with the nucleus is treated as the interaction of an incident nucleon with the individual nucleons inside the target nucleus.

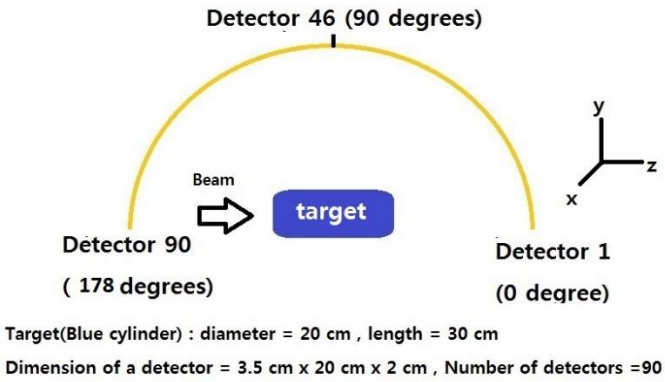

Figure 3.11: Schematic view of detectors and target placed in GEANT4 simulation

Detectors were placed around the target at various angles between 0 and 180 degrees with respect to the proton beam direction. A 30 cm long and 20 cm diameter natural lead

(Pb) target was simulated, and 90 detectors of 3.5 cm x 20 cm x 2 cm each were placed around the target. Each detector was positioned at an angle, with the angles increasing by 2 degrees from the z-axis. In this simulation, a proton energy range of 30 MeV to 1.1 GeV was used in 10 MeV increments. This enables a comparison between the neutron yields at each proton beam energy. The detectors were set to record the kinetic energies of the neutrons passing through the volume.

When the simulation was designed, it was set to run with the QGSP_BIC_HP physics list for GEANT4. This is the recommended physics for secondary particle production for incident particle beams of up to a few GeV [26], [27], which was the reason for its use in this study. Every simulation treats the mass and condition of particle interaction differently. It is understandable that section 3.5 suggests otherwise, but that study was conducted with the aim of benchmarking a known experiment. Hence, it is considered that the findings in section 3.5 do not significantly reflect those of this section.

3.8.3 Results

In the simulations, 5×10^6 protons were fired onto the lead spallation target in order to establish a reliable data set for neutron yields.

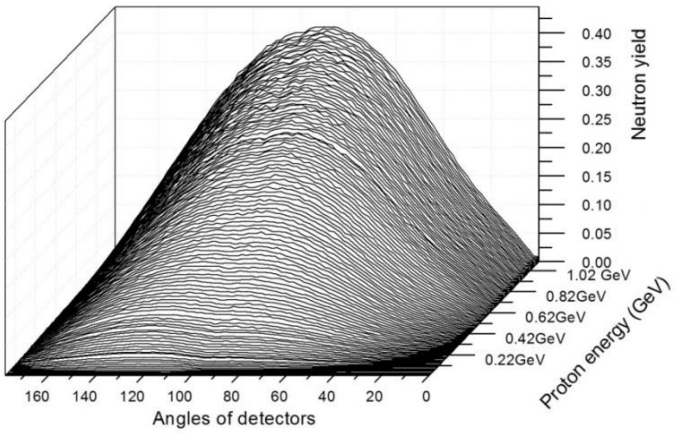

Figure 3.12: Neutron yields per proton beam at each detector angle

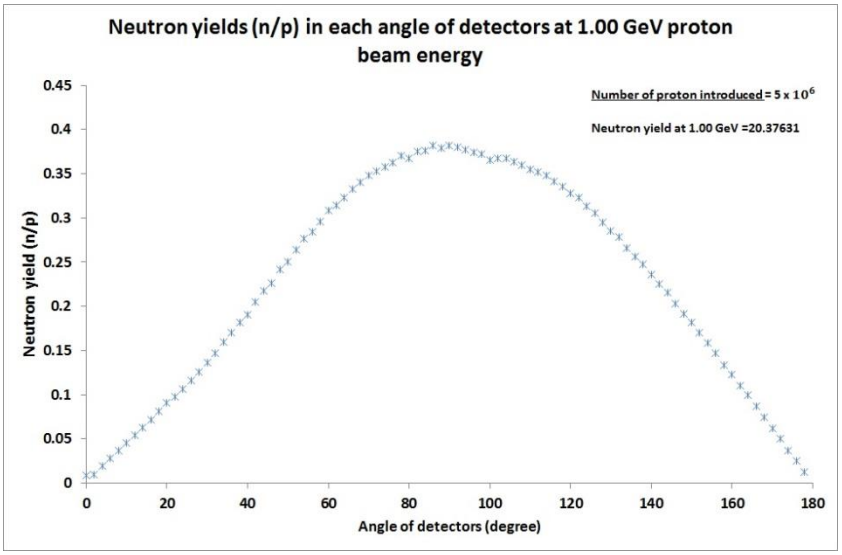

Figure 3.13: Neutron yield (neutrons per incident proton) at proton beam energy of 1000 MeV

The number of neutrons per proton at different proton beam energies was plotted for each 2 degree angle as shown in Figure 3.12. The figure shows that most of the neutrons escaped from the target at large angles and fewer neutrons were detected at angles closer to the forward direction (the beam travels, near detector 1). The neutron yield increased until it peaked at the detector which was at 90 degrees to the z-axis.

Figure 3.13 represents the neutron yield calculated for a 1000 MeV proton beam. The neutron yield data in Figure 3.13 were extracted for validation purposes from the dataset depicted in Figure 3.12. As stated earlier in this chapter, it was intended that a range of proton energies (30MeV - 1100MeV) would be simulated in this work. However, since analytical verification of the entire range of proton energies would be difficult, it was necessary to extract the result for one proton energy in the range to conduct the validation of data. In Seltborg's study [28], a total of 21 neutrons per proton were produced in the lead spallation target. Similarly, MYRRHA [29] states that "A lead target bombarded with 1 GeV proton can yield about 25 neutrons per incident proton". Thus, the simulation results in this work, of 20.4 neutrons per proton are consistent with the neutron yield values quoted by Seltborg and MYRRHA. Neutron yield is highly

dependent on target geometry and size, so it was considered likely that there would be some differences in the neutron yield value.

The angular distributions of neutrons of different energies, as recorded by each detector for 100, 300, 600 and 1000 MeV proton beams, are plotted in Figure 3.14 to Figure 3.17. Sets of results related to these proton beam energies were selected in order to observe the pattern of neutron energy spectra as the proton beam energy increased. As shown in the figures below, neutron energies up to their corresponding incident beam energy were selected, which enabled precise analysis of secondary and low energy neutrons. Each graph represents the number of neutrons by the distances from the centre. As the distance from the centre increased, the number of neutrons detected for each particular energy also increased. The dots are depicted in different colours to represent different neutron energy ranges.

Firstly, a comparison between Figure 3.14 and Figure 3.15 indicates that as the proton energy increased, the number of neutrons detected also increased. More specifically, the number of neutrons with low energy (i.e. neutrons with energy higher than 0.1 but below 1 MeV) rose significantly as the proton beam energy increased from 100 MeV to 300 MeV. The most distinctive feature of the results is that the high energy neutrons were emitted in a forward direction with respect to the direction of the beam travels (at between 0 and 90 degrees as represented in the figures). This means that these high energy neutrons were emitted at the back of the spallation target (opposite the place where the proton beam first impacted on the target). It is also noticeable that the high energy neutrons are close to the centre of the graph, which means that there were fewer neutrons in the high energy range compared to the number of lower energy neutrons. All these findings corroborate G.S Bauer's statement in [30], which refers to findings originally reported in [31] (see Figure 2.5 in Chapter 2). It was important to validate the results based on G.S Bauer's paper [30], because the original reference [31] indicates that the source was based on private communication. Hence, the GEANT4 simulations were able to confirm the claims in both [30] and [31].

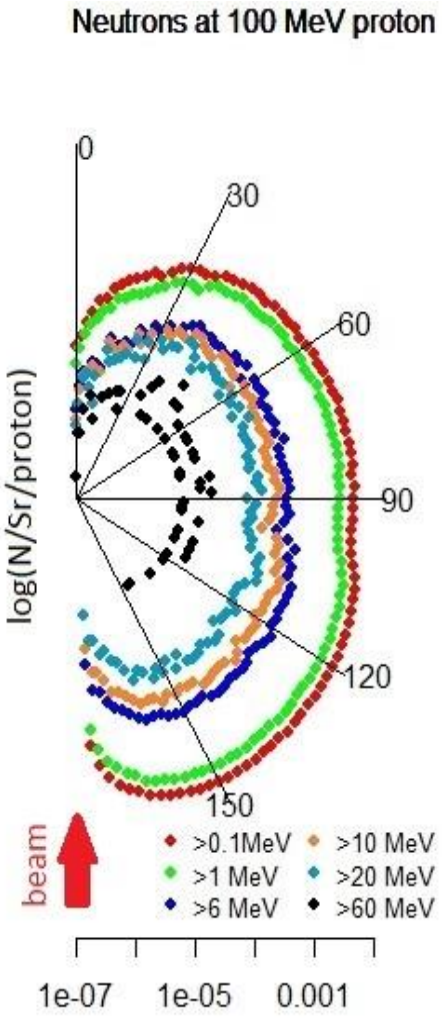

Figure 3.14: Angular distribution of neutrons of different energies at 100 MeV proton beam energy

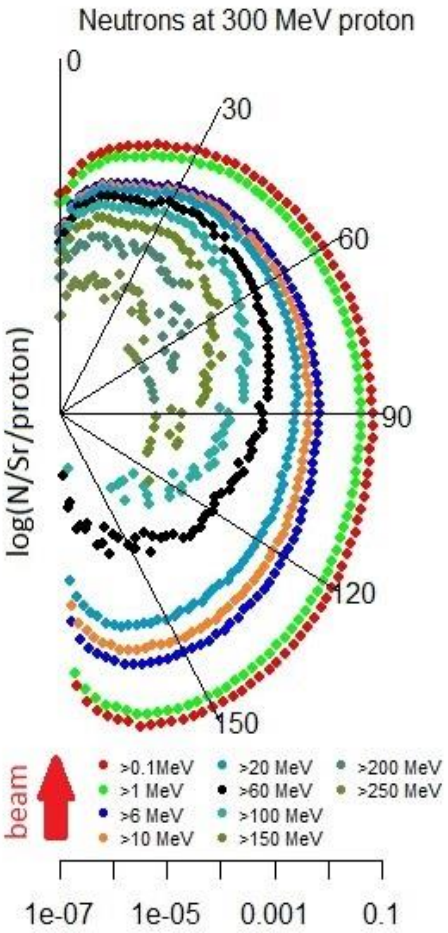

Figure 3.15: Angular distribution of neutrons of different energies at 300 MeV proton beam energy

This study continued by analysing the results for the angular distribution of neutrons at 600 MeV and 1000 MeV, which are shown in Figure 3.16 and Figure 3.17. As in the previous results for 100 MeV and 300 MeV proton beam energies, many neutrons produced from the spallation target were categorised as having neutron energies between 0 and 1 MeV, represented as red and green dots. These low energy neutrons are

approximately isotropic. It is also interesting to note that as the neutron energy increased, the angular distribution was concentrated in the area between 0 and 90 degrees, as shown in the figures. Hence, this study can confirm that the high energy neutrons were probably spalled in a forward direction, i.e. in the beam direction.

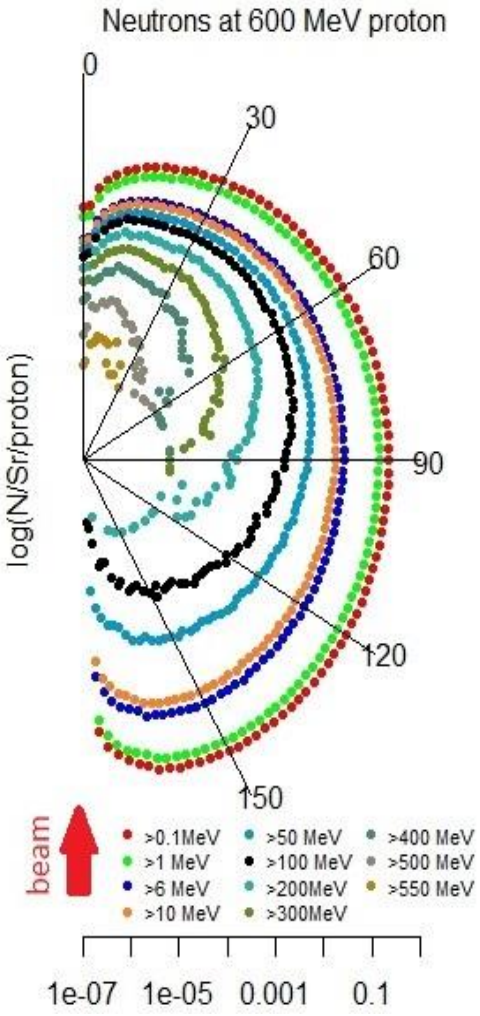

Figure 3.16: Angular distribution of neutrons of different energies at 600 MeV proton beam energy

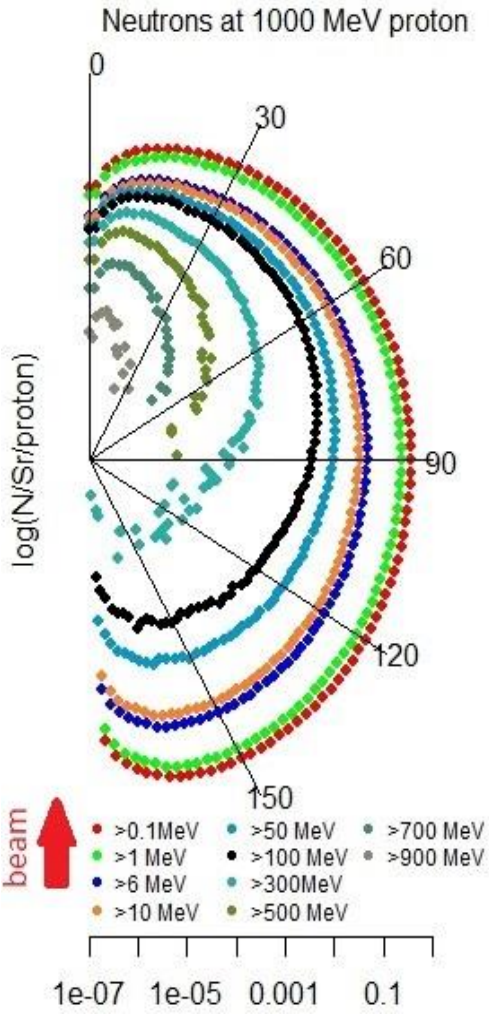

Figure 3.17: Angular distribution of neutrons of different energies at 1000 MeV proton beam energy

Overall, most neutrons had low energies (below 10 MeV). Furthermore, this result shows that a significant fraction of the neutrons were scattered in many directions, despite the fact that a 30 cm long target was used in this study. Figure 2.5 in Chapter 2

from G.S Bauer [30] validates the finding that highly energised neutrons were scattered in the same direction as the beam. According to Bauer, “The small fraction of cascade neutrons whose energy can reach up to that of the primary particles driving the reaction are emitted mainly in the forward hemisphere relative to the proton beam”. Close comparison shows that the results obtained from this simulation corroborate this statement.

3.8.4 Conclusion

This study was conducted with the purpose of finding the angular distribution of neutrons from a spallation target. It was also conducted as a benchmarking exercise in relation to G.S Bauer’s results on the angular distribution of neutrons. The simulation found that the total neutron yield from spallation increased with the proton beam energy. Most of the low energy neutrons between 0 and 10 MeV escaped at large angles from the target, while a significant fraction of neutrons at a high energy close to that of the incident beam were produced at between 0 and 90 degrees. A lower number of neutrons with high energy were also detected in the backward direction. A large number of neutrons had energies below 2 MeV. Furthermore, the number of neutrons detected near detector 46 (at 90º to the target) was significantly higher than elsewhere (see Figure 3.12 and Figure 3.13). These findings will aid the design of an efficient ADS spallation target in terms of improving moderation, shielding and activation.

3.9 Bibliography

[1] NIST Center of neutron research, “Neutron scattering lengths and cross sections for lead,” 2017. [Online]. Available: https://www.ncnr.nist.gov/resources/n-lengths/elements/pb.html. [Accessed: 23-Sep-2017].

[2] V. Zerkin and IAEA-NDS, “Multi-platform EXFOR-CINDA-ENDF,” 1999. [Online]. Available: https://www-nds.iaea.org/exfor/servlet/E4sMakeE4. [Accessed: 24-Oct-2016].

[3] Geant4 Collaboration, “a toolkit for the simulation of the passage of particles through matter, version geant4.9.6.p01,” 2012. [Online]. Available: http://geant4.web.cern.ch/geant4. [Accessed: 30-Jun-2014].

[4] L. S. Waters and et.al , “MCNPX user’s manual version 2.3.0” Los Alamos National Laboratory, Rep. LA-UR-02-2607, April, 2002.

[5] S. Meigo *et al.*, “Measurements of neutron spectra produced from a thick lead target bombarded with 0.5- and 1.5-GeV protons,” *Nucl. Instruments Methods Phys. Res. Sect. A Accel. Spectrometers, Detect. Assoc. Equip.*, vol. 431, no. 3, pp. 521–530, Jul. 1999.

[6] C. Bungau, R. Cywinski, and R. Barlow, “Neutron spallation studies for an accelerator driven subcritical reactor,” in *Particle Accelerator Conference*, Vancouver, Canada, May 4-8 2009.

[7] D. H. Wright, “An Overview of Geant4 Hadronic Physics Improvements,” in *Joint International Conference on Supercomputing in Nuclear Applications and*

Monte Carlo (SNA + MC2010), Hitotsubashi Memorial Hall, Tokyo, Japan, October 17-21, 2010

[8] J. Sanchez, "Simulation of the SOFIA experiment at GSI for fission studies in inverse kinematics," Ph.D dissertation, Universidad de Santiago de Compostela, 2012.

[9] J. Yarba, "Recent Developments and Validation of Geant4 Hadronic Physics," *J. Phys. Conf. Ser.*, vol. 396, no. 2, pp. 0–11, Dec. 2012.

[10] J. Apostolakis, *et.al.*, "Geant4 simulation of nuclear spallation reactions," *InProc. International Topical Meeting on Nuclear Research Applications and Utilization of Accelerators. Satellite Meeting on Spallation Reactions* , May 2009, pp. 4-8.

[11] Y. E. Titarenko *et al.*, "Experimental and Computer Simulation Study of Radionuclide Production in Heavy Materials Irradiated by Intermediate Energy Protons,",Los Alamos National Laboratory, Rep. LA-UR-99-4489, 1999.[Online] Available: arXiv:nucl-ex/9908012. [Accessed: 30-10-2016]

[12] R. Serber, "Nuclear Reactions at High Energies," *Phys. Rev.*, vol. 72, no. 11, pp. 1114–1115, Dec. 1947.

[13] A. Heikkinen, N. Stepanov, and J. P. Wellisch, "Bertini intra-nuclear cascade implementation in Geant4," *Comput. High Energy Nucl. Phys.*, La Jolla, California, March 24-28, 2003, pp. 24–28. [Online] Available: arXiv preprint nucl-th/0306008 [Accessed 30-09-2016]

[14] M. P. Guthrie, R. G. Alsmiller and H. W. Bertini, Nucl. Instr. Meth, 66, 1968, 29

[15] J. J. Griffin, "Statistical Model of Intermediate Structure.," *Phys. Rev. Lett.*, vol. 19, no. 1, p. 57, Jul. 1967.

[16] J. Yarba, “Recent developments and validation of Geant4 hadronic physics,” *J. Phys. Conf. Ser.*, vol. 396, no. PART 2, pp. 0–11, 2012.

[17] S. Agostinelli, J. Allison, K. Amako, and Et.al, “GEANT4 - A simulation toolkit,” *Nucl. Instruments Methods Phys. Res. Sect. A Accel. Spectrometers, Detect. Assoc. Equip.*, vol. 506, no. 3, pp. 250–303, 2003.

[18] H. Nifenecker, O. Meplan, and S. David, *Accelerator Driven Subcritical Reactors (Series in Fundamental and Applied Nuclear Physics)*. London, IOP Publishing Ltd, 2003

[19] D. C. Howell, “Chi-Square Test: Analysis of Contingency Tables,” in *International Encyclopedia of Statistical Science*, Berlin, Heidelberg: Springer Berlin Heidelberg, 2011, pp. 250–252.

[20] R. Barlow, “Private Conversation,” 2016.

[21] R. L. Wasserstein and N. A. Lazar, “The ASA’s Statement on p-Values: Context, Process, and Purpose,” *Am. Stat.*, vol. 70, no. 2, pp. 129–133, Nov. 2016.

[22] Social Science Statistics, “P value from Chi-square calculator.” [Online]. Available: http://www.socscistatistics.com/pvalues/chidistribution.aspx. [Accessed: 13-Oct-2017].

[23] MEDCALC software, “Values of the Chi-squared distribution.” [Online]. Available: https://www.medcalc.org/manual/chi-square-table.php. [Accessed: 13-Oct-2017].

[24] S. Mongelli and J. Maiorino, “Spallation physics and the ADS target design,” *Brazilian J. Phys.*, vol. 35, no. 3B, pp. 894–897, 2005.

[25] C. Bungau, R. Cywinski, and R. Barlow, “Neutron Spallation Studies in Thick Lead Targets for an Accelerator Driven Subcritical Reactor,” *Nucl. Instruments Methods Phys. Res. Sect. A Accel. Spectrometers, Detect. Assoc. Equip.*, 2013.

[26] J. Allison, K. Amako, J. Apostolakis, and et.al, “Geant4 developments and applications,” *IEEE Trans. Nucl. Sci.*, vol. 53, no. 1, pp. 270–278, 2006.

[27] Geant4 Collaboration, “Reference Physics Lists.” [Online]. Available: http://geant4.cern.ch/support/proc_mod_catalog/physics_lists/referencePL.shtml. [Accessed: 20-Apr-2016].

[28] P. Seltborg, “External Source Effects and Neutronics in Accelerator-driven Systems”, Licentiate dissertation, Royal Institute of Technology Stockholm, 2003.

[29] SCK•CEN, “Applications catalogue of MYRRHA.” [Online]. Available: http://myrrha.sckcen.be/en/MYRRHA/Applications. [Accessed: 21-Apr-2016]

[30] G. S. Bauer, “Physics and technology of spallation neutron sources,” *Nucl. Instruments Methods Phys. Res. Sect. A Accel. Spectrometers, Detect. Assoc. Equip.*, vol. 463, no. 3, pp. 505–543, May 2001.

[31] V. . Yurevitch, “Review and analysis of the experimental data on neutron production in lead targets obtained at p/d-beam of the dubna synchrophasotron during 1986-1992;preprint.”

Chapter 4. A Comparison of Lead and Lead Bismuth Spallation Targets

4.1 Introduction

During the 1950s, according to [1], lead and Lead-Bismuth Eutectic (LBE) were investigated for their potential to meet the requirements for use as a fast reactor coolant. Such a coolant is required to provide effective heat transfer with no significant thermalisation of the neutron spectrum. The pure composition of lead has a high melting point (327 ºC), but this temperature reduces to 127 ºC for LBE. This unique feature enables the material to transfer heat inside the reactor efficiently without the risk of corrosion of the metal. The benefit of the lower melting point is that LBE provides a lower operational temperature range, which improves safety by lowering the corrosion rate [1]. This feature, together with that of being a heavy metal, makes LBE an attractive material for a spallation target. Many facilities have studied LBE as their target material. For example, both MEGAPIE [2] at PSI[1] and HYPER [3] at KAERI[2] have used LBE as a coolant, and MYRRHA[3] proposes to use LBE as both coolant and spallation target [4]. MYRRHA is a research reactor still under development by SCKCEN in Belgium. This chapter focuses upon a comparison of neutron production with LBE and pure lead as spallation targets. In order to facilitate this study, the GEANT4 simulation geometry was set up as described in Chapter 3. The incident beam energies considered were 0.6 and 1.0 GeV. The 0.6 GeV proton beam energy was chosen as this is MYRRHA's target proton beam energy [5], and hence was considered to be reasonable for testing both the lead and LBE targets and the beam energy in

[1] PSI stands for Paul Scherrer Institut

[2] KAERI stands for Korean Atomic Energy Research Institute

[3] MYRRHA stands for multipurpose Hybrid Research Reactor for high-tech applications

relation to neutron production. A 1.0 GeV proton beam energy was also chosen as this energy is considered the optimum choice for a proton beam in Accelerator-Driven Sub-critical Reactor (ADSR) applications [6]. In order to achieve optimal operation in an ADSR, it is important to balance the beam power and the rate of neutron production in the spallation reaction with the fuel core of the ADSR. A key report [6] suggests that a 1.0 GeV proton beam with 20 mA beam current would be the most suitable parameters for an ADSR to achieve its maximum performance rate for energy production.

In this study, the standard composition for lead-bismuth eutectic was used [1], [7]which is 55.5% bismuth and 44.5 % lead. In comparison to pure lead, lead-bismuth eutectic has a lower melting point (125 ºC) but a higher boiling point (1670 ºC). These properties make the material suitable for use as a coolant in a reactor core where the thermal stress is high. The composition for natural lead was used which is 52.4% ^{208}Pb, 24.1% ^{206}Pb, 22.1% ^{207}Pb and 1.4 % ^{204}Pb [8].

In this study, bismuth is also used as the one of a source for neutron production through spallation process. Natural Bismuth which was used in this simulation is pure ^{209}Bi, and cross sections are shown in Table 4.1.

Table 4.1: the cross section of ^{209}Bi taken from [8], [9]

	Thermal cross section (barn)	Fast cross section (barn)
Elastic	9.390	2.804
Inelastic	0.0342	2.565
Capture	0.0342	0.000756

This finding shows that bismuth is likely to undergo elastic scattering reaction for a similar range of neutron energy to ^{207}Pb's cross section (see Chapter 3). In addition, it is noticeable that the inelastic scattering is higher in the fast neutron cross-section than in the thermal neutron cross-section. This indicates that bismuth can also be utilised as a source of neutron production for spallation purposes.

4.2 GEANT4 simulation environment for lead and LBE target station

In order to establish the appropriate conditions for the study of neutron spectra created from spallation reactions in lead and LBE, the same simulation environment was set up as that used in the benchmarking process, described in Chapter 3.

To analyse the large amounts of data produced from GEANT4 efficiently, the QGSP_BERTINI_HP physics list was chosen based on the findings in Chapter 3. The previous benchmarking results had indicated that the Bertini model can simulate neutron spectra accurately from a spallation reaction of a reasonable duration. It was considered that the method of choosing multiple physics lists would not be suitable at this time, since the quantity of data produced by GEANT4 would be too much to analyse within a single project. Moreover, the benchmarking process described in Chapter 3 had shown that there was no significant discrepancy in the accuracy of results produced by other physics lists (QGSP_INCLXX_HP and QGSP_BIC_HP).

4.3 Results

The following graphs represent the results of the numerical simulations performed using Geant4 for 0.6 and 1.0 GeV proton beams onto LBE and lead, where the neutron energy spectra for both incident beam energies are shown for 0-1000 MeV and 0-1 MeV.

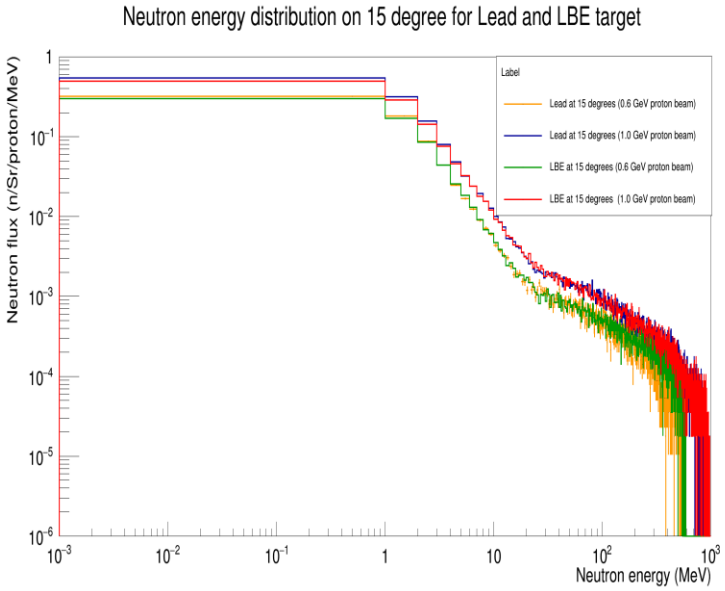

Figure 4.1: Neutron energy spectra for lead and LBE at 15 degrees (0-1000 MeV neutron energies)

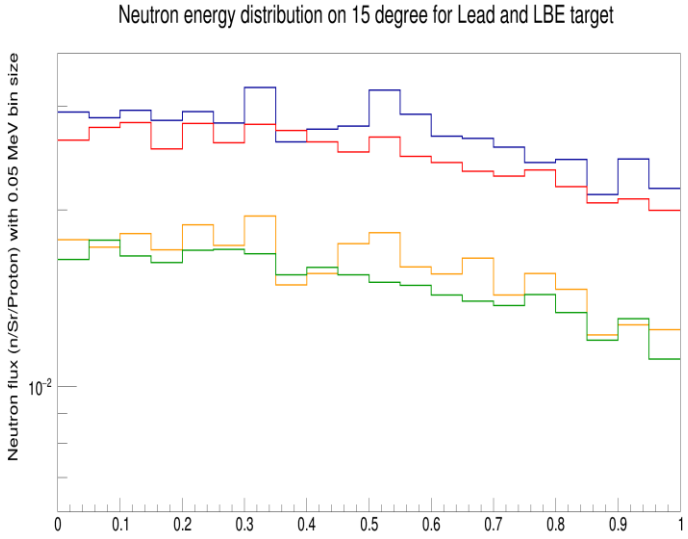

Figure 4.2: Neutron energy spectra for lead and LBE at 15 degrees (0-1 MeV neutron energies)

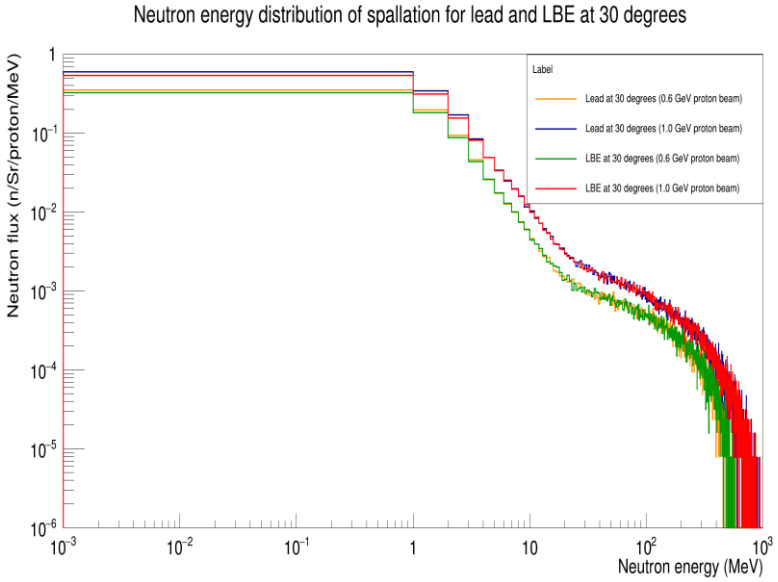

Figure 4.3: Neutron energy spectra for lead and LBE at 30 degrees (0-1000 MeV neutron energies)

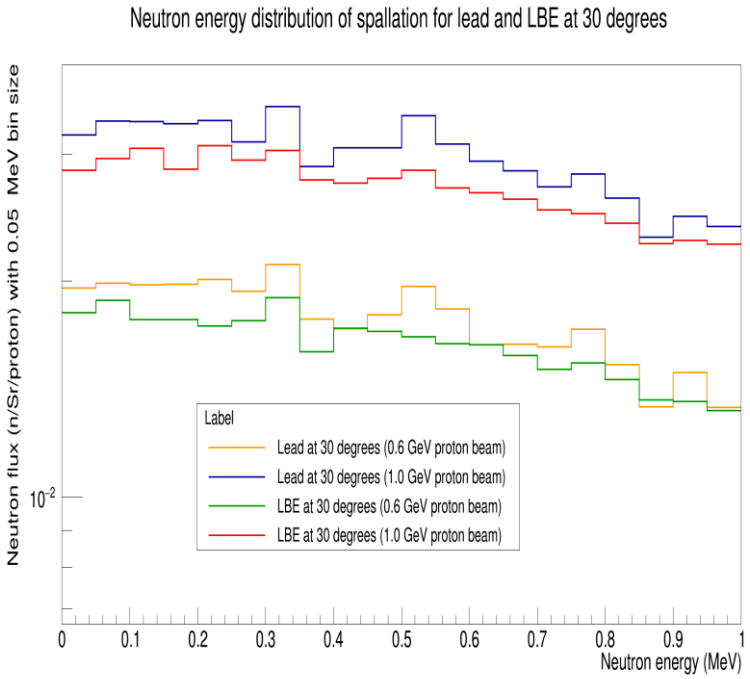

Figure 4.4: Neutron energy spectra for lead and LBE at 15 degrees (0-1 MeV neutron energies)

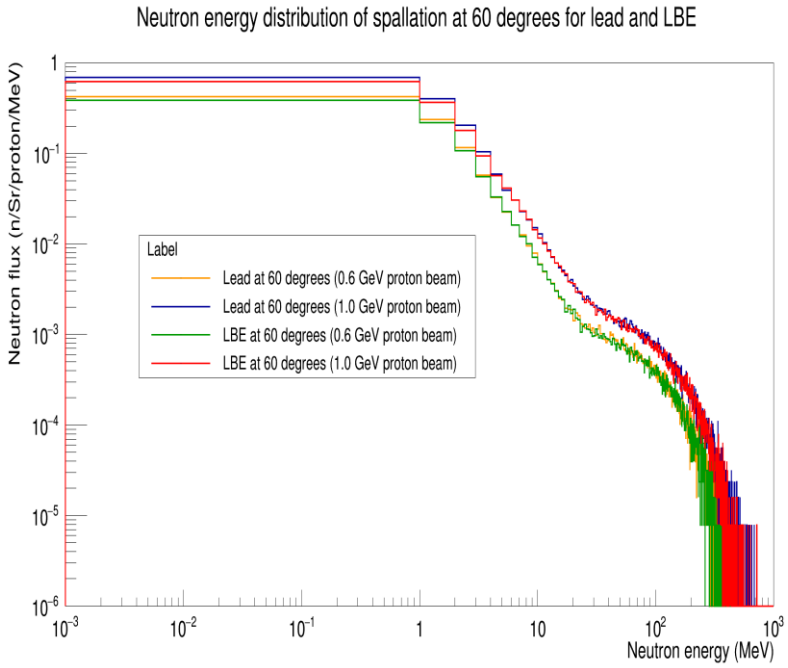

Figure 4.5: Neutron energy spectra for lead and LBE at 60 degrees (0-1000 MeV neutron energies)

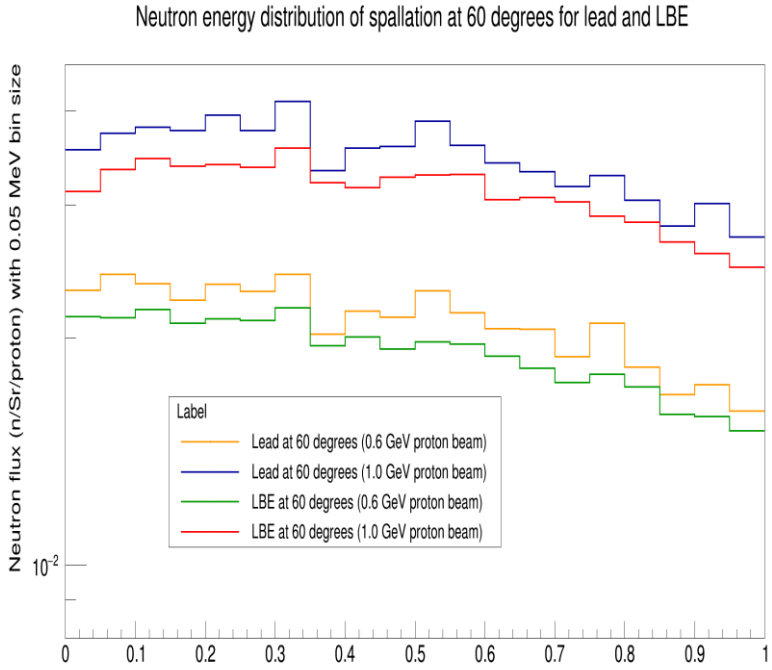

Figure 4.6: Neutron energy spectra for lead and LBE at 60 degrees (0-1 MeV neutron energies)

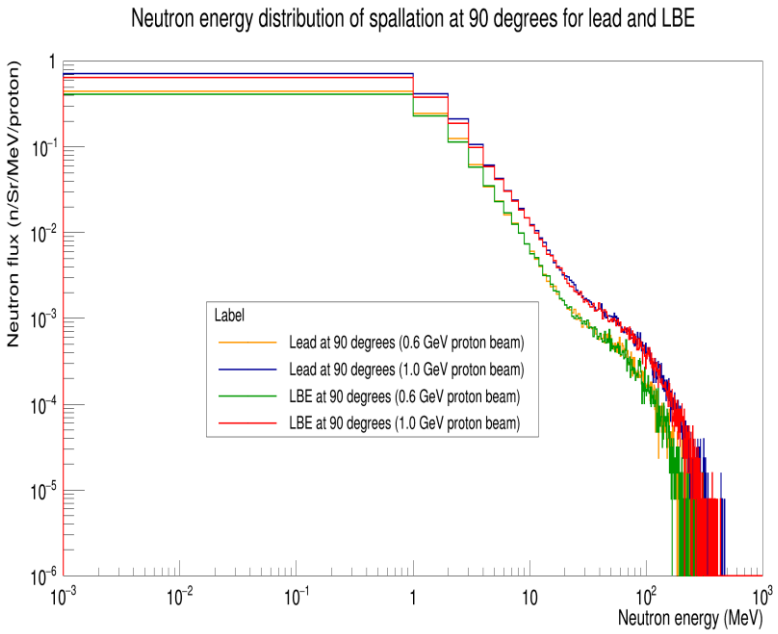

Figure 4.7: Neutron energy spectra for lead and LBE at 90 degrees (0-1000 MeV neutron energies)

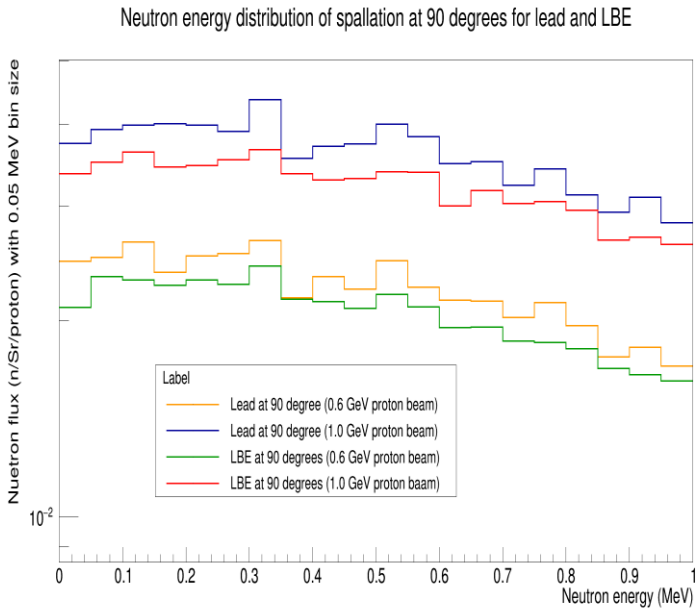

Figure 4.8: Neutron energy spectra for lead and LBE at 90 degrees (0-1 MeV neutron energies)

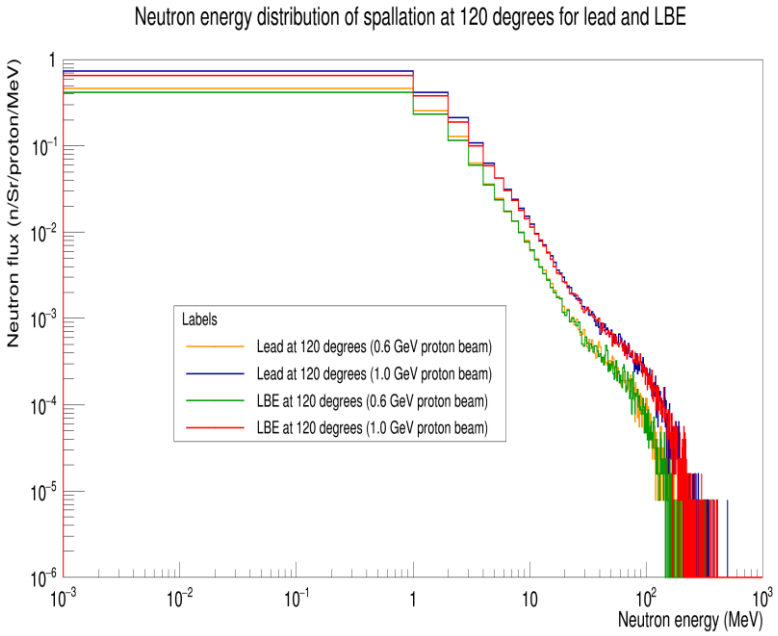

Figure 4.9: Neutron energy spectra for lead and LBE at 120 degrees (0-1000 MeV neutron energies)

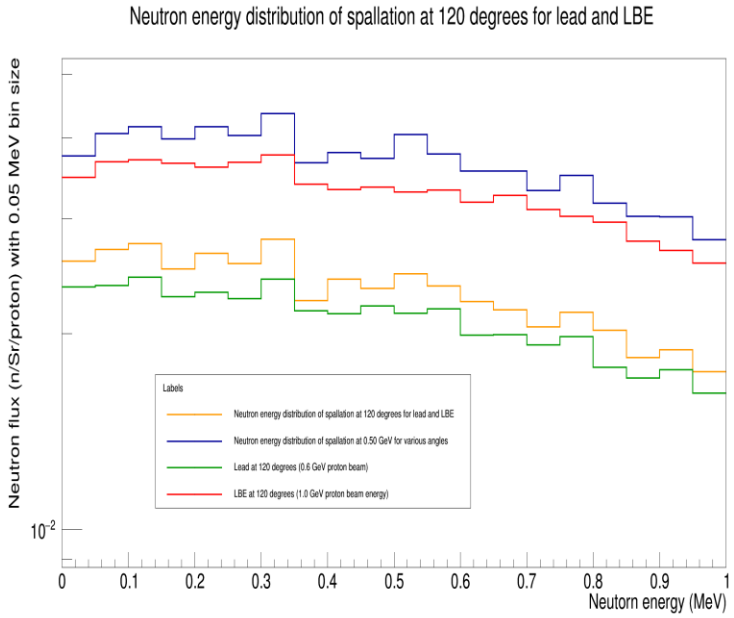

Figure 4.10: Neutron energy spectra for lead and LBE at 120 degrees (0-1 MeV neutron energies)

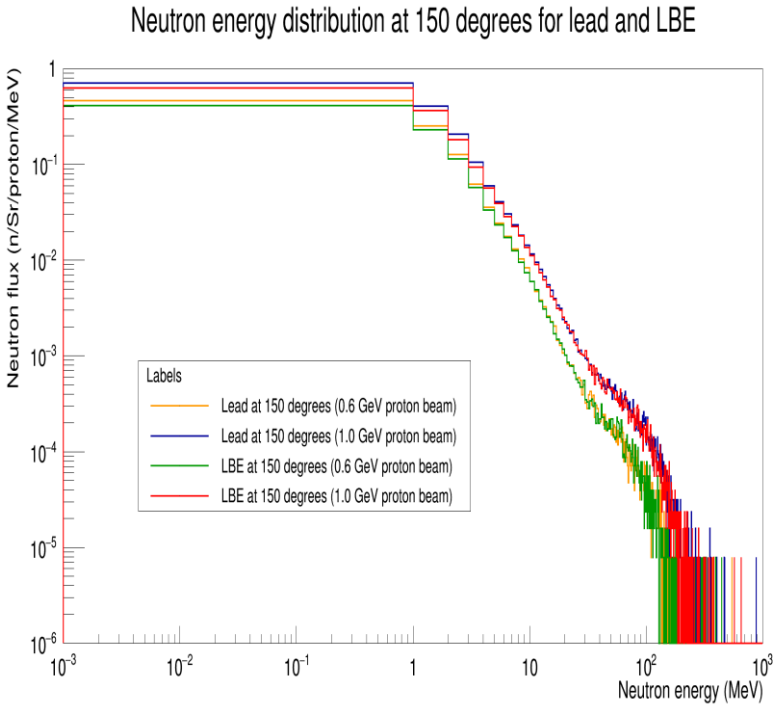

Figure 4.11: Neutron energy spectra for lead and LBE at 150 degrees (0-1000 MeV neutron energies)

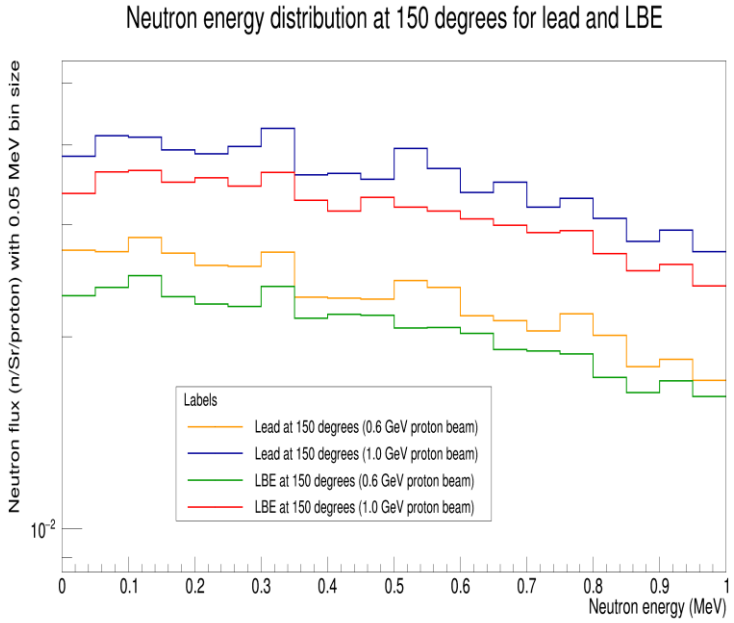

Figure 4.12: Neutron energy spectra for lead and LBE at 150 degrees (0-1 MeV neutron energies)

Overall, the comparison between neutron flux in lead and LBE targets showed that there is little difference between lead and lead-bismuth eutectic in relation to neutron production. The results in Figure 4.1 to Figure 4.12 indicate that pure lead provides higher neutron fluxes at neutron energies below 10 MeV. However, the difference in neutron fluxes between the two materials is under 1 order of the scale of neutron flux. At the higher neutron energies, the neutron fluxes for LBE were perhaps very slightly greater than those for lead (see Figure 4.1, Figure 4.3, Figure 4.5, Figure 4.7, Figure 4.9 and Figure 4.11) However, it is noted that the accuracy of the data is very limited considering the fact that there were fewer neutrons present in the high energy neutron spectrum. This finding is likely to be due to the relative atomic masses of bismuth and lead. Bismuth is approximately one mass unit heavier than lead. Since neutron production by spallation is related to atomic mass, and these are so similar, it can be considered that the rate of neutron production should also be similar. The trend of the neutron spectra observed in the full spectrum (0 – 1000 MeV neutron energies) followed that in the low energy neutron spectrum between 0 and 1 MeV (see Figure 4.2, Figure 4.4, Figure 4.6, Figure 4.8, Figure 4.10 and Figure 4.12). The low energy neutron spectrum data indicate that the neutron spectra for lead are a little higher than for LBE at low energies.

4.4 Conclusion

From the results described above, it is clear that the findings of the simulation show some difference between lead and LBE in terms of neutron production. The comparison between neutron fluxes in lead and LBE also showed that lead produced a higher number of neutrons than LBE in the range between 0 and 10 MeV neutron energies, which is likely to be related to the cross sections of the target materials on neutron capture. It may be due to the fact that lead has a higher absorption cross section than bismuth. The difference in neutron flux (neutrons/incident proton) was less than 1 order of magnitude. It may be concluded on the basis of these findings that mixing bismuth with lead has little effect in terms of varying neutron production at the energies in this study. The neutron spectra for both 0.6 and 1.0 GeV proton beams show that the highest

number of neutrons from both targets was produced at a neutron energy range between 0 and 1 MeV. The graph data show that at higher neutron energy there was a lack of neutrons present in the energy range.

It may be concluded from this study that LBE can be as effective a material as lead in terms of neutron production. However, mixing bismuth with lead provides the additional benefit of a lower melting point while the heavy metal property remains the same. Furthermore, this study has confirmed that there is no indication that the mixture of lead and bismuth will change significantly in the neutron spectra or the rate of neutrons produced from a spallation target. The neutron absorption cross section (1MeV) for lead is reported as 6.001mb, while that for LBE is 1.492 mb [10].

Since LBE has only 44.5% lead and the rest is composed of bismuth, the chance of neutrons being captured inside the target may also differ compared with the pure Pb-207 target tested in this study. This information correlates with the results showing neutron flux for neutron energies between 0 and 1 MeV, where the pure lead target produced a higher rate of neutrons than LBE.

4.5 Bibliography

[1] Nuclear Energy Agency and OECD, “Handbook on Lead-bismuth Eutectic Alloy and Lead Properties, Materials Compatibility, Thermal -hydraulics and Technologies,” OECD/NEA Nuclear Science Committee, Rep. NEA. No 7258, 2015.

[2] W. Wagner, F. Gröschel, K. Thomsen, and H. Heyck, “MEGAPIE at SINQ – The first liquid metal target driven by a megawatt class proton beam,” *J. Nucl. Mater.*, vol. 377, no. 1, pp. 12–16, Jun. 2008.

[3] W. S. Park, U. Shin, S.-J. Han, T. Y. Song, B. H. Choi, and C. K. Park, “HYPER (Hybrid Power Extraction Reactor): A system for clean nuclear energy,” *Nucl.*

Eng. Des., vol. 199, no. 1–2, pp. 155–165, Jun. 2000.

[4] P. Baeten, M. Schyns, R. Fernandez, and et.al, "MYRRHA : A multi-purpose nuclear research facility," *EPJ Web Conf.*, vol. 79, no. 3001, Nov. 2014.

[5] P. Baeten, "MYRRHA Project - status update MYRRHA - Accelerator Driven System," in *ESNII Conference*, 2012, Brussel, June 25, 2012. [Online] Available: http://www.gedeon.prd.fr/ATELIERS/Juillet_2012/exposes/6_juillet/3_GEDEPEON_MYRRHA_vandenende.pdf [Accessed: 30-09-2016]

[6] R. Cywinski, *et.al*., "Towards an Alternative Nuclear Future," The Thorium Energy Amplifier Association (ThorEA), 2009.

[7] V. Sobolev *et.al.*, "Chapter 2: Thermophysical and Electronic Properties, Handbook on lead-bismuth eutectic alloy and lead properties material compatibility, thermal hydraulic and technologies,", OECD/NEA Nuclear Science Committee, Rep. NEA. No 6195, 2007.

[8] JAEA Nuclear data center, "Cross Section Table (83-Bi-207)," 2018. [Online]. Available: http://wwwndc.jaea.go.jp/cgi-bin/Tab80WWW.cgi?lib=J40&iso=Bi209. [Accessed: 21-Feb-2018].

[9] V. Zerkin and IAEA-NDS, "Multi-platform EXFOR-CINDA-ENDF," 1999. [Online]. Available: https://www-nds.iaea.org/exfor/servlet/E4sMakeE4. [Accessed: 24-Oct-2016].

[10] N. E. Todreas, *et.al.*, "Medium-power lead-alloy reactors: Missions for this reactor technology," *Nucl. Technol.*, vol. 147, no. 3, pp. 305–320, 2004.

Chapter 5. A study of Neutronic Behaviours involved with Thorium Fuelled ADSR with MYRRHA Configuration

5.1 Introduction

The idea of an Accelerator-Driven System (ADS) with subcritical core operation was first proposed in the early 1990s. While the primary operational aim was focused on developing an advanced nuclear fuel cycle, some institutes considered the ADS concept for transmutation technology [1]. For example, there were some movements from the Department of Energy (DoE) in the USA to establish a roadmap for developing accelerator transmutation of waste (ATW) technology [2].

The Rubbia group has studied the use of ADS in thorium-fuelled reactors [3] and Aker/Jacobs' ADTR design has been considered for the use of power generation [4]. Studies of ADS have connected the following characteristics of thorium fuel with boosting the net consumption of minor actinides [5]:

- The use of fast neutrons due to the relative size of the (n,gamma) and (n,f) cross sections above ~ 1 MeV; at this point, neutrons are more likely to cause the MA nucleus to undergo further fission, whereas at lower energies, it is far more likely to be absorbed.
- Use of thorium rather than uranium; the exact number of fertile to fissile fuel components required depends on the cross sections and decay rates involved. However, basically, ^{232}Th has six fewer nucleons than ^{238}U, and the chance of a nucleus absorbing enough neutrons to produce an isotope like ^{241}Am is much smaller.

Noted from [6], demonstration of the technology was first announced by the Belgian government with their proposed construction of MYRRHA at the Belgian nuclear research centre (SCKCEN). MYRRHA is the first test reactor with specifications designed according to the ADS concept. The MYRRHA project was started in 1998, aiming at the design, construction and operation of an accelerator-driven, lead-bismuth-cooled subcritical or critical fast neutron reactor (LFR). MYRRHA was intended to be a flexible fast neutron irradiation facility, able to work in either subcritical or critical mode. Substantial investment has been made into the creation of a Sodium-cooled Fast Reactor (SFR), due to the limited stock of bismuth globally. However, the high chemical reactivity of sodium causes an SFR to be more difficult to operate. Hence, the choice of using LFR operation would be more suitable for MYRRHA. Currently, MYRRHA's reactor design is running with plutonium-based MOX fuel; however, ADS technology is able to operate with thorium.

This study aims to understand the effect on neutronic behaviour when thorium is introduced as a main source of fuel in nuclear core compartments. The MYRRHA facility houses a nuclear core filled with plutonium based MOX fuel (low-enriched uranium, 20% or less)[7], [8], with a uranium-plutonium fuel cycle [10]. Thorium is a fertile material which uses a ^{232}Th to ^{233}U fuel cycle. ^{232}Th has the cross section of 7.4 barns for the thermal neutron absorption, 0 for fission and inelastic scattering and 13.0 barns for elastic scattering [7], [8]. These values show that thorium has the interaction mostly in elastic scattering and neutron capture process. ^{232}Th has three times higher in neutron capture cross section than ^{238}U (i.e. 2.7 barns). This indicates that thorium has a higher conversion to fissile material (i.e. ^{233}U for ^{232}Th) than ^{238}U to ^{239}Pu [7].

It is assumed that there will be many characteristic differences in neutron production compared with the original uranium-plutonium fuel cycle applied in MYRRHA. Under this assumption, various aspects of MYRRHA were carefully studied using Geant4. The physics list of GEANT4 is QGSP_BERT_HP, which is regarded as the optimal choice for spallation studies, as described in Chapter 3.

Following previous studies which used a baseline core structure derived from the core assembly schematics provided in [9], the components of the assemblies described were configured to fit thorium as a main source of fuel. This study intended to monitor neutron emission outside the core structure while different materials composed the inner and outer layers of the core assembly. The study would then investigate the propagation of neutrons as they passed through the core structure. Hence, a simple structure consisting of multiple layers of fuel and shielding materials was created, the size of each layer being the same as the thickness of the core assembly used in MYRRHA. The structure was designed as an object consisting of simple cylindrical-shaped layers. This feature was tailored to mimic the structural components of the original core structure of MYRRHA. It was also designed to enable the Geant4 simulation to monitor neutrons each time they passed through each layer.

5.2 Introduction to the MYRRHA facility

The development of the MYRRHA project was initiated by SCKCEN, the Belgian Nuclear Research Centre. The project set out to create a multipurpose neutron source which was designed to encourage R & D applications based on the Accelerator-Driven System (ADS). According to [4],[5], MYRRHA's first aim was to demonstrate the feasibility of ADS technology and to show that this could fit into the European strategy for nuclear waste transmutation.

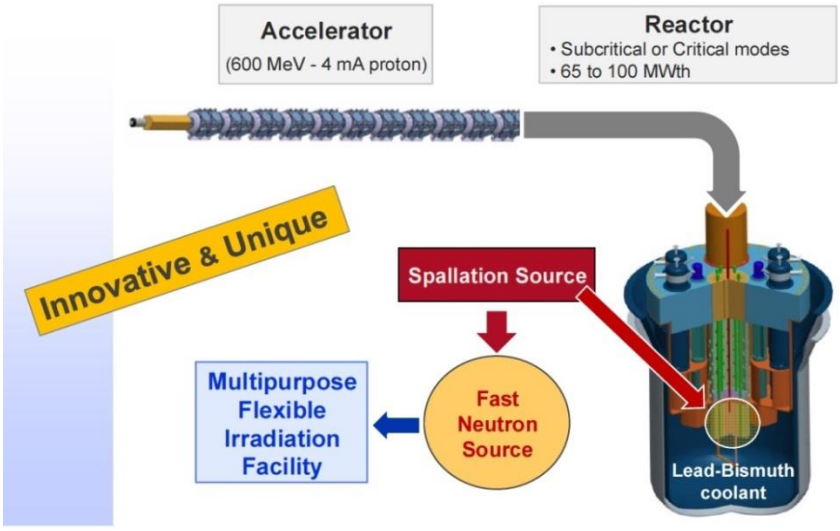

Figure 5.1: Overview of MYRRHA facility, taken from [11]

The design of MYRRHA consists of three main areas (see Figure 5.1). These areas comprise a proton accelerator, which produces an incident proton beam to the target; a spallation target area, where fast neutrons are created for supply to the core structure; and the fuel core structure, where the fission reactions take place for both energy production and transmutation of minor actinides and other wastes.

Firstly, the proton accelerator is driven by a linear accelerator, which has 600 MeV and a beam current of 4 mA in CW mode. The accelerator consists of a double injector as part of a 'fault tolerant' scheme [1]. This feature increases the reliability of the accelerator beam delivery system by ultimately acting as a redundancy in the entire operation within the MYRRHA facility.

Secondly, the spallation target area is composed of liquefied Lead Bismuth Eutectic (LBE), which is poured into a reservoir descending to the central area core. As previously mentioned, MYRRHA operates in both subcritical and critical mode. In subcritical mode, a spallation reaction will take place where the proton beam is guided into contact with the target material. The guideline, which is also referred to as a beam tube, is installed as part of a windowless or windowed design. The placement of the spallation area is conceived to ensure optimal conditions for spallation and minimal

energy loss, taking into consideration difficulties in engineering. The LBE material circulates from the core region to the reservoir, where the material is used as a primary coolant. The choice of LBE as coolant offers a lower inlet operating temperature, which decreases the risk of corrosion [3],[4]. By combining this with a passive shut-down system and adaptation technique, the target area can deliver high fast-flux intensity [9].

Finally, the reactor core structure is situated in an area surrounding the spallation target. The reactor core system was originally named MYRRHA-FASTEF. The primary core system was designed to operate with a maximum core power of 100 MWth. Due to the closed system of the primary neutron source (i.e. spallation source) and its surrounding areas, all reactor components are configured to be accessed by the remote on-site handling system [9]. This system controls component replacement, inspection and handling of the reactor core.

The reactor core consists of inner and outer vessels to ensure the safety and functionality of the reactor. While the reactor core vessel stays inside as part of the primary system, the outer vessel acts as containment for any possible leaks or breaks, as well as improving the capability of the vessel's air cooling system (see Figure 5.2) [12].

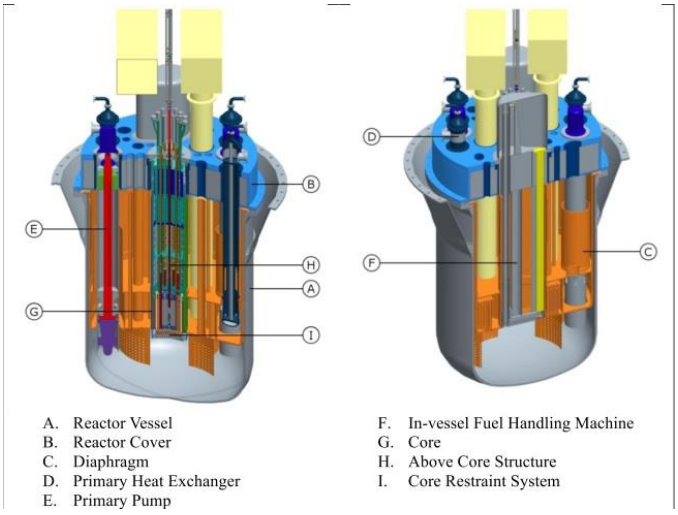

Figure 5.2: Section of MYRRHA-FASTEF core, taken from [12]

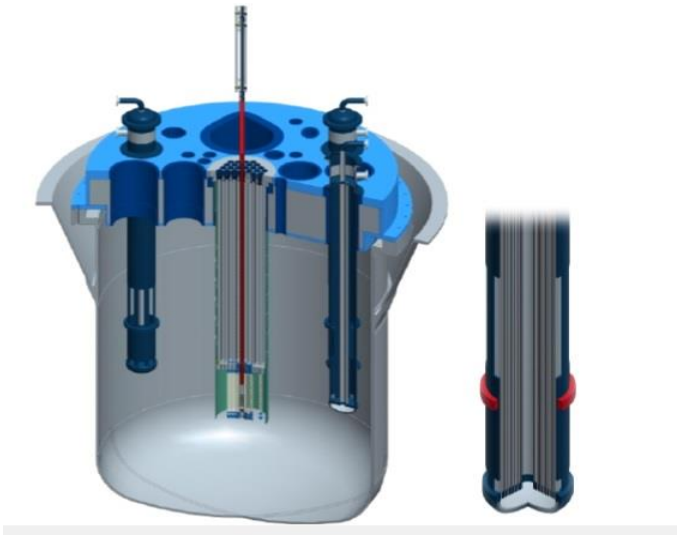

Figure 5.3: Primary heat exchanger, taken from [12]

The primary cooling system runs with LBE to the core through pumps. While the primary cooling system is the first mechanism to cool the reactor core, the secondary cooling system is designed to cool the reactor temperature down using water. The tertiary system, which is run by an air-cooling method, will be activated during operation and in passive mode for 'decay heat removal' [12].

The main fuel in the reactor core is composed of uranium-based MOX fuel, which is typically used in nuclear reactors throughout the world. The core structure has several assemblies in what is named the In-Pile test Section (IPS), which functions as a loading area for fission actinides [9]. This capability fulfils one of the primary objectives, i.e., transmutation using ADS specifications. Having assemblies dedicated to IPS makes the unit easy to remove or replace [9].

MYRRHA has a special modification in critical mode operation, which is the placement of six control rods filled with buoyancy-driven LBE and three scram rods (gravity-driven LBE). These loads replace the control rods adopted in subcritical mode.

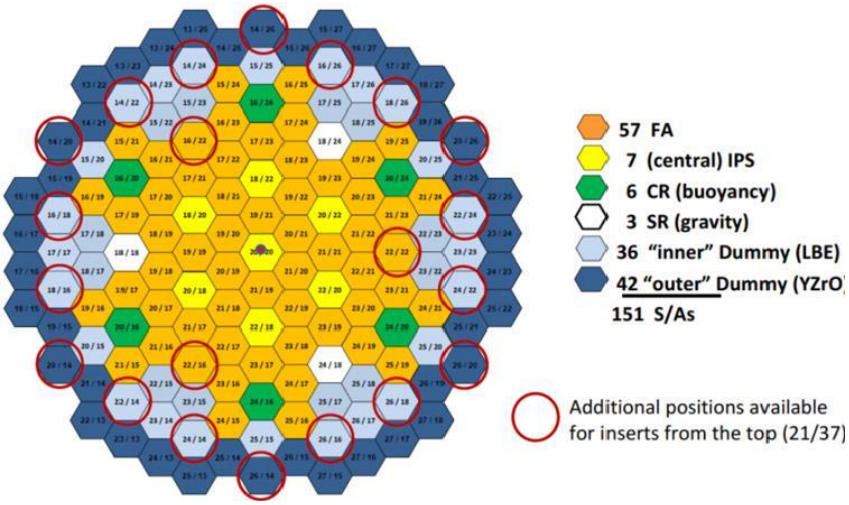

Figure 5.4: Cross-section of the MYRRHA-FASTEF core, showing the central target, the different types of fuel assemblies and dummy components, taken from [9]

To increase neutron flux inside the core, the area surrounding the fuel assemblies filled with LBE is composed of dummy assemblies. These assemblies increase neutron reflection toward the central core area. After this inner dummy area, there are assemblies in the outer dummy area filled with YZrO pellets to act as a shield around the core.

It is intended that MYRRHA, with its unique features in terms of flexible irradiation facilities, will be fully operational by 2025 and the facility will be the first operational ADS-conceived reactor [13]. Overall, the aim of MYRRHA is to address the following research output:

- Demonstration of ADS technology
- Demonstration of transmutation of minor actinides in both subcritical and critical mode
- Demonstration of innovative reactor systems in fast spectrum
- Material research for Generation IV systems
- Research for radio isotope production and industrial applications.

5.3 Neutron energy distribution in different region of core assemblies

In this study, thorium is considered to be a potential fuel source in the ADS environment. MYRRHA's core geometry (see Figure 5.4) was chosen and this would be reconfigured with thorium in the main fuel area. In order to see the neutron production in each region, a simple geometry was constructed mimicking MYRRHA's core structure. The size of each layer was created to be the same size as the fuel assembly in MYRRHA's core, which is 97.55 mm wide and 1400 mm long [14]. Figure 5.5 shows the configuration of the geometry and Table 5.1 gives its specifications. Within the geometry, the GEANT4 program was set to monitor neutrons and their energies as they passed the outer layer in each region. The results of this study have been presented in the proceedings of the International Particle Accelerator Conference 2016, Busan, Korea [15] and the proceedings of the ADST workshop [16] as part of the PhD project.

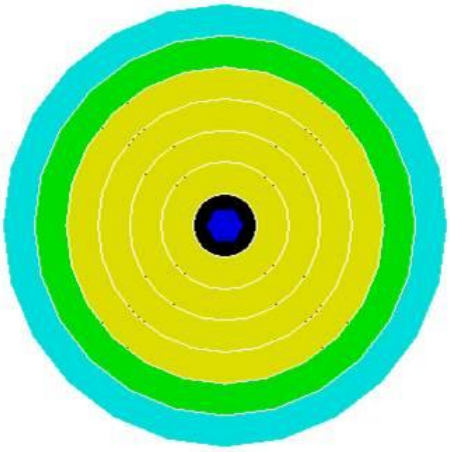

Figure 5.5: Simple geometry with MYRRHA configuration in GEANT4

Table 5.1: Specifications of the MYRRHA-configured simple geometry

Area	Material	Size (mm^2) (Annular radius × Length)
Spallation target (Blue)	Lead Bismuth Eutectic	97.55 × 300
Fuel (Yellow)	Metallic Thorium	97.55 × 1400
Reflector (i.e. inner dump) (Green)	Lead Bismuth Eutectic	97.55 × 1400
Inner shielding (i.e. outer dump) (Cyan)	Y_2O_3	97.55 × 1400

In Figure 5.5, each assembly area has a different colour corresponding to the materials of which it is composed. For example, blue is used for the spallation target, yellow is thorium fuel, green is the reflector region and cyan is the inner shielding. The reflector region referred to in this text is also named the 'inner dump' in [9], while the inner shielding area is named the 'outer dump'. However, the original MYRRHA paper [9] states that the inner dump area, composed of LBE, has the effect of reflecting neutrons, and thus has been renamed in order to enable the function of the area in the structure to be easily recognised. Similarly, the outer dump area has been renamed the inner shielding area in this study, due to the fact that there would be an outer shielding area in place for shielding the core. In this study, the metallic thorium was used as main source of fuel which has the density of 11.72 g/cm^2.

Each region shown as an annular shape in Figure 5.5 has a distance from the centre of the core equal to the size of a fuel assembly (i.e. Region 1 is at 97.55 cm, Region 2 is at 195.1 cm etc.). The results of the GEANT4 simulations presented in Figure 5.6 show the energy spectra of neutrons travelling from one region to another in the core.

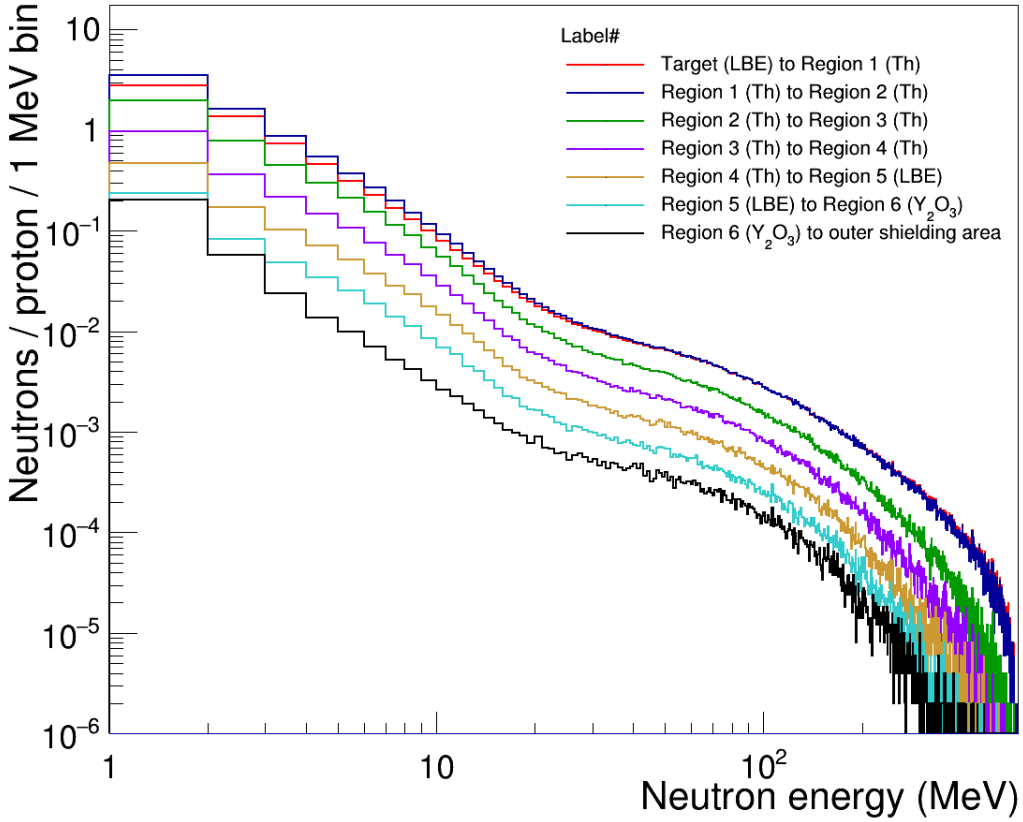

Figure 5.6: Number of outgoing neutrons through each region in the core as a function of neutron energy

It can be seen from Figure 5.6 that the neutron flux (number of outgoing neutrons per proton in 1 MeV bin size) for Regions 1 to 2 (red line) is higher than the line representing the neutron flux from the target to Region 1 (blue line). This indicates that more neutrons have been created from the neutron spallation target. The neutrons created from the spallation target are mostly below 2 MeV. By allowing these neutrons to induce further reactions which produce neutrons in the first fuel region, thorium can produce additional neutrons. In addition, the absorption cross-section for thermal neutrons of ^{232}Th is nearly three times that of ^{238}U [8]. This demonstrates that thorium can catch not only fast neutrons but also thermal-ranged neutrons. Hence, further cascaded reactions can occur inside the thorium material to create more neutrons.

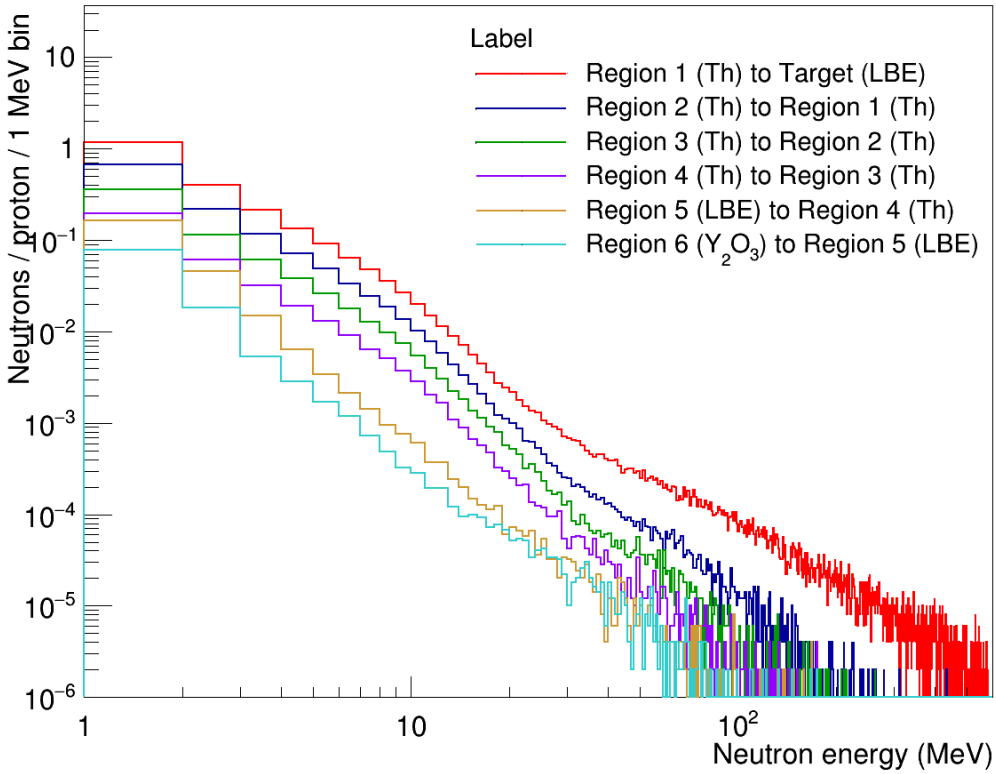

Figure 5.7: Number of back-scattered neutrons through each region in the core as a function of neutron energy

Neutrons travel not only toward the outside but also back-scatter toward the centre of the core, as shown in Figure 5.7. The results shown in this figure indicate that, of all regions in the structure, Region 1 had the highest rate of neutrons back-scattering toward the centre. Region 1 is the first region in contact with neutrons created from the spallation target and composed of thorium. Hence, it is to be expected that the highest rate of back-scattered neutrons will be found in the area closest to the centre of the core structure. Furthermore, there is no structure absorbing back-scattered neutrons between the spallation target and Region 1. Hence, there is no medium in place to interact with back-scattered neutrons and lead to the emission of neutrons. It was also noted that there were no back-scattered neutrons detected between Region 6 (inner shielding area) and Region 5, which is the LBE-composed reflector region.

In order to verify the capability of thorium fuel to contribute to neutron production, the neutron flux was calculated in the first region shown in Figure 5.5. This region is approximately similar to the region MYRRHA uses for loading minor actinides for transmutation [12].

According to [10], the neutron flux at the locations for minor actinides transmutation was reported as 10^{15} n/cm^2 · s and 10^{13} to 10^{14} n/cm^2 s for the locations of structural material and fuel irradiation for neutron energies higher than 0.75 MeV. The GEANT4 simulation was configured to obtain the neutron path length which was then used to calculate the neutron flux by this formula below.

$$neutron\ flux\ (n/cm^2) = \frac{\sum neutron\ path\ length}{volume\ of\ the\ region \times No\ of\ particle} \cdot \frac{current}{1.60 \times 10^{-19}} \quad (5.1)$$

where current is 4mA in MYRRHA facility. In this formula, the following values were used

Table 5.2: The values used to calculate neutron flux in the first region of fuel in the GEANT4 simulation

Volume of the first fuel region	41853 cm^3
Number of particles in the simulation	2.0E6
Neutron path length	≈2.0E09
Current	4 mA

The neutron flux was calculated as 5.90E14 n/cm^2 ·s. This value is comparable with the neutron flux reported from the MYRRHA paper mentioned above despite that this study used thorium based fuel instead of uranium based fuel. Hence, this finding indicates that thorium might be capable to be utilised to produce neutrons to meet the requirement of transmutation in MYRRHA's configuration. Similarly one can calculate the rate of incineration that could be achieved for a minor actinide. The incineration would mean in this case the conversion of the minor actinide to another isotope with a shorter half-life than the original isotope. This process would mainly go through fission process by

neutrons. This study used following formulas to calculate the rate of incineration for ^{237}Np [25].

$$Probability\ of\ MA\ to\ be\ fissioned\ by\ neutron\ (\int \sigma(E)\varphi(E)dE\ ) = \sum neutron\ flux\ \times \sigma\ dE \tag{5.2}$$

Where φ is the flux, defined as the total track length per second of all neutrons in the object, divided by its volume, and σ is the neutron-induced fission cross section for ^{237}Np between 0 and 2 MeV retrieved from [17].

$$The\ rate\ of\ incineration = Probability\ \times (protons/sec)\ \times No\ of\ ^{237}Np\ nuclei \tag{5.3}$$

Using this formula, a ROOT program was created to collect neutron path length in each energy bin of 50 keV bin size. The cross-section converted to cm^2 was then extracted from [17] and multiplied with the neutron path length in the corresponding energy bin. The sum of the values was then normalised with the volume of the cell where minor actinides are loaded. The value is the probability that any particular ^{237}Np nucleus will get converted by the neutrons through the fission reaction which is 7.06E-27. This probability was then used to calculate the rate of incineration using formula 5.3. The number of protons per second is 2.5E16 and the number of ^{237}Np nuclei as 1.22E18. The rate of incineration is approximately 0.0215 g/second. According to [18], there is 2100 metric tonnes of spent nuclear fuel produced in United State in a year. The production of the transuranic element by the neutron irradiation of ^{235}U constitute 1% of the total spent nuclear fuel [18]. (This is not 100% ^{237}Np, but we will use this as an illustration.) Hence, this would mean 21000000 grams of ^{237}Np produced from the neutron irradiation of ^{235}U in a year. In order to incinerate this amount of ^{237}Np with the rate of incineration mentioned above, it would take approximately 976744186 seconds which is equivalent to 271317 hours approximately. This would be equivalent to 11304 days

approximately. This value is comparable with Berthors' finding. According to Berthors [19], the times that ^{237}Np would burn-up are 14961 days with the fast neutron flux of 3E14 n/cm^{2}s and 4407 for fast neutron flux of 1E15 n/cm^{2}s. Despite the different conditions used in [19], the days that burn-up was taken is in the similar length of time. Hence, it is reasonable that the rate of incineration for ^{237}Np is well estimated. This calculation assumes that the neutrons are continuously supplied.

5.4 Energy distribution of neutrons escaping from the core structure

5.4.1 Effect of reflectors blocking neutrons from the core structure

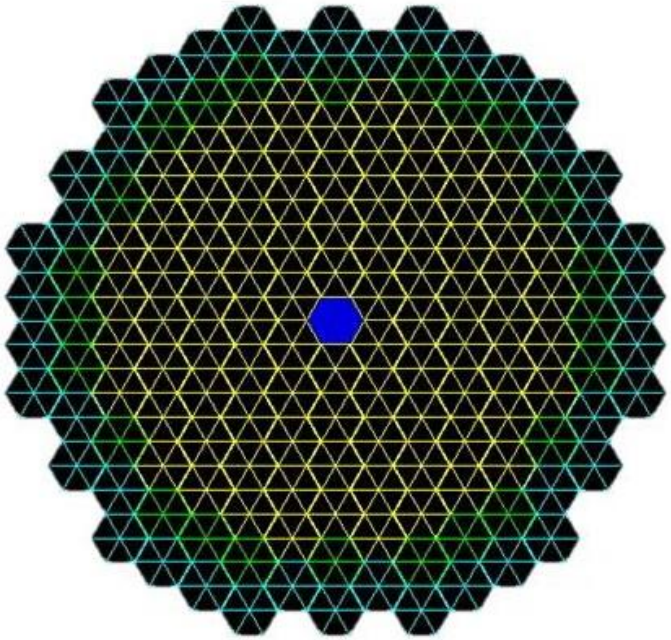

Figure 5.8: MYRRHA core configuration created in GEANT4 simulation (spallation target = blue; thorium fuel = yellow; reflectors = green; inner shielding = cyan). This diagram was first presented in [15]

In relation to the findings described in section 5.3 above. The study was primarily focused on the effect of reflecting neutrons within the core structure and any resultant increase in neutron flux under various environments. It was expected that the

effectiveness of preventing neutrons escaping from the core would be demonstrated when various materials were introduced into the regions outside the central fuel region shown in yellow in Figure 5.8. This design was created based on the original design of the MYRRHA core, which is shown in Figure 5.4.

In order to understand the effect of an LBE-composed reflector on reflecting neutrons within the core, the simulations were firstly carried out by removing the shielding assemblies surrounding the core at this time.

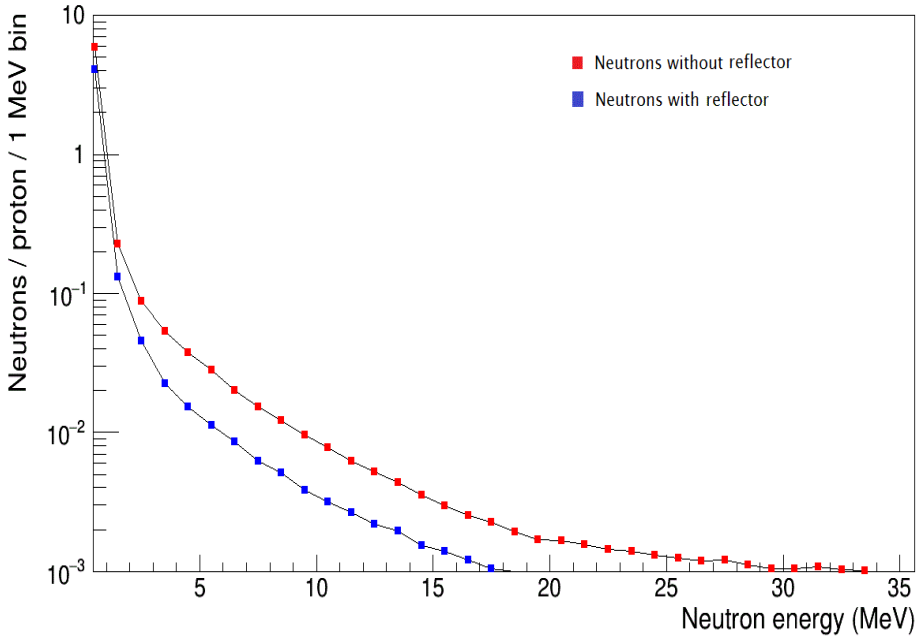

Figure 5.9: Neutron flux (number of neutrons per proton) escaping from the core as a function of neutron energy. This figure was first presented in [15]

While the full geometry of core assemblies was created under similar specifications to the original MYRRHA design, the specifications shown in Table 5.3 were used in this study.

Table 5.3 : Specifications of core assemblies used in the GEANT4 simulation

Area	Material	Size (cm^2)	Number of assemblies placed in the core
Spallation target	**PbBi (LBE)**	**97.55 × 30**	**1**
Fuel	**Thorium**	**97.55 × 140**	**76**
Reflector	**PbBi (LBE)**	**97.55 × 140**	**36**

Figure 5.9 shows the variation in neutron energy spectra (neutrons per incident proton in 1 MeV energy bins) between the reflector and non-reflector assemblies. It can be seen from the figure that the reflectors decreased the number of neutrons per proton especially for high-energy neutrons. More specifically, the figure shows that the highest neutron energy for the non-reflector structure was recorded at 33.5 MeV, while the reflector managed to reduce the maximum energy to 17.5 MeV. LBE is known as a weak absorber of neutrons. However, it is known as a good scatterer [20]. As a result of this effect, LBE may increase the chance of neutrons undergoing collisions inside the material, thereby ultimately reducing neutron energy. This will beneficially affect the neutron-physical characteristics of the reactor [20]. It was also noted that neutron flux in the neutron energy range between 0 and 2 MeV remained high (approximately 4 neutrons per incident proton). This finding indicates that extra shielding may be required to prevent neutrons escaping from the core. Overall, the results indicate that the reflector material (i.e. LBE) was effective in reducing the number of highly energised neutrons escaping from the structure. However, it is also conclusive that the material was not effective in blocking neutrons with an energy range of between 0 and 2 MeV. These neutrons can induce further collisions to produce low energy neutrons, such as epi-thermal or thermal neutrons, if there is more LBE-like material present in the immediate area. However, the original MYRRHA schematic [9] indicates that any assemblies placed after this LBE-composed reflector region are intentionally placed for radiation shielding and containment of the reactor core. Hence, the reflector did a good job in containing the neutrons. Any neutrons escaping from this reflector region would then be moderated further as they collided with the outer shielding material.

5.4.2 Effect of inner shielding on neutron energy distribution

As previously mentioned, the inner shielding, referred to as the outer dummy area in the original MYRRHA core specification, is placed after the reflector area to shield the core barrel [9]. Although this study initially attempted to create the material (YZrO) used in MYRRHA in order to deliver the same environment, without knowing the exact composition of the material, the attempt was unsuccessful. Due to a lack of information regarding the material, three different materials that were close to YZrO were chosen and the energy distribution of neutrons escaping from these materials was compared.

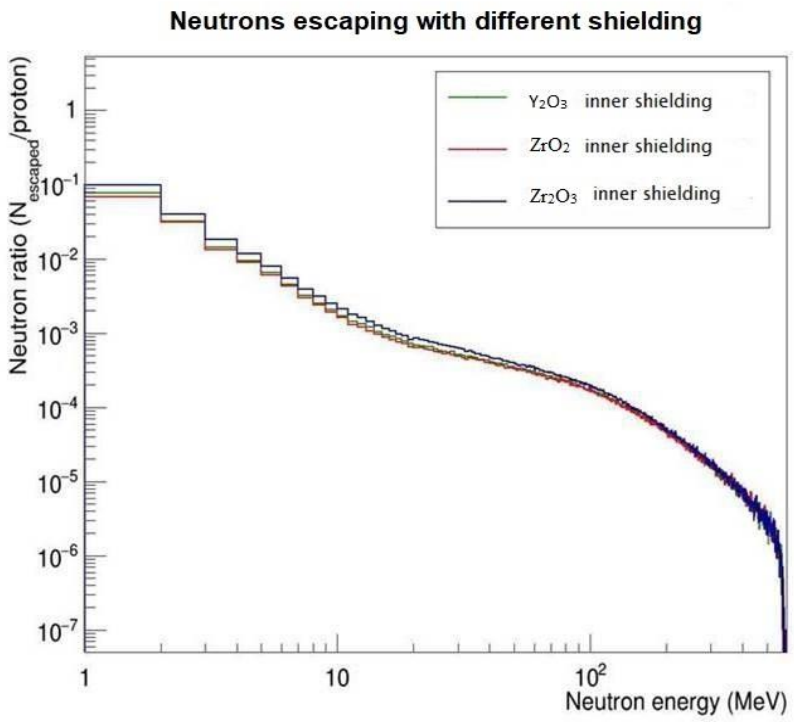

Figure 5.10: Energy distributions of neutrons escaping from the core under three different inner shielding materials as a function of neutron energy between 0 and 600 MeV with 1 MeV bins (red=ZrO_2, green=Y_2O_3 and blue=Zr_2O_3)

The materials Y_2O_3, ZrO_2 and Zr_2O_3 were used, since all three materials have the components of YZrO. Variants of these materials are widely used as thermal barriers in high temperature environments and medical applications due to their high compression resistance and chemical inertness [21]–[23], which fits their usage in a nuclear core

structure. Thus, this study examined the effect on neutron spectra using these materials in such a way that the anticipated effectiveness of YZrO on the neutron energy distribution could be assessed.

Figure 5.10 shows a comparison between the neutron energy spectra resulting from the use of the three different materials mentioned. It can be observed from Figure 5.10 that the result with ZrO_2 shows the lowest rate of neutrons escaping from the core in the neutron energy range between 0 and 2 MeV. Y_2O_3 shows the second highest rate of blocking neutrons, followed by Zr_2O_3.

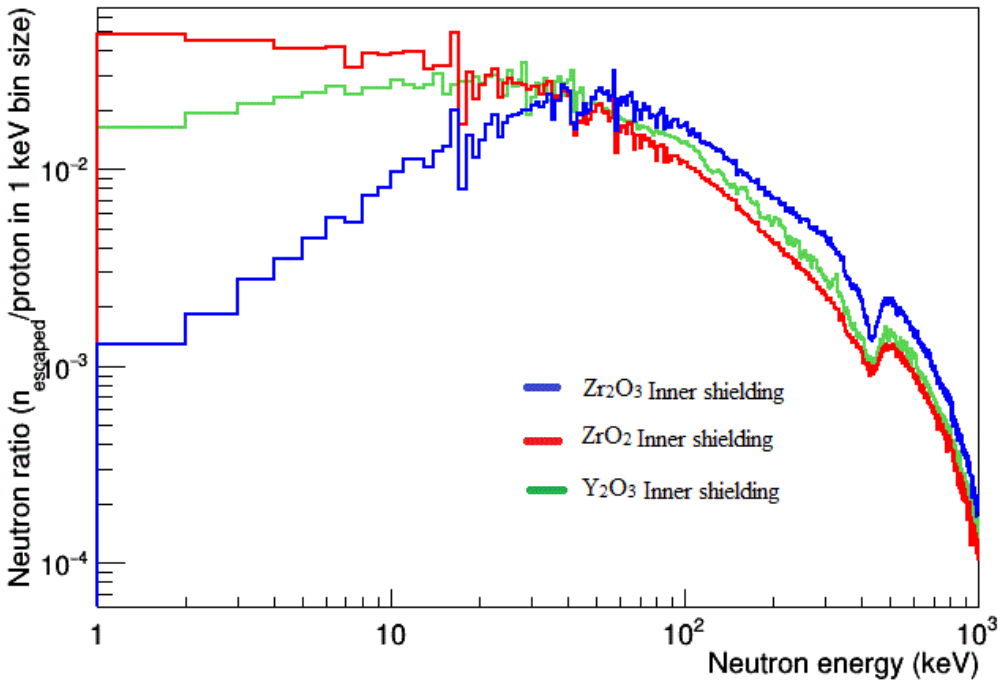

Figure 5.11: Energy distribution of neutrons escaping from the core with different inner shielding materials as a function of neutron energy between 0 and 1000 keV with 1 keV bins (red=ZrO_2, green=Y_2O and blue= Zr_2O_3).

To examine these results more closely, Figure 5.11 shows the energy distribution of escaping neutrons in the neutron energy range between 0 and 1 MeV. As the figure clearly demonstrates, the ZrO_2 material showed the highest rate of blocking low energy neutrons. It can be seen from this figure that ZrO_2 has the lowest rate of letting neutrons

escape from the material at a neutron energy below approximately 40 keV. It also appears that the change in neutron rate occurred at a neutron energy of 40 keV for both the other materials. The pattern below 40 keV indicates that ZrO_2 was the material with the highest rate of neutron escape, followed by Y_2O_3. Zr_2O_3 had the lowest rate of neutron escape below 40 keV. This finding shows that ZrO_2 is not effective in preventing the escape of neutrons with energy below 40 keV. The cause of this behaviour might be related to the neutron capture cross sections of the materials. According to the ENDF nuclear data library, both ^{89}Y and ^{91}Zr have the high neutron capture cross sections at neutron energies between 10^{-5} and 0.75 MeV (see Figure 5.12), which suggests that there is a high probability of neutrons in this energy range being captured by all three materials. Therefore, despite the differences in composition of all three materials used in the inner shielding area, it is likely that low energy neutrons being captured changes the number and energy spectrum of emitted from the materials.

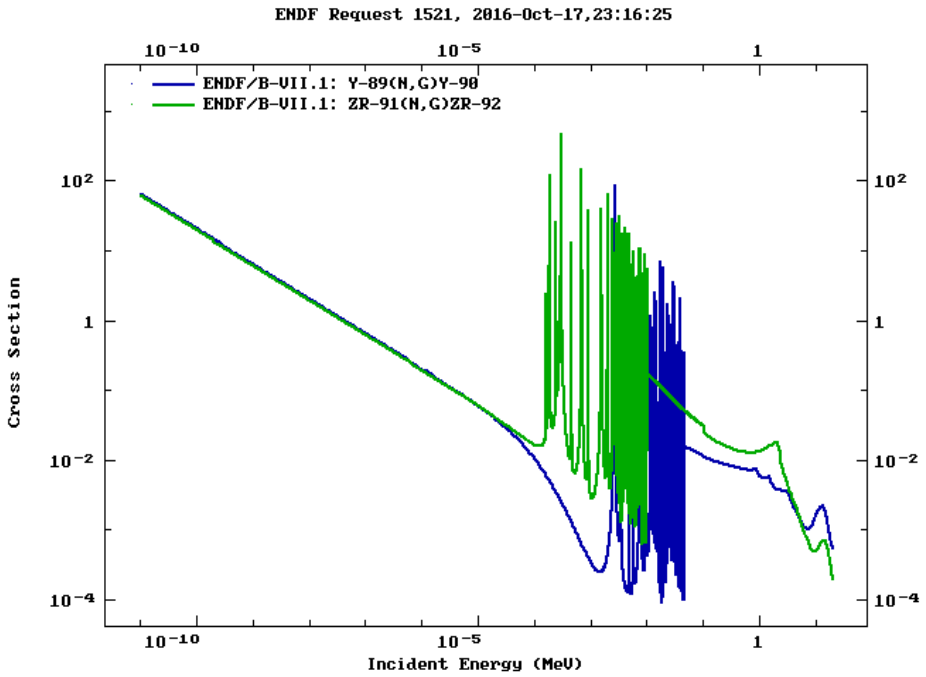

Figure 5.12: Neutron capture cross section taken from ENDF data library online database (blue=Yttrium and green=Zirconium) [24]

In general, the number of neutrons escaping per incident proton was similar in all three materials for neutron energies above 10 MeV. However, there was a clear difference in the blocking of low energy neutrons depending on the material in the shielding area. Hence, it might be possible that the placement of a further shielding area could vary the energy spectra of neutrons escaping from this area.

5.4.3 Effect of outer shielding on neutron energy distribution

As shown in section 5.4.2, the inner shielding area decreases the average neutron energy. However, there is still a need for an outer shielding area to shield the reactor core and reflect any escaping neutrons back into the core, or to remove any that may have escaped. MYRRHA's original schematic, as shown by Professor R. Barlow [25], indicates that beryllium is used for the outer shielding. Beryllium is known to be effective for stopping thermal neutrons [26], though according to [27], several alternative materials can be used in high temperature environments, such as tungsten and stainless steel.

In this study three different materials, namely beryllium, stainless steel-347 and tungsten carbonate (WC), were selected to fill the assemblies placed in the outer shielding area. These materials were selected based on the fact that they are used in nuclear applications [28]. It is noted by [28] that, due to its characteristic of having a low thermal neutron absorption cross section, beryllium is known to be a unique material that has previously been used successfully as a neutron reflector. Beryllium is also effective in reducing the energy of neutrons. On the other hand, tungsten carbide was chosen since this material is known as a neutron reflector [29], as well as the fact that its carbon element has low activation characteristics which make it ideal as a shielding material. The combination of carbon and tungsten into one material enables it to possess both stability at high temperature and good shielding capability [29]. Stainless steel-347 is one of the common materials used in nuclear reactor shielding due to its strength in a high temperature environment [28], [30].

In this study, the energy spectra of neutrons escaping from these materials were analysed in order to observe the effects of the materials on neutrons that had passed from the previous inner shielding areas. In order to understand neutronic behaviour in every environment under this ADSR configuration, this study was processed with the placement of all three inner shielding materials discussed in section 5.4.2.

Firstly, the energy spectra of neutrons escaping from Y_2O_3 inner shielding and interacting with the three forms of outer shielding were examined. Figure 5.13 shows the neutron energy distribution after the neutrons had passed the inner shielding and collided with the outer shielding area. As can be seen from the figure, the energy spectra differed for the different outer shielding materials.

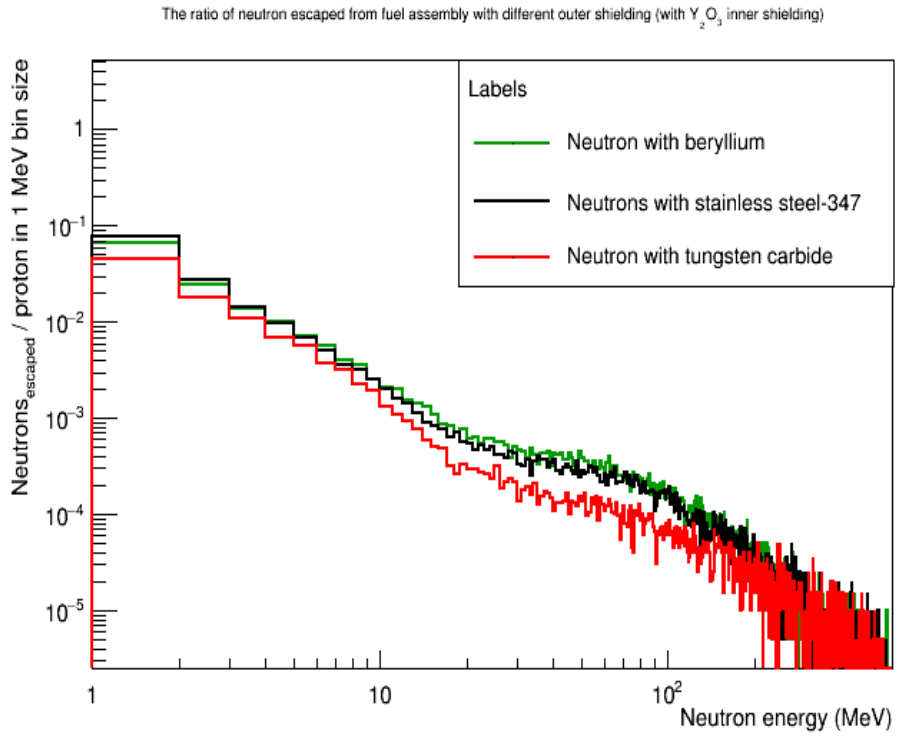

Figure 5.13: Energy spectra of neutrons escaping from outer shielding with Y_2O_3 inner shielding as a function of neutron energy between 0 and 600 MeV with 1 MeV bins (red=tungsten carbide, green=beryllium and black = stainless steel-347)

It can be seen from Figure 5.13 that all three materials show a similar energy pattern throughout the whole spectrum. However, it is also evident that tungsten carbide

(portrayed as a red line) gives the greatest rate of preventing neutrons escaping from the structure. This is then followed by stainless steel-347 and beryllium. It is noticeable that stainless steel-347 shows a slightly better rate of blocking neutrons than beryllium in the energy range between 0 and 2 MeV. However, after 2 MeV, beryllium shows a better rate of blocking neutrons than stainless steel-347. Overall, it is clear that tungsten carbide is the most effective in preventing neutron escape compared with the other two candidates.

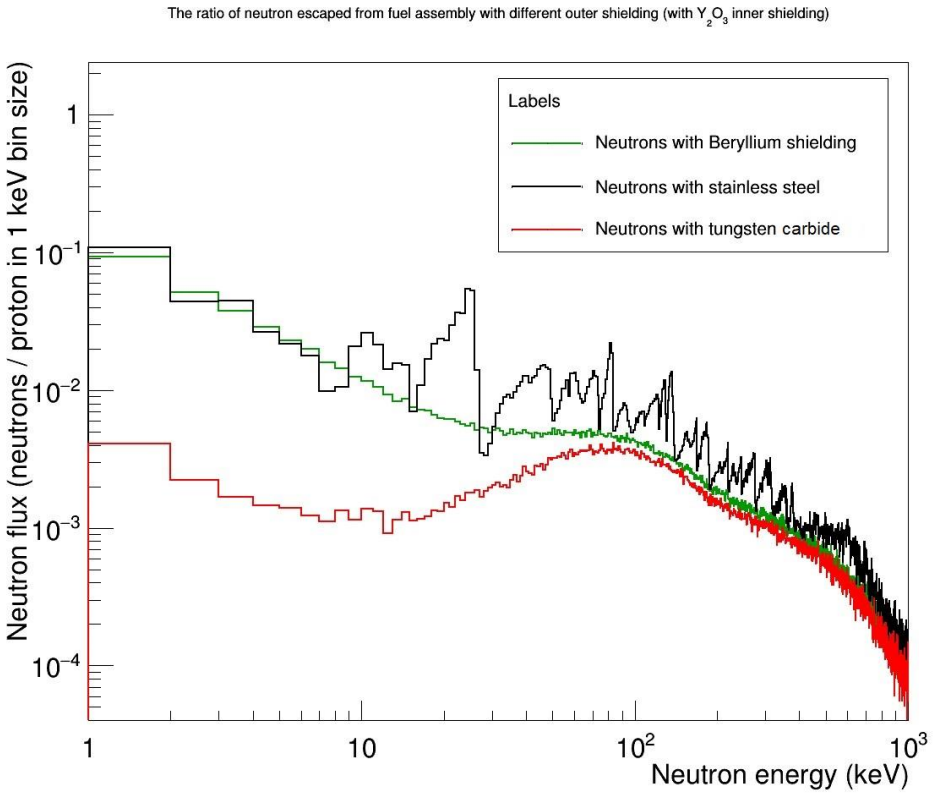

Figure 5.14: Energy spectra of neutrons escaping from outer shielding with Y_2O_3 inner shielding as a function of the neutron energy between 0 and 1000 keV with 1 keV bins (red=tungsten carbide, green=beryllium and black = stainless steel-347).

The study then closely analysed the neutron spectra between 0 and 1 MeV for all three outer shielding materials. It can be observed from Figure 5.14 that tungsten carbide's rate of neutron blockage is most effective at a low energy range, while beryllium and stainless steel-347 show a similar rate. Closer observation reveals that beryllium has a slightly better rate of blocking neutrons. It is also noticeable that stainless steel-347

shows a fluctuating pattern of neutron energy spectra. This might be related to the fact that stainless steel-347 is composed of eight different elements [31].

Secondly, the energy spectra of neutrons escaping from ZrO_2 inner shielding and interacting with the outer shielding materials were examined; the results are shown in Figure 5.15.

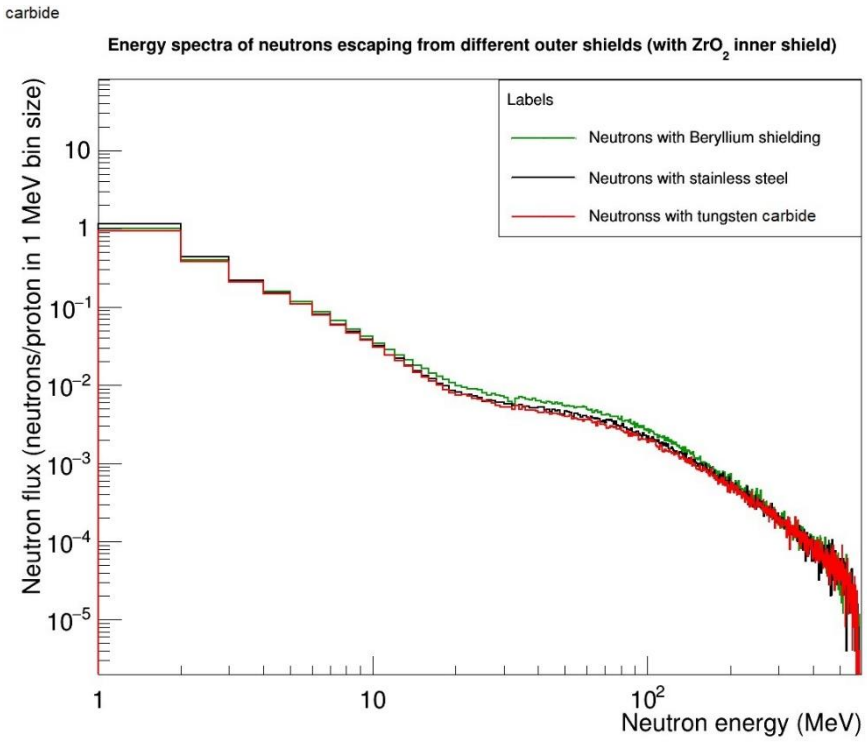

Figure 5.15: Energy spectra of neutrons escaping from outer shielding with ZrO_2 inner shielding as a function of neutron energy between 0 and 600 MeV with 1 MeV bins (red=tungsten carbide, green=beryllium and black = stainless steel-347)

Again, the figure shows the neutron energy distribution after the neutrons had passed the ZrO_2 inner shielding and collided with the outer shielding area. It can be seen from Figure 5.15 that all three materials show a similar energy pattern throughout the whole spectrum. It is also noticeable that the difference in neutron spectra between the three materials appears reduced in comparison with the results shown in Figure 5.13. The ZrO_2 inner shielding allows more neutrons to escape from the volume than the Y_2O_3 shielding. The capability of the outer shielding materials to block neutrons escaping

from the volume remained the same as in the previous study. A similar rate of neutron flux was shown by all three outer shielding materials, the number of neutrons escaping being relatively high compared with the study with Y_2O_3. The study then analysed the neutron spectra between 0 and 1 MeV more closely for all three outer shielding materials with ZrO_2 inner shielding in place. It can be seen from Figure 5.16 that all three materials showed a similar rate of preventing neutrons escaping as the neutron energy increased. At energies between 0 and 10 keV, however, tungsten carbide showed the lowest rate of allowing neutrons to escape from the volume, while closer observation revealed that beryllium had a better rate of blocking neutrons at a neutron energy range between 10 and 100 keV. This finding might be related to the total cross section of beryllium retrieved from the ENDF online data library [17], as shown in Figure 5.17.

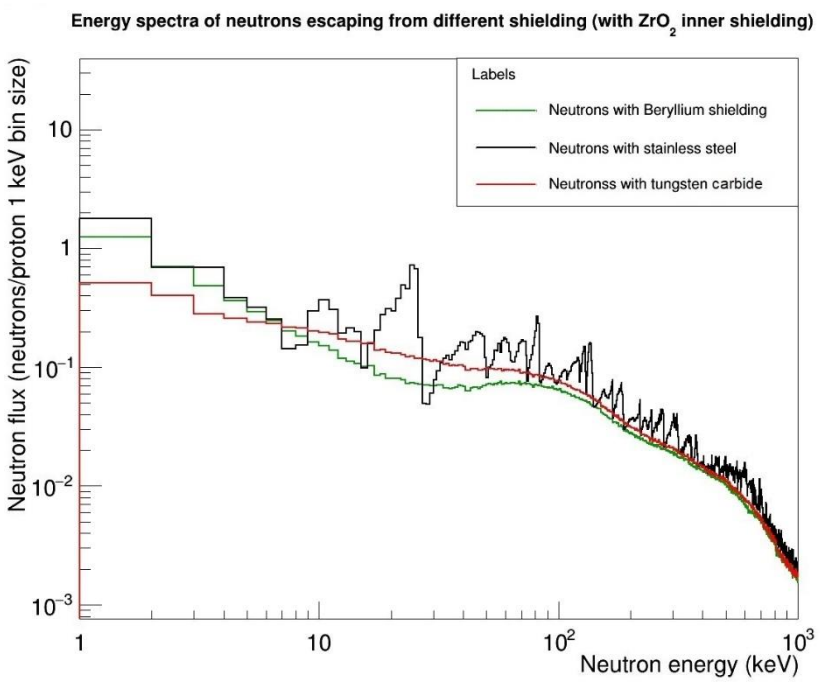

Figure 5.16 : Energy spectra of neutrons escaping from outer shielding with ZrO_2 inner shielding as a function of neutron energy between 0 and 1000 keV with 1 keV bins (red=tungsten carbide, green=beryllium and black = stainless steel-347)

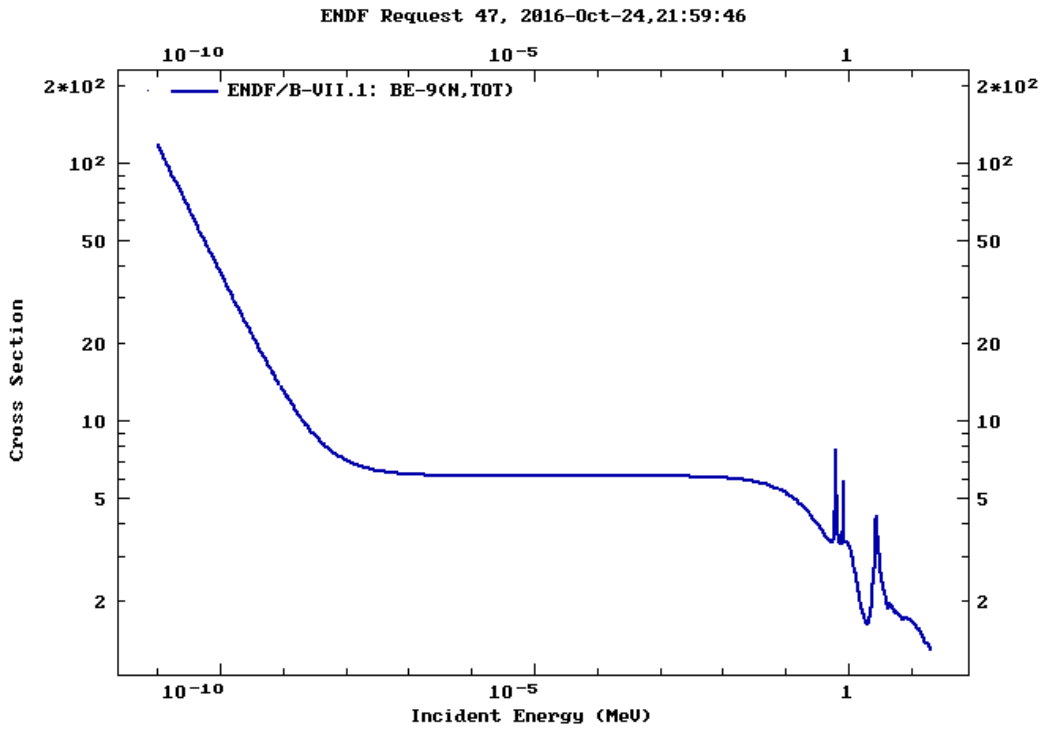

Figure 5.17: Total neutron cross section of ^{9}Be retrieved from [17] **originally taken from** [23]

Figure 5.17 shows that there is a sudden increase in the cross section between approximately 100 keV and 1 MeV. This might suggest that many interactions have occurred between the neutrons and the beryllium nucleus, causing fewer neutrons to be emitted at ranges between 10 keV and 100 keV. A further finding of this study was that stainless steel-347 shows a fluctuating pattern of neutron energy spectra; this feature was also observed in Figure 5.14.

A final study was conducted to analyse the energy spectra of neutrons escaping from the outer shielding materials while Zr_2O_3 inner shielding was in place. The figure below shows the neutron energy distribution after the neutrons had passed the Zr_2O_3 inner shielding and collided with the outer shielding area. As can be seen from Figure 5.18, the energy spectra of neutrons emerging from the various outer shielding materials differed.

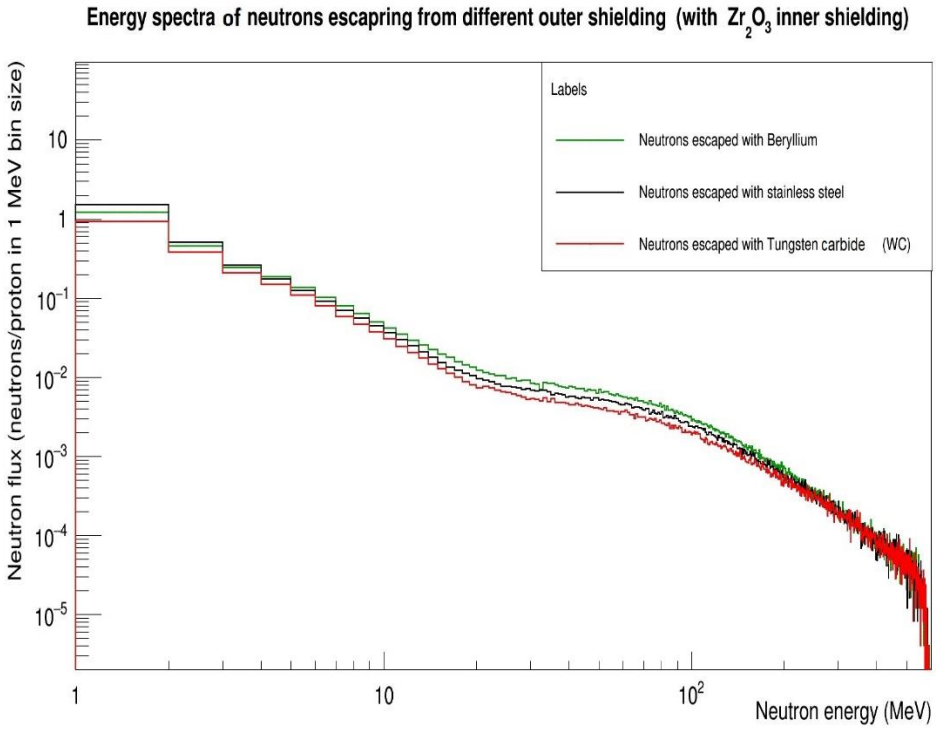

Figure 5.18: Energy spectra of neutrons escaping from outer shielding with Zr_2O_3 inner shielding as a function of neutron energy between 0 and 600 MeV with 1 MeV bins (red=tungsten carbide, green=beryllium and black = stainless steel-347)

Figure 5.18 shows similar patterns to the other two results previously discussed. Tungsten carbide showed the lowest rate of allowing neutrons to escape from the structure; this was then followed by beryllium and stainless steel-347, which showed similar rates. The graph also indicates that beryllium showed a better rate of blocking neutrons than stainless steel-347 at neutron energies between 0 and 2 MeV. After that, the stainless steel showed a better rate of blocking neutrons. This may correspond with the earlier discussion about the total neutron cross section of beryllium (see Figure 5.17). The cross section not only increases between 0.1 and 1 MeV, but also between 1 and 2 MeV. This may suggest that more neutrons have interacted with the beryllium nucleus, which is reflected in the number of neutrons emitted from the volume.

The study then looked more closely at the energy spectra between 0 and 1 MeV for the data presented in Figure 5.18.

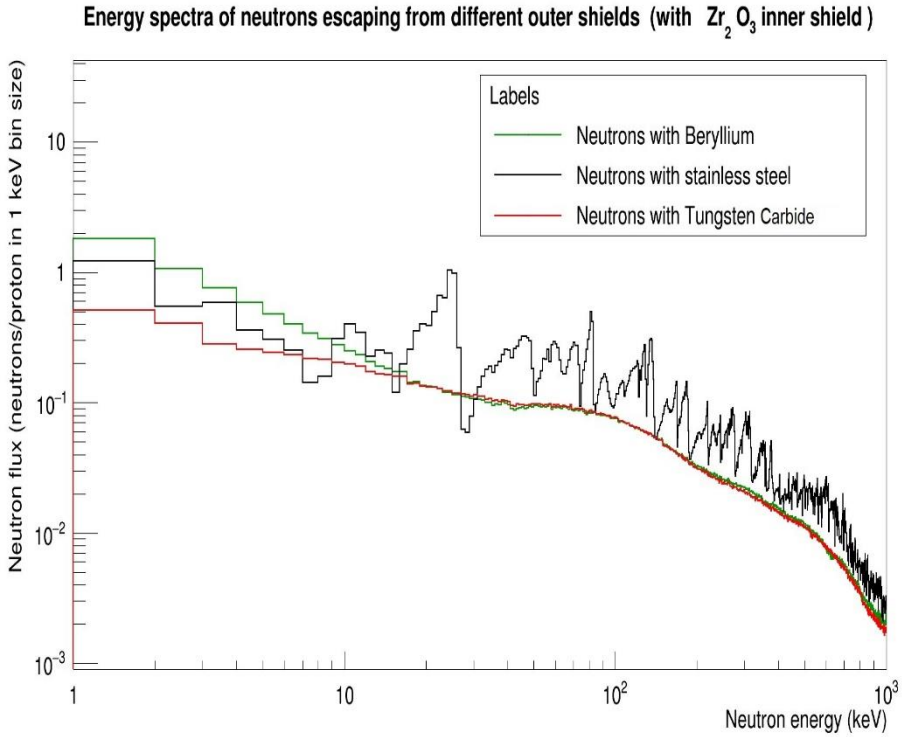

Figure 5.19: Energy spectra of neutrons escaping from outer shielding with Zr_2O_3 inner shielding as a function of neutron energy between 0 and 1000 keV with 1 keV bins (red=tungsten carbide, green=beryllium and black = stainless steel-347)

Figure 5.19 shows the energy spectra of neutrons that escape from the Zr_2O_3 inner shielding interacting with each of the three outer materials. The figure provides a close examination of the results for neutron energies between 0 and 1000 keV in 1 keV increments. As with the neutron spectra for the other two materials at this energy range (see Figure 5.14 and Figure 5.16), tungsten carbide showed the greatest rate of blocking neutrons escaping from the outer shielding area, since its energy spectrum was the lowest in terms of neutrons escaping per proton. This was then followed by stainless steel-347 and finally beryllium. This pattern of neutron spectra continued up to 10 keV. From that point to the end of the neutron energy range, both tungsten carbide and beryllium showed the lowest rate of allowing neutrons to escape from the outer shielding area. Thus, of the three materials, stainless steel-347 showed the highest rate of allowing neutrons to escape from the volume after 10 keV. Moreover, fluctuation of the neutron spectrum for stainless steel-347 was continuously shown at this energy

range. These findings suggest that both tungsten carbide and beryllium are good shielding materials at 10 to 1000 keV.

5.5 Conclusion

This chapter has discussed the potential of thorium fuel in an Accelerator-Driven Subcritical Reactor (ADSR). Firstly, this study examined the neutron population and energy distribution within each section of the core assembly by creating a geometry which mimicked MYRRHA's core specifications. The findings show that more neutrons were produced in the first thorium fuel region, where the interaction between spallation neutrons primarily took place. The results also show that the rate of neutron production decreased as the distance from the centre of the core increased. In terms of backscattering, a significant number of neutrons were found to be scattered backward in every region, but especially from the first thorium-fuelled area to the spallation target area. This finding indicates that the first fuel region was where the highest rate of neutron production occurred within the core structure. This study is therefore able to say that it is possible for thorium to be utilised for neutron production in an ADSR core. Furthermore, neutrons produced from the thorium-fuelled region were mostly categorised as fast neutrons with a neutron energy of 1-2 MeV. This feature may be beneficial in fulfilling an ADSR's purpose of transmuting nuclear waste, since fast neutrons are favourable for the transmutation of minor actinides due to the high neutron flux environment needed, and there is more chance of neutrons inducing fission in minor actinides [32]–[34].

The chapter has also discussed the escape of neutrons from various shielding areas surrounding the core assembly. The aim was to analyse the neutron energy spectra after the neutrons had interacted with various materials within these shielding areas. The assembly consisted of a reflector and both inner and outer shielding areas. Each area was specifically composed of various materials to fulfil the purpose of reflecting and removing neutrons if they passed through the region. Firstly, the reflector area was placed after the thorium fuel area. The choice of material was Lead Bismuth Eutectic

(LBE), which is the material used in the MYRRHA reactor. The findings show that LBE was effective in reducing the number of high energy neutrons. The materials helped to moderate the neutrons and primarily to block their escape from the volume. It was still evident that more neutrons need to be removed, however, due to the presence of 17.5 MeV neutrons detected outside the reflector region, as well as a significant number within the fast neutron spectrum (i.e. in the energy range 1 - 2 MeV).

The next part of the study examined inner shielding materials. Since the primary material used in MYRRHA (YZrO) could not be utilised in this study due to the lack of reference to its specifications in any MYRRHA publications, three materials close to YZrO (i.e. ZrO_2, Y_2O_3 and Zr_2O_3) were selected as they comprised the same elements as YZrO. The findings indicate that these materials have similar characteristics in terms of their interaction with neutrons across the full range of neutron spectra between 0 and 600 MeV. However, closer examination showed that at neutron energies between 0 and 1000 keV they showed different rates of blocking neutrons. At up to 40 keV neutron energy, Zr_2O_3 was the material with the lowest rate of allowing neutrons to escape, but ZrO_2 was the most effective in preventing neutrons from escaping after that point. This finding suggested that a variety of outer shielding materials would be required to enforce the blockage of neutrons escaping from the final shielding area, since the results for all three materials used in the inner shielding area showed varying results at low neutron energies.

Finally, the study analysed the energy spectra of neutrons escaping from various outer shielding materials while the materials previously discussed were in place as inner shielding. Since the previous exploration of the effect of inner shielding on escaping neutrons suggested variations in neutron spectra, the study then aimed to see the combined effect of both inner and outer shielding on the neutrons escaping. Three materials known be effective in neutron moderation and reflection were selected; tungsten carbide, stainless steel-347 and beryllium. The study examined the effect of each of the chosen materials placed in the outer shielding area on neutrons which had escaped through the inner shielding material. In most cases, tungsten carbide showed

the best rate of preventing neutrons escaping from the structure. This was then followed by stainless steel-347 and beryllium, which showed similar rates. In particular, it was found that tungsten carbide's effectiveness began from the low end of the energy spectrum (0 -1000 keV neutron energy). This suggests that tungsten carbide could be the best candidate to place in the outer shielding area of a thorium ADSR environment. As for the combination of both inner and outer shielding, the combination of Y_2O_3 and tungsten carbide (WC) showed the best rate of preventing neutrons escaping compared with the other combinations. As discussed in section 5.4.2, Y_2O_3 was the second best material in terms of blocking neutrons effectively. By combining its effect on neutron reflection with tungsten carbide's effective neutron removal, the maximum neutron flux (neutrons escaping per proton in 1 MeV bin) was kept under 10^{-1} (see Figure 5.13). This was not achieved by the other set-ups involving ZrO_2 and Zr_2O_3 as the inner shielding.

Overall, this study has shown that thorium can produce a large quantity of neutrons within the fast neutron spectrum. From the range of high energy production shown by this study, it can be concluded that a combination of neutron removal and reflection may need to be in place to increase neutron flux inside the core. This would increase the number of fissions for the production of energy or for the transmutation of minor actinides if those are loaded in the reactor.

5.6 Bibliography

[1] H. A. Abderrahim, J. Galambos, Y. Gohar, S. Henderson, G. Lawrence, and T. Mcmanamy, "Accelerator and Target Technology for Accelerator Driven Transmutation and Energy Production," , DOE white paper on ADS. Rep. 17;1(1):1-23, September, 2010. [Online] Available: https://192.107.175.200/~/media/hep/pdf/files/pdfs/ADS_White_Paper_final.pdf [Accessed on 30-07-2016]

[2] "A Roadmap for Developing Accelerator Transmutation of Waste (ATW) Technology: A Report to Congress," Department of Energy, US, Rep. DOE/RW-

0519,October,1999. [Online] Available: http://www.wipp.energy.gov/science/adtf/ATW.pdf. [Accessed: 30-07-2016]

[3] C. Rubbia, J. A. Rubio, S. Buono, and et.al, "Conceptual design of a fast neutron operated high power energy amplifier," European Organization for Nuclear Research, Rep. CERN/AT/95-44 (ET),1995.

[4] V. Ashley and R. Ashworth, "The Technically Viable ADTRTM Power Station," *Nuclear Future Volume 7 issue 3* . 2011.pp.41-46.

[5] R. Barlow, J. Burlison, T. Edwards, and et.al, "Studies of MYRRHA using thorium fuel," *Int. J. Hydrogen Energy*, vol. 41, no. 17, pp. 7175–7180, May 2016.

[6] OECD/NEA, "Independent evaluation of the MYRRHA project Report by an international team of experts," OECD Nuclear Energy Agency, Rep. NEA No. 6881, 2009.

[7] NIST Center of neutron research, "Neutron scattering lengths and cross sections for lead," 2017. [Online]. Available: https://www.ncnr.nist.gov/resources/n-lengths/elements/pb.html. [Accessed: 23-Sep-2017].

[8] International Atomic Energy Agency, "Thorium fuel cycle-Potential benefits and challenges," IAEA, Vienna,Rep. IAEA-TECDOC-1450, May 2005.

[9] P. Baeten, M. Schyns, R. Fernandez, D. De Bruyn, and G. Van den Eynde, "MYRRHA: A multipurpose nuclear research facility," *EPJ Web Conf.*, vol. 79, no. 3001, p. 3001, Dec. 2014.

[10] H. A. Abderrahim, *et.al*, "MYRRHA: A multipurpose accelerator driven system for research & development," *Nucl. Instruments Methods Phys. Res. Sect. A*

Accel. Spectrometers, Detect. Assoc. Equip., vol. 463, no. 3, pp. 487–494, 2001.

[11] P. Baeten, "MYRRHA Project - status update MYRRHA - Accelerator Driven System," presented in *ESNII Conference*, 2012, Brussel, June 25, 2012. [Online] Available:http://www.gedeon.prd.fr/ATELIERS/Juillet_2012/exposes/6_juillet/3_GEDEPEON_MYRRHA_vandenende.pdf [Accessed: 30-09-2016]

[12] P.Baeten., *et.al*, "MYRRHA, a Flexible Fast Spectrum Irradiation Facility," in European Reactor Research Conference, Rome, Italy March 20-24, 2011.

[13] D. De Bruyn, H. A. Abderrahim, P. Baeten, and P. Leysen, "The MYRRHA ADS Project in Belgium Enters the Front End Engineering Phase," *Phys. Procedia*, vol. 66, no. April 2014, pp. 75–84, 2015.

[14] M. Sarotto, "MYRRHA-FASTEF FA / core design," presented in *international Workshop on Innovative Nuclear Reactors cooled by HLM*, Pisa ,Italy April 17-20,2012.[Online]Available:http://www.nr.titech.ac.jp/~mtakahas/X13/4.3%20(M.%20Sarotto).pdf [Accessed: 09-05-2015]

[15] S. C. Lee, C. Bungau, and R. Cywinski, "Geant4 simulations of proton-induced spallation for applications in ADSR systems," in *Proceedings of IPAC 2016, Busan, Korea*, 2016, pp. 1943–1945.

[16] D. S. Lee, R. Cywinski, C. Bungau, and R. Seviour, "Geant4 simulations of proton induced spallation for applications in ADSR systems," in *4th Workshop on ADS and thorium*, 2016, no. PoS(ADST2016)011.

[17] V. Zerkin and IAEA-NDS, "Multi-platform EXFOR-CINDA-ENDF," 1999. [Online]. Available: https://www-nds.iaea.org/exfor/servlet/E4sMakeE4. [Accessed: 24-Oct-2016].

[18] A. G. Croff, C. Member, L. T. Tavlarides, J. H. Flack, C. Staff, and H. J. Larson, “Background, Status, and Issues Related To the Regulation of Advanced Spent Nuclear Fuel Recycle Facilities ”, United States Nuclear Regulatory Comission, Rep. NUREG-1909, 2007.

[19] V. Berthou, C. Degueldre, and J. Magill, “Transmutation characteristics in thermal and fast neutron spectra: application to americium,” *J. Nucl. Mater.*, vol. 320, no. 1–2, pp. 156–162, Jul. 2003.

[20] G. Toshinsky and V. Petrochenko, “Modular Lead-Bismuth Fast Reactors in Nuclear Power,” *Sustainability*, vol. 4, no. 12, pp. 2293–2316, Sep. 2012.

[21] J. Chevalier and L. Gremillard, “Zirconia as a Biomaterial,” in *Comprehensive Biomaterials*, vol. 20, no. 1999, Elsevier, 2011, pp. 95–108.

[22] J. R. Kelly and I. Denry, “Stabilized zirconia as a structural ceramic: An overview,” *Dent. Mater.*, vol. 24, no. 3, pp. 289–298, 2008.

[23] P. F. Manicone, P. Rossi Iommetti, and L. Raffaelli, “An overview of zirconia ceramics: Basic properties and clinical applications,” *J. Dent.*, vol. 35, no. 11, pp. 819–826, Nov. 2007.

[24] P. . Rose, “Cross Section Evaluation Working Group, ENDEIB-VI Summary Documentation,.” National Nuclear Data Center, Brookhaven National Laboratory, Upton, NY, USA, 1999.

[25] R. Barlow, “Private Conversation,” 2017.

[26] R. Cywinski, “Private conversation,” 2016.

[27] P. Elliott and others, “Choose materials for high-temperature environments.”,

Chemical Engineering Progress, vol 92., no 2, pp75-91, Feb. 2001.

[28] T. a. Tomberlin, "Beryllium – a Unique Material in Nuclear Applications," in *36th International SAMPE Technical Conference*, San Diego, California 2004.[Online]Available:http://citeseerx.ist.psu.edu/viewdoc/summary?doi=10.1.1.543.4019. [Accessed: 29-09-2015]

[29] Y. Gohar and D. L. Smith, "Multiplier, moderator, and reflector materials for lithium-vanadium fusion blankets.," *J. Nuclear Material*., Vol 283-287, Part 2 pp.1370-1374, 2000.

[30] N. B. Prasad and G. S. Tendolkar, "Application of Stainless Steels in Nuclear Technology," pp. 455–457, 1958.[Online] Available: http://eprints.nmlindia.org/3675/1/455-457.PDF [Accessed: 05-11-2016]

[31] ESPI Metals, "Stainless Steel 304 - Alloy Composition," *ESPI metal Corp*, 2015. [Online]. Available: http://www.espimetal.com/index.php/technical-data/204-Stainless Steel 347 - Alloy Composition. [Accessed: 30-Mar-2016].

[32] D. Mathers, "The Thorium Fuel Cycle," presented in *Thorium Energy Conference 2013*, *013*,CERN,Geneva, October.27-31., 2013. [Online] Available: http://www.thoriumenergyworld.com/uploads/6/9/8/7/69878937/the_thorium_fuel_cycle_-_daniel_p._mathers_-_nnl_-_thec13.pdf .[Accessed: 03-11-2016]

[33] National Nuclear Laboratory, "Minor Actinide Transmutation Position Paper." National Nuclear Laboratory, Warrington, UK [Online] Available: http://www.nnl.co.uk/media/1053/minor_actinide_transmutation_-_position_paper_-_final_for_web1.pdf [Accessed: 28-10-2016]

[34] A. Stanculescu, "Accelerator Driven Systems (ADSs) for nuclear transmutation," *Ann. Nucl. Energy*, vol. 62, pp. 607–612, Dec. 2013.

Chapter 6. Conclusion and Future Work

6.1 Conclusion

This thesis has investigated neutron production in an ADSR environment when thorium is adopted as the main source of fuel. While the potential of ADSRs has been publicly recognised, few actual studies of neutron production using thorium fuel in an ADSR have been formally presented. Furthermore, current demonstration facilities based on ADSR operation have not considered thorium as their main fuel source. For example, the MYRRHA reactor, which is still under construction, is designed around the use of plutonium-based MOX fuel [1]. It is assumed that preliminary studies prior to the construction of MYRRHA would have been based on the neutronic behaviour of uranium. Hence, this thesis has provided an overview of neutron production with thorium fuel in order to explore the possibility of using thorium in an ADSR facility to fulfil the purpose of energy production and/or transmutation of minor actinides. In order to facilitate this study, the GEANT4 program was used. GEANT4 is a Monte Carlo transport code specialising in particle interaction and secondary production, which fits the purpose of this study [2].

The world's nuclear technology has been developed through the fission process using uranium, and most nuclear research has been based on using uranium as the fuel in a reactor. In order to use uranium in a reactor, the uranium ore has to be extracted, refabricated and enriched. Moreover, despite the fact that uranium-based nuclear power generation produces long half-life nuclear wastes such as plutonium and americium, nuclear technology never seems to change direction by seeking an alternative energy source which is much cleaner and cheaper to operate. Thorium has been acknowledged as an attractive new form of nuclear fuel and the abundance of thorium ore is three times greater than uranium [3] . A thorium fuel cycle from ^{232}Th to ^{233}U offers the advantage of producing almost no plutonium by-product from the fission process. Hence, it could be a candidate for future nuclear energy.

Meanwhile, Accelerator Driven Subcritical Reactors (ADSR) have the capability of producing energy subcritically and transmuting minor actinides to short-lived elements such as ^{134}Cs and ^{104}Rb. With their subcriticality of operation and external supply of neutrons through spallation, ADSRs offer safer nuclear energy with a potential capability of reducing nuclear waste.

Chapter 3 has discussed GEANT4's capability of simulating the spallation process and neutron production in an ADSR, which was validated by benchmarking the results of experiments conducted by KEK, Japan, for neutron spectra from 0.5 and 1.5 GeV proton beams on a lead target. The chapter has described how the GEANT4 program was configured to replicate the KEK experiment in a simulation and the neutron energy spectra results were collected. In order to accurately recreate the simulation and identify the best model to describe neutron production through the spallation process effectively, the study chose three different physics lists provided in the GEANT4 code to benchmark the experiment. These physics lists, which are recommended by GEANT4 for secondary particle production [4], are QGSP_BERT_HP, QGSP_BIC_HP and QGSP_INCL_HP. The results show that all three models are reasonably effective for reproducing experimental data. More specifically, QGSP_INCL_HP showed a remarkable likeness to the experiment results across the entire neutron energy spectrum. This was then followed by QGSP_BERT_HP and finally QGSP_BIC_HP. This finding indicates that each physics list, driven by its major physics models, calculates neutron propagation differently. The accuracy of modelling neutron production in the spallation process is dependent on the physics model used. The study shows that QGSP_INCL_HP described the experimental results most accurately. However, it also reveals that this physics list took approximately twice as long to complete as the other two lists. For simulation processes with complicated geometry, such as an ADSR core, it was anticipated that the time for completion would be much longer. It is concluded in Chapter 3, therefore, that the QGSP_BERT_HP physics list is the best candidate with which to proceed for further ADSR study, or for any other studies involving a large number of neutron interactions with limited resources.

This thesis has described neutron production primarily through the spallation process. Hence, the choice of spallation material is important as it is directly related to neutron yield. It is commonly known that the neutron yield from a spallation target depends on a high Z number, so it is common that spallation targets are composed of heavy metals such as lead. Lead and its variant Lead Bismuth Eutectic (LBE) are frequently identified as ideal spallation targets. For example, the previous study used in the benchmarking was based on a lead target, and liquefied LBE is currently chosen as a spallation target material and coolant for the MYRRHA reactor. Chapter 4 of this thesis has focused on analysing whether there are any differences in neutron production between lead and lead bismuth eutectic. It was anticipated that neutron distribution would be similar due to the presence of lead in both materials. The comparison between these two materials in terms of neutron energy spectra showed that lead produced a higher number of neutrons than LBE in the range between 0 and 10 MeV neutron energies, but it was clear that the mixture of bismuth with lead had only a minor effect on neutron production. Although the quantity of lead in LBE is much smaller than in pure lead, which would ultimately cause some reduction in neutron production, given the fact that LBE provides the advantages of a low melting point and high boiling point, this study has concluded that there is no solid reasoning for not using LBE.

Having determined the neutron spectra for lead and LBE, this thesis then focuses on the viability of using thorium in the MYRRHA reactor, which is based on the Accelerator Driven System (ADS). The findings from previous chapters have provided an in-depth understanding of the spallation target and neutron energy distribution from the target material. MYRRHA, which is operated by SCKCEN, has been designed with the purpose of demonstrating ADS technology. The reactor has been designed to operate in both critical and subcritical mode and, in the latter, certain sections of the core assemblies are loaded with minor actinides for transmutation purposes. Chapter 5 has explained how thorium has been found to be useful for running as a main fuel in an ADSR system. Hence, this study configured the core assembly design of MYRRHA to place thorium in the central fuel region. The study firstly investigated neutron production in each region of the core assembly and the analysis focused on the energy

spectra of the neutrons as they passed through each region. It was found that the first thorium region, with which the spallation neutrons are first in contact, showed a significantly greater increase in the emittance of neutrons than other regions. This appears to indicate that this region contributes substantially to the boost in neutron production, and suggests that the neutrons created from the first fuel region may play a major role in increasing neutron flux inside the core as they interact with subsequent fuel regions.

In order to maintain the fission process inside the core structure, it is important to keep the neutron flux high so that reactions continuously occur. Hence, the reflector region was placed after all the thorium fuel regions. The reflector region, composed of LBE, functioned to reduce the number of high energy neutrons escaping from the fuel region and to retain the neutrons within the core region as much as possible. The comparison between reflector and non-reflector assemblies showed that the reflector had a significant effect in reducing the number of high energy neutrons emitted outside the region. This indicates that the placement of a reflector region is ideal, even using thorium fuel. Furthermore, lowering the energy of high-energy neutrons would allow more opportunities to interact for those neutrons, which could provide a way to increase neutron flux inside the core.

After discussing the main compartment for neutron production, the study has addressed the containment of neutrons and the issue of shielding surrounding the core structure. There were two shielding areas involved in this study. Firstly, the inner shielding area, which is also referred as “outer dummy” area in [1], was placed for the primary containment of neutrons escaping from the structure. The aim was to remove neutrons which were escaping, or possibly to reflect them back toward the main core area. The original material, YZrO, could not be replicated in this study due to the fact that its chemical composition was unknown. Hence, three materials (Y_2O_3, ZrO_2 and Zr_2O_3) which are close to the original material chosen by the MYRRHA facility were chosen. The study anticipated that the rate at which the materials prevented neutrons escaping from the volume would be similar. The results showed that there were differences at

neutron energies between 0 and 1 MeV. Most notably, ZrO_2 showed the best rate of blocking neutrons, which was then followed by Y_2O_3 and Zr_2O_3, based on the spectra shown from 40 keV to the end of the spectrum. However, the neutron energy spectra below 40 keV showed a different outcome, with Zr_2O_3 showing the highest rate of blocking neutrons. This was followed by ZrO_2 and finally Y_2O_3. These findings indicate the multiple neutron reaction cross sections of these materials, which significantly alter neutron leakage at the end when the installation of outer shielding materials is in place.

As previously discussed, the effect of inner shielding varied at different neutron energy ranges. The neutron moderation of each inner shielding material showed a different trend at the point where the neutron energy exceeded 40 keV. The study then proceeded to explore the combined effect of both inner and outer shielding in terms of the effect on neutrons escaping from the final barrier of the core structure. Three materials known to be good for neutron reflection and moderation were chosen for this study; tungsten carbide, beryllium and stainless steel-347 [5],[6]. It was found that of all the combinations, the combination of Y_2O_3 and tungsten carbide (WC) showed the best rate of preventing neutrons from escaping. Despite the fact that each combination showed various outcomes, especially at neutron energies between 0 and 1 MeV, it was concluded that the Y_2O_3 and tungsten carbide (WC) combination showed the most compelling results for blocking neutrons, both in a low energy range and across the entire neutron spectrum explored in this study. Further work on testing various materials, including the original inner shielding material (i.e. YZrO), would be an ideal way of developing a better understanding of neutronic behaviour.

The results throughout this thesis have shown compelling evidence that neutron production using thorium is feasible. The neutrons produced from thorium fuel have a relatively high energy, enabling the reactor to run in a fast neutron spectrum which is ideal for transmutation. It is obvious that further study on thorium fuel in ADSRs is still needed, particularly in terms of thorium fuel cycle conversion inside the core over a specific time interval. However, this thesis has provided an understanding that from a neutron energy perspective, thorium could be used as a main fuel source in an ADSR

system. Hence, it could incite follow-up work designed to evaluate whether the choice of thorium as a fuel source could be retained in the long term, and also whether reactor facilities should carry out further research into improving the thorium fuel cycle.

6.2 Future work

In addition to the aspects mentioned above, the following areas of study could be considered to extend the current research.

6.2.1 A study of time dependent neutron production in thorium fuel

Since GEANT4 code simulations are based on time-independent simulations, time-dependent simulations of how changes in neutron economy occur through the fission process would be in order. Furthermore, isotope creation through the fission process inside the thorium fuel region could be interesting to research. Hence, further research could be carried out for ^{232}Th conversion to ^{233}U. In order to conduct such research, the study would need to use a program called EASY-II, which works in cooperation with FISPACT-II [7]. EASY, which stands for European Activation System, was developed by the Culham Centre for Fusion Energy. This program can simulate activation and transmutation processes [7]. Most importantly, the program can simulate "fission product nuclide inventory calculations". Hence, if the EASY program produces time-dependent data for a nuclear chemical inventory of isotopes created inside thorium fuel, the input data can be integrated into GEANT4 for simulating particle interaction from these data. Thereby, time-dependent neutron production in thorium fuel can be simulated.

6.2.2 A study identifying the physics processes involved in neutron production

This thesis has thoroughly discussed the energy spectra of neutrons produced in each region, i.e. the fuel, reflector and shielding regions. It is possible that the neutrons can

be traced back to the physics process that produced them using the GEANT4 program. By understanding the process involved in neutron production, a study could then proceed to identify the place where a particular process occurred most. Hence, the research could explore how to increase a particular energy to enhance neutron economy.

6.2.3 A study of neutron-induced spallation through D-T source

A further idea is suggested by Professor R. Seviour regarding the use of a D-T source as an initial source of neutrons. The current study has discussed the fact that proton-induced spallation is the main source of neutron supply in an ADSR system. If the neutrons can be directly fed into the reactor channel from a D-T source, this could provide a supply of neutrons with a consistent neutron energy of 14.96 MeV [8].

6.2.4 Study of neutron production using time-dependent GEANT4 method

The studies discussed in this thesis are based on the use of GEANT4, which is a time-independent Monte Carlo transport code. It would be useful to carry out a further study of the time evolution of neutron production and fission processes on the basis of time-dependent GEANT4 codes. These codes are developed by Dr Cristian Bungau [9]. By adapting Dr Bungau's time-dependent codes for use with the GEANT4 programming applied in this study, the results for neutron production in the fission process could be analysed on various time scales.

6.3 Bibliography

[1] P. Baeten *et al.*, "MYRRHA : A multi-purpose nuclear research facility," *EPJ Web Conf.*, vol. 79, no. 3001, Nov. 2014.

[2] S. Agostinelli *et al.*, "GEANT4 - A simulation toolkit," *Nucl. Instruments Methods Phys. Res. Sect. A Accel. Spectrometers, Detect. Assoc. Equip.*, vol. 506, no. 3, pp. 250–303, 2003.

[3] R. Cywinski *et al.,* "Towards an Alternative Nuclear Future," The Thorium

Energy Amplifier Association (ThorEA), 2009.

[4] A. Heikkinen *et al.*, “A Geant4 physics list for spallation and related nuclear physics applications based on INCL and ABLA models,” *J. Phys. Conf. Ser.*, vol. 219, no. 3, p. 32043, Apr. 2010.

[5] T. A. Tomberlin, “Beryllium – a Unique Material in Nuclear Applications,” in *36th International SAMPE Technical Conference*, 2004.

[6] Y. Gohar and D. L. Smith, “Multiplier, moderator, and reflector materials for lithium-vanadium fusion blankets.,” 1999.

[7] Culham Centre for Fusion Energy, “EASY-II archive,” 2016. [Online]. Available: http://www.ccfe.ac.uk/archive_easyii.aspx. [Accessed: 01-Nov-2106].

[8] M. Ragheb and A. Nour Eldin, “Fissile and fusile breeding in the thorium fusion fission hybrid,” in *2010 1st International Nuclear & Renewable Energy Conference (INREC)*, 2010, vol. 2, pp. 1–9.

[9] C. Bungau, R. Barlow, and R. Cywinski, “Optimisation Studies of Accelerator Driven Fertile to Fissile Conversion Rates in Thorium Fuel Cycle,” in *Proceedings of IPAC 2012, New Orleans, Louisiana, USA*, 2012, pp. 4112–4114.

Appendix I – IPAC 2016 proceeding paper

GEANT4 SIMULATIONS OF PROTON-INDUCED SPALLATION FOR APPLICATIONS IN ADSR SYSTEMS

S.C. Lee†, [1], C. Bungau[1], R. Cywinski[1],

[1]International Institute for Accelerator Applications, University of Huddersfield, Huddersfield, UK

Abstract

In order to assess the feasibility of spallation driven fission and transmutation, we have simulated proton induced neutron production using GEANT4, initially benchmarking our simulations against published experimental neutron spectra produced from a thick lead target bombarded with 0.5 and 1.5 GeV protons. The Bertini and INCL models available in GEANT4, coupled with the high precision (HP) neutron model, are found to adequately reproduce the published experimental data. Given the confidence in the GEANT4 simulations provided by this benchmarking, we have then proceeded to simulate neutron production as a function of target geometry and thence to some preliminary studies of neutron production in an ADSR with the geometry similar to that of the proposed Belgian MYRRHA project. This paper presents the results of our GEANT4 benchmarking and simulations.

INTRODUCTION

Spallation is exploited as a reliable technique for the production of high intensity neutron fluxes. Spallation sources generally use high intensity proton beams with energies of typically 1-2 GeV and a geometrically and materially optimised target. Spallation reactions can be simulated by Monte-Carlo based transport codes. In principal, the simulation codes record as many particle histories and probabilistic interactions as possible with the simulated events determined by sampling associated probability distributions. GEANT4, a Monte-Carlo based transport code developed by CERN, provides an extensive set of hadronic physics models for energies up to 10 - 15 GeV, both for the intranuclear cascade region and for modelling of evaporation [1]. These features enable the programme to describe the spallation process. We have evaluated the suitability of the GEANT4 code in simulating the spallation process by benchmarking GEANT4 results against published experimental observations [2] for various spallation target geometries. Having confirmed the suitability of GEANT4 for such simulations our subsequent goal is to optimise the target geometry for optimal neutron yield. Additionally, we have also generated the neutron energy spectrum resulting from embedding a spallation target within an assembly of thorium fuel rods and reflectors with a geometry similar to that of the proposed ADSR project MYRRHA [4,5].

Reference [2] provides the validation study of MCNP-4A code against experimental data taken from KEK, Japan. The experiment was designed to measure neutron spectra for a thick lead target bombarded with 0.5 and 1.5 GeV proton beams. The experiment was originally carried out at KEK in an attempt to resolve the discrepancy of neutron spectra between their calculated results and an experiment results in lead and tungsten targets 500 MeV protons. For these experiments the chosen target material was lead. The geometry is shown in Figure 1.

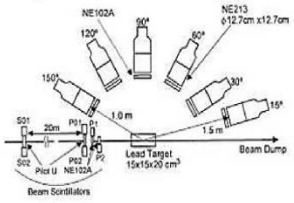

Figure 1: Experimental arrangement, taken from [2].

In the KEK study, a 12 GeV proton synchrotron supplied a stream of proton beams onto the spallation target after passing through a bending magnet. This process configured proton beams with a unique momentum suitable for the thick spallation target.

GEANT4 SIMULATION GEOMETRY

For our simulations the geometry was chosen to be as similar as possible to the configurations used in the experiments [2]. The spallation target was placed at the centre of a simulated space with detectors placed at 15, 30, 60, 90, 120 and 150 degrees with respect to the target and incoming proton beam; in most cases these were at a distance of 1 metre, though the detector at 15 degrees was placed at 1.5 metres [2]. GEANT4 provides numerous hadronic physics models describing particle interactions.

The physics lists used in this study were QGSP_BERT_HP which uses the Bertini intranuclear cascade model to describe the inelastic interactions of protons and neutrons, QGSP_BIC_HP which uses the Binary Cascade model, and QGSP_INCLXX_HP which uses the Liège model. All three physics lists were coupled with a high precision (HP) neutron model which uses evaluated neutron data libraries for neutron cross-sections below 20 MeV [5]. These physics lists were chosen because they are capable of predicting neutron production with a precise range of neutron energies, and they are the recommended physics models for simulating the neutron spallation processes [6, 7].

The area of "detectors" were set to $12.7 \times 12.7 \text{cm}^2$, the same size as the NE213 scintillator used in the KEK experiment.

† email address sangcheol.lee@hud.ac.uk

ISBN 978-3-95450-147-2

RESULTS OF THE SIMULATIONS

Figure 2 and 3 show the neutron spectra measured at various angles. It can be seen that there is a good agreement between the GEANT4 results and the experimental data. Furthermore, the GEANT4 simulations are closely comparable to those obtained from the earlier MCNP-4A simulations in [2].

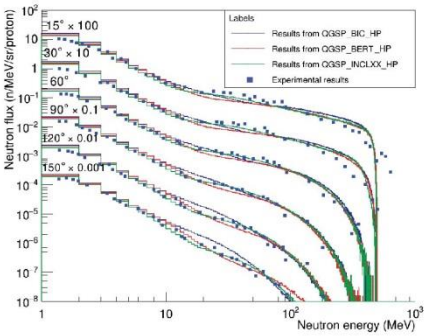

Figure 2: Neutron flux at 0.5 GeV proton beam energy using GEANT4, with the experimental data taken from [2].

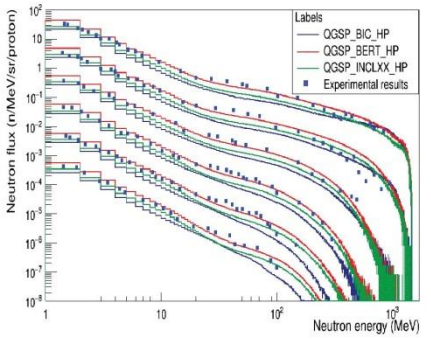

Figure 3: Neutron flux at 1.5 GeV proton beam energy using GEANT4, with the experimental data taken from [2].

In terms of the relative accuracy of the three physics models we have used, the QGSP_INCLXX_HP physics list produced the closest results to the experimental results, followed by the Bertini, whilst the Binary Intranuclear Cascade (BIC) proved to be the least accurate. The results from INCL at 0.5 GeV proton beam energy showed a match to the experimental results at every angle. The Bertini model also produced accurate results at between 0 and 10 MeV neutron energy (see Figure 2). At 1.5 GeV, INCL produced the most accurate outcome in relation to the experimental results in the neutron energy range between 0-10 MeV and 100-1000 MeV. However, the Bertini model produced better results than the INCL at the range between 10-100 MeV.

MYRRHA THORIUM FUEL STUDY

The above simulations indicate that GEANT4 is capable of modelling spallation neutron reactions in an energy regime useful for exploitation in an ADSR. We therefore carried out a preliminary simulation of neutron distributions in a thorium fuelled ADSR. MYRRHA (the multipurpose hybrid research reactor for high-tech applications) was chosen as an appropriate design geometry for the simulated ADSR. MYRRHA is a flexible fast spectrum research reactor (50-100 MWth), which is being designed to operate in sub-critical and critical modes [3]. The MYRRHA design proposes the use of a 600 MeV proton accelerator, a spallation target and a multiplying core with uranium based MOX fuel. The core area is cooled by liquid lead-bismuth [8], which also provides the spallation target material [9].

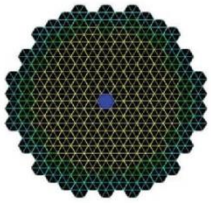

Figure 4: GEANT4 MYRRHA core configuration (Blue, spallation target, yellow thorium fuel, reflectors green, shields cyan).

For the purpose of this study, we have replaced the reactor fuel by fertile thorium, a material which is currently attracting considerable interest as both a potential fuel and a matrix for transmutation of nuclear waste. In order to understand the effect of the reflector, the simulations were carried out with the shielding assemblies removed.

Table 1: Core specification Used in the Simulation

Area	Material	Size (cm^2)	Number place
Spallation target	PbBi	97.55 × 30	1
Fuel	Thorium	97.55 × 140	76
Reflector	PbBi	97.55 × 140	36
Shielding	Zirconia Y-TZP	97.55 × 140	42

The results of the GEANT4 simulations, figures 5 and 6, show the energy spectra of neutrons travelling from one region to another in the core. Each region was measured from the centre of the core on the size of a fuel assembly (i.e. region-1 97.55 cm, region-2 195.1cm etc.). Figure 5 shows the number of outer going neutrons per proton. In the figure, the neutron spectrum for the region 1 to 2 shows the highest number of neutrons per proton. This result indicated that this region contributed to neu-

ISBN 978-3-95450-147-2

tron production significantly. The number of neutrons produced from the spallation target is 16.68 neutrons per incident proton.

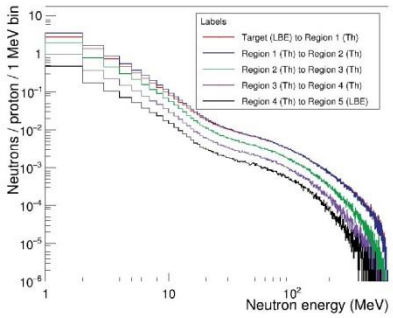

Figure 5: Number of outer going neutrons into each region in the core as a function of neutron energy.

In Figure 6, the highest number of neutron back-scattered was recorded from the region 1 to the spallation target. The figure also shows that the neutron energy spectrum representing region 5 to region 4 is lower than in other regions.

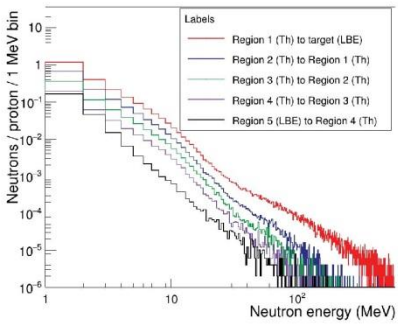

Figure 6: Number of neutrons back-scattered into each region in the core as a function of neutron energy.

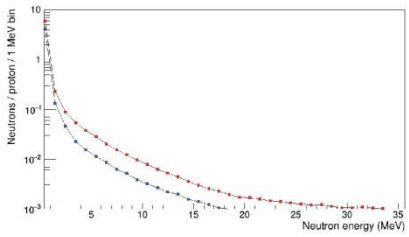

Figure 7: Number of neutron escaped from the core as a fucntion of neutron energy.

Comparing neutron energy spectra between the reflector and the non-reflector as shown in Figure 7, the reflectors decrease the number of neutrons per proton in high neutron energy. The figure also indicates that the maximum neutron energy of the non-reflector result was recorded at 33.5 MeV while the highest neutron energy for the reflector was at 17.5 MeV. Regarding the number of neutrons escaping from the core per proton, there is no significant difference between the reflector and the non-reflector at the neutron energy range of 0-2 MeV. This result indicates that the nuclei of the reflector material (i.e. LBE) were not effective for stopping neutrons escaping from the reflector.

CONCLUSION

We have shown that GEANT4 simulations of experimental spallation neutron production, at least as accurate if not more than MCNPX. The QGSP_INCLXX_HP physics list appears to reproduce the experimental results most closely.

For MYRRHA configuration study, it is conclusive that reflectors showed a significant effect to reduce the neutrons escaping from the core. However, the number of escaping neutrons per proton from the core was still at the high level. This suggests that extra shielding area is necessary for increasing neutron flux inside the core which reflects the rate of thorium-uranium conversion.

ACKNOWLEDGEMENT

Sangcheol Lee would like thank the Institute of Physics, UK for financial support to attend this conference.

REFERENCES

[1] C. Bungau, et.al., "Neutron spallation studies for an accelerator driven subcritical reactor," in *Particle Accelerator Conference*, 2009.

[2] S. Meigo, et.al., "Measurements of neutron spectra produced from a thick lead target bombarded with 0.5- and 1.5-GeV protons," *Nucl. Inst. Meth A* 431 (1999): 521–530.

[3] P. Baeten, et.al., "MYRRHA : A multi-purpose nuclear research facility," *EPJ Web Conf.*, vol. 79, no. 03001, Nov. 2014.

[4] M. Sarotto, "MYRRHA-FASTEF FA / core design," in *international Workshop on Innovative Nuclear Reactors cooled by HLM*, 2012.

[5] S. Agostinelli, et.al., "GEANT4 - A simulation toolkit," *Nucl. Instruments Methods Phys. Res. Sect. A Accel. Spectrometers, Detect. Assoc. Equip.*, vol. 506, no. 3, pp. 250–303, 2003.

[6] Geant4 Collaboration, "Reference Physics Lists," 2009. `http://geant4.web.cern.ch/geant4/support/physicsLists/referencePL/referencePL.shtml`.

[7] Geant4 Collaboration, "Physics lists - Use cases." `http://geant4.cern.ch/support/proc_mod_catalog/physics_lists/useCases.shtml`.

[8] H. Abderrahim, "MYRRHA An innovative and unique irradiation research facility," *... Inf. Exch. Meet. San Fr. USA*, 2010.

[9] SCK•CEN, "Applications catalogue of MYRRHA." `http://myrrha.sckcen.be/en/MYRRHA/Applications`.

ISBN 978-3-95450-147-2

Appendix II – PoS (ADST 2016) proceeding paper

PROCEEDINGS OF SCIENCE

Geant4 simulations of neutron production in a thorium fuelled Accelerator Driven Subcritical Reactors

David Sangcheol Lee[1]
International Institute for Accelerator Applications, University of Huddersfield
IIAA, University of Huddersfield, Queensgate, Huddersfield, West Yorkshire, UK HD1 3DH
E-mail: Sangcheol.lee@hud.ac.uk

Robert Cywinski
International Institute for Accelerator Applications, University of Huddersfield
IIAA, University of Huddersfield, Queensgate, Huddersfield, West Yorkshire, UK HD1 3DH
E-mail: R.Cywinski@hud.ac.uk

Cristian Bungau
International Institute for Accelerator Applications, University of Huddersfield
IIAA, University of Huddersfield, Queensgate, Huddersfield, West Yorkshire, UK HD1 3DH
E-mail: C.Bungau@hud.ac.uk

Rebecca Seviour
International Institute for Accelerator Applications, University of Huddersfield
IIAA, University of Huddersfield, Queensgate, Huddersfield, West Yorkshire, UK HD1 3DH
E-mail: R.Seviour@hud.ac.uk

Spallation taken from the middle English spalle, is an efficient process for producing an intense neutron flux suitable for exploitation in Accelerator Driven Subcritical Reactors (ADSRs) for energy production and the transmutation. In order to assess spallation driven fission and transmutation we have simulated proton induced neutron production using GEANT4. Benchmarking our simulations against experimental neutron spectra produced from a thick lead target bombarded with 0.5 and 1.5 GeV protons. The Bertini and INCL models available in GEANT4, coupled with the high precision (HP) neutron model, are found to reproduce the published experimental data. Given the confidence in the GEANT4 simulations provided by this benchmarking we then proceed to study neutron production in an ADSR using Thorium in a geometry similar to that of the proposed Belgian MYRRHA project with 0.6 GeV proton beam energy that proposed by SCKCEN.

4th Workshop on ADS and thorium
31 August - 2 September 2016
University of Huddersfield, England

[1]Speaker

http://pos.sissa.it/

PoS(ADST2016)011

1. Introduction

Spallation is a reliable technique for the production of high intensity neutron fluxes. These sources use high intensity proton beams with energies of typically 1-2 GeV, optimised target producing neutrons. In this paper we use a Monte-Carlo based transport simulation to model spallation reactions. GEANT4, a Monte-Carlo based transport code developed by CERN, provides an extensive set of hadronic physics models for energies up to 10 - 15 GeV, both for the intranuclear cascade region and for modelling of evaporation [1]. GEANT4 codes records particle histories and probabilistic interactions, with the simulated events determined by sampling associated probability distributions. In this paper we evaluate the suitability of GEANT4 to simulate the spallation process, by benchmarking GEANT4 results against published experimental observations [2]. Having confirmed the suitability of GEANT4 to model the spallation process we can then use GEANT4 to optimise the target geometry for optimal neutron yield. We also present the neutron energy spectrum resulting from embedding a spallation target within an assembly of thorium fuel assemblies, reflectors and shielding in a geometry similar to that of the proposed ADSR project MYRRHA [3,4]. The MYRRHA design uses a 600 MeV proton linear accelerator, a spallation target and a multiplying core with uranium based MOX fuel where the core area is cooled by liquid lead-bismuth [5],which also provides the spallation target material [6]. A schematic of MYRRHA reactor core is shown in Figure 3

2.Geant4 benchmarking study

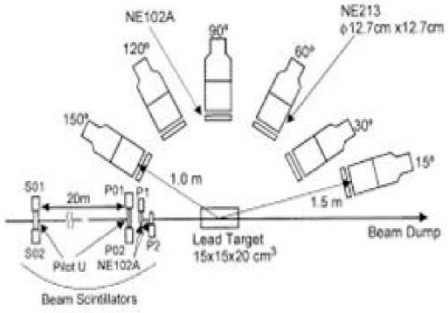

Figure 1: Experimental arrangement, taken from [2].

For our initial simulations, we choose a configuration similar to that used in the experiments [2]. The experimental setup of [2] is shown in Figure 1 where proton beam incident onto a lead spallation tater. The spallation target was placed at the centre of a simulated space with detectors placed at 15, 30, 60, 90, 120 and 150 degrees with respect to the target and incoming proton beam, at a distance of 1 metre, except the 15° detector which was placed at 1.5 metres [2]. The area of each detector was set to 12.7×12.7 cm² the same size as the detector in [2].

GEANT4 provides numerous hadronic physics models describing various particle interactions. For the work presented in this paper, the following GEANT4 physics list were used. QGSP_BERT_HP which uses the Bertini intranuclear cascade model to describe the inelastic interactions of protons and neutrons, QGSP_BIC_HP which uses the theory based Binary Cascade model capable of simulating secondary particle production by creating more physical path of particle interaction [7], and QGSP_INCLXX_HP which uses the latest developed Liège model that has improved interpretation of pre-equilibrium and other particle interactions [8]. Coupled with a high precision (HP) neutron model using data for neutron cross-sections below 20 MeV [4].

2.2.Result of the simulation for benchmarking

Figure 2a show the neutron spectra (neutrons/ incident proton / steradians in 1 MeV bin size) at various projectile angles between 0 and 100 MeV neutron energy. It can be seen that there is a good agreement between the GEANT4 results and the experimental data throughout the whole spectrum. More specifically, the green line shown in Figure 2a which represents the results produced by QGSP_INCLXX_HP physics list show closest to the experimental results. While this physics produced most accurate results to the experimental result throughout the entire neutron energy range, the graphs shows that INCL based physics list produced result significantly close with the experimental result in the range between 0- 10 MeV neutron energy.

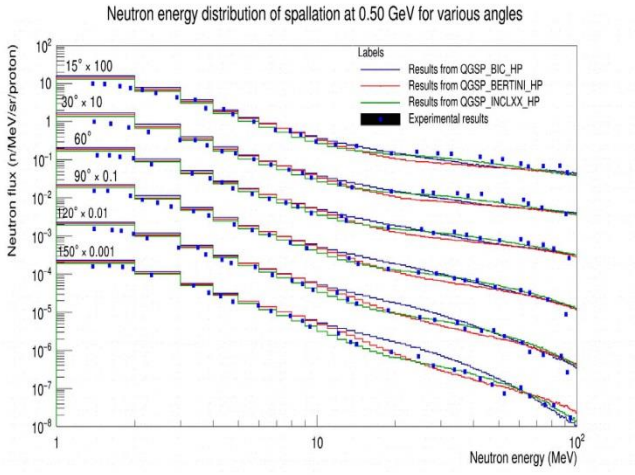

Figure 2a: Neutron flux at 0.5 GeV proton beam energy using GEANT4 at the neutron energy between 0 and 100 MeV with the experimental data taken from [2]

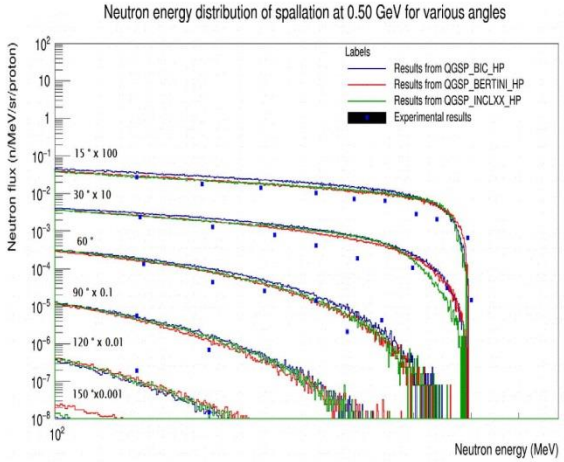

Figure 2b: Neutron flux at 0.5 GeV proton beam energy in the range of neutron energy between 100 and 600 MeV using GEANT4 with the experimental data taken from [2]

In Figure 2a, the least accurate result from INCL based physics list to the experimental result is found to be 0.0488, which is 4.88% error at neutron energy 91 MeV in 120°. This error estimate supports that Geant4 is capable of producing reliable results for spallation reaction. On the other hand, The Figure 2b shows a decrease in the accuracy of Geant4 to experimental results. However, the curves in each angle folllows the trend of experimental results. The least accurate point by QGSP_INCLXX_HP in Figure 2b is found as, 3.11×10^{-3} which is 5.99 % error at neutron energy 437 MeV in 15°.

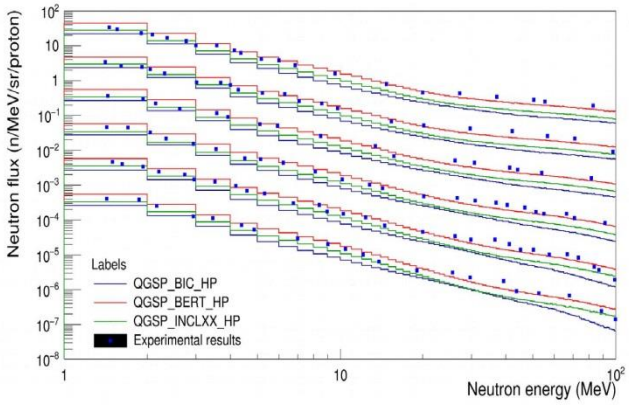

Figure 2c: Neutron flux at 1.5 GeV proton beam energy in the range of neutron energy between 0 and 100 MeV using GEANT4 with the experimental data taken from [2]

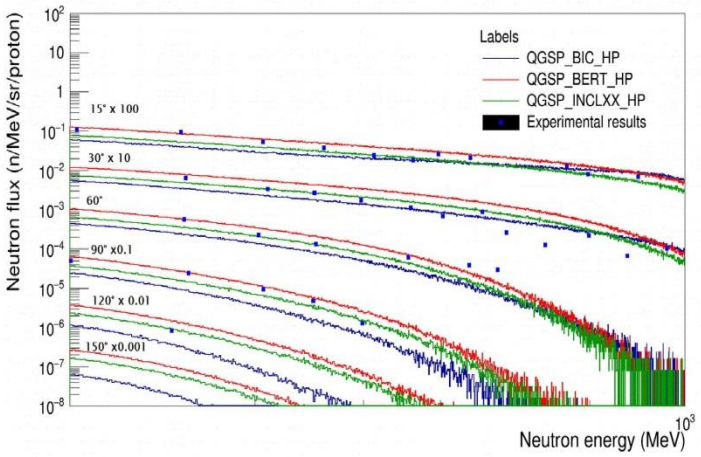

Figure 2d: Neutron flux at 1.5 GeV proton beam energy in the range of neutron energy between 100 and 1000 MeV using GEANT4 with experimental data taken from [2]

Similarly, the Geant4 results with experimental results at 1.5 GeV beam energy shown in Figure 2c and 2d indicate similar trend as the results shown in Figure 2a and 2b. Initially, it was anticipated that there would be a significant difference between simulation and experiment due to the difficulty measuring of high energised neutrons in both experiment and simulation methods. It can be seen from that Geant4 produces fairly accurate results to the experiment results as shown in Figure 2c. The least accurate point is found to be at neutron energy of 55 MeV in 30° with the difference of 3.89×10^{-6} which is 6.64%. The accuracy of Geant4 simulation result to the experiment is decreasing as the neutron energy spectrum increases. In Figure 2d, it shows that the Geant4 results get fragmented in high energy range due to the low number of neutrons presented. The difference between Geant4 result and the experimental results of neutron energy of 697 MeV in 30° was 8.61×10^{-5} which is 27.97 %. As previously mentioned, the accuracy of measuring high energy neutron is low in both experimental and simulation methods. Hence, the reliability for measuring such high neutron energies can not be certain. In overall, of the three physics models we have used, the QGSP_INCLXX_HP physics list produced the closest results to the experimental results, followed by the Bertini, whilst the Binary Intra-nuclear Cascade (BIC) proved to be the least accurate. The results from INCL at 0.5 GeV proton beam energy showed a match to the experimental results at every angle. The Bertini model also produced accurate results at between 0 and 10 MeV neutron energy (see Figure 2a). At 1.5 GeV, INCL produced the most accurate outcome in relation to the experimental results in the neutron energy range between 0-10 MeV and 100-1000 MeV (see Figure 2d). However the Bertini model produced better results than the INCL at the range between 10-100 MeV (see Figure 2c). The above simulations indicate that GEANT4

is capable of modelling spallation neutron reactions in an energy regime useful for exploitation in an ADSR.

3.Neutron energy distribution in different regions with MYRRHA's core configuration

For the paper we consider a reactor geometry similar to MYRRHA where we have replaced the Uranium based reactor fuel by fertile thorium. Thorium is currently attracting interest as both a potential fuel and a matrix for transmutation of nuclear waste. In order to understand the effect of the reflector, in this paper the simulations were carried out with the shielding assemblies removed. The configured geometry of core assembly with thorium fuel is shown in figure 3 and its specification in table 1. In figure 3, each assembly area has different colours corresponding to those composed materials such as blue is spallation target, yellow is thorium fuel, green as reflector and cyan as inner shielding.

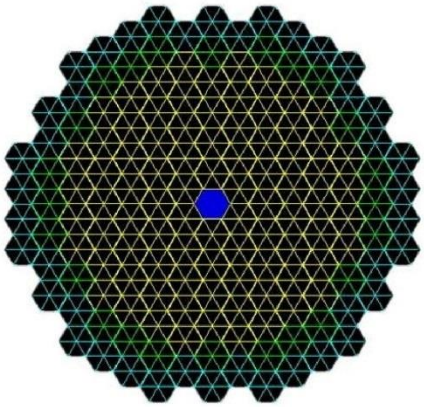

Figure 3: Geant4's MYRRHA core configuration (Blue: spallation target, Yellow: thorium fuel, Green: reflectors, Cyan: inner shielding)

Area	Material	Size (mm^2)	Number of core units
Spallation target	PbBi	97.55×300	1
Fuel	Thorium	97.55×1400	76
Reflectors	PbBi	97.55×1400	36
Shielding	Y_2O_3 ZrO_2 Zr_2O_3	97.55×1400	42

Table 1: Core specification used in the simulation

The results of the GEANT4 simulations, figures 3a,3b and 3c, show the energy spectra of neutrons travelling from one region to another in the core. The distance of each annular region from the centre of core is set as the size of a fuel assembly (i.e. region-1 97.55 cm, region-2 195.1cm etc.). In figure 3a, it can be seen that the number of outer going neutrons per proton for fuel region 1 to 2(red line) is higher than the number of neutrons from target to region 1 (blue line). This result indicated that the first fuel region contributed to neutron production significantly. On the other hand, figure 3b shows differently that the difference of the results between the target to region 1 and region 1 to region 2 is very small which indicates that the production of high energy neutrons is not increased significantly by thorium fuel area.

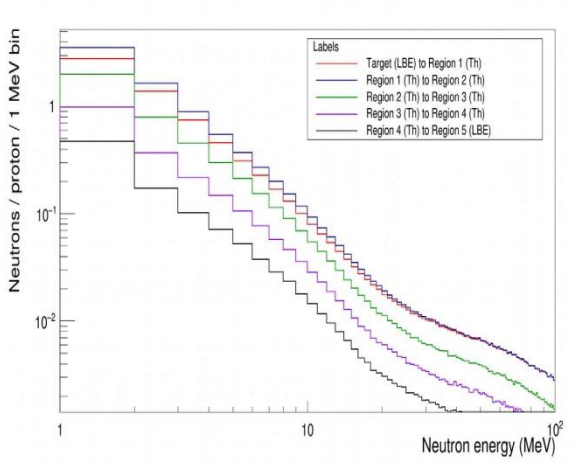

Figure 3a: Number of outer going neutrons into each region in the core as the function of neutron energy between 0 and 100 MeV

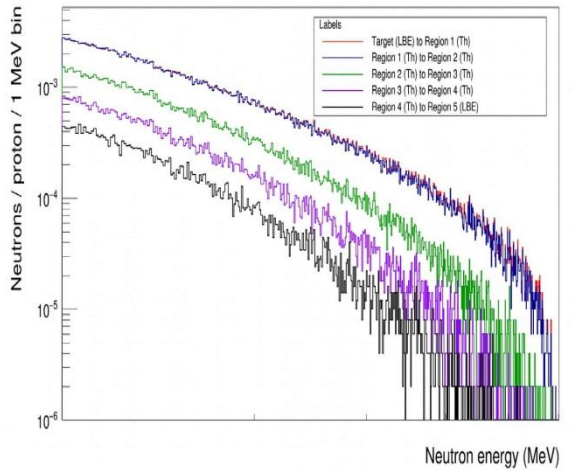

Figure 3b: Number of outer going neutrons into each region in the core as a function of neutron energy between 100 and 1000 MeV

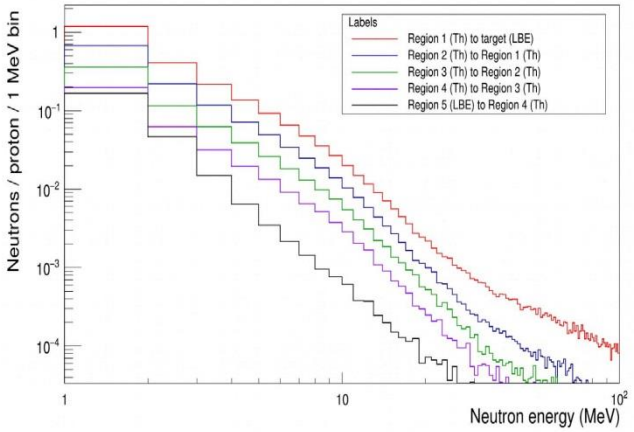

Figure 3c: Number of neutron back-scattered into each region in the core as a function of neutron energy between 0 and 100 MeV

In figure 3c, the area that neutrons are most travelling backward is the area from region 1(composed with thorium) to the spallation target(composed with lead bismuth eutectic) The area where neutrons travelling from the region 1 to the spallation target is the first region placed after spallation target. Hence, it is expected to get the results of having the high rate of neutrons back-scattered in the closest area from the centre of core.

3.1The energy distribution of neutron escaping from the core with reflectors.

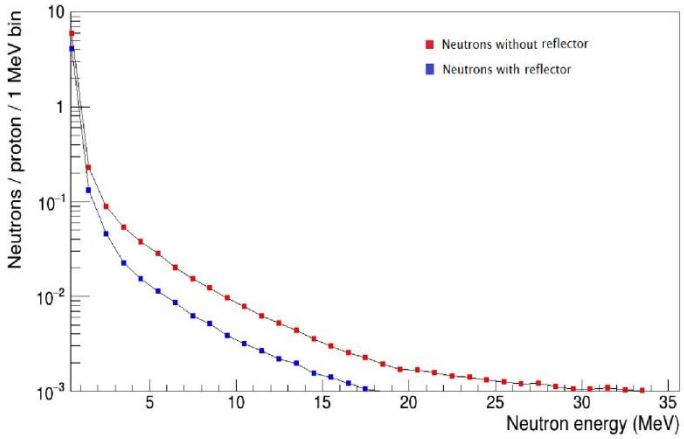

Figure 4: Number of neutrons escaped from the core as a function of neutron energy taken from [10]

Comparing neutron energy spectra between the reflector and the non-reflector as shown in Figure 7, the reflectors decrease the number of neutrons per proton in high neutron

energy. The figure also indicates that the maximum neutron energy of the non-reflector result was recorded at 33.5 MeV while the highest neutron energy for the reflector was at 17.5 MeV. Regarding the number of neutrons escaping from the core per proton, there is no significant difference between the reflector and the non-reflector at the neutron energy range of 0-2 MeV. This result indicates that the nuclei of the reflector material (i.e. LBE) were not effective for stopping neutrons escaping from the reflector.

3.2 The energy distribution of neutron escaping from the core with inner shielding.

The core consists of many areas of shielding in the structure to increase neutron flux and block radiation emitting from the core. The original MYRRHA core specification indicated that there is an 'outer dummy' area in placed after the reflector region for shielding purpose. Due to the lack of information of the composition of YZrO listed in [9], three different materials close to YZrO were tested to investigate the effect of blocking neutrons escaping from the core. In this text, this area of shielding is named as 'inner shielding' to express the purpose of the area in the core.

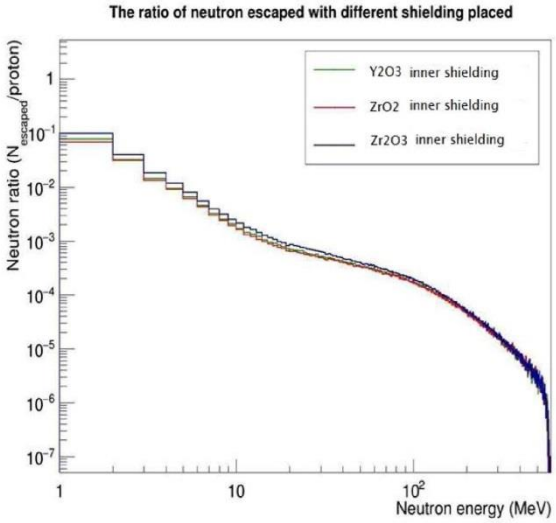

Figure 5: Energy distribution of neutrons escaping from the core with different inner shielding as a function of neutron energy

Comparing the neutron energy spectra between the three materials shown in Figure 8, the number of neutrons escaping per incident proton is similar in all three materials, especially for high neutron energies. Figure 8 also indicates that the highest rate of neutrons blocking for neutron energies between 0 and 2 MeV was achieved by ZrO_2. However the difference between ZrO_2 with other two candidate(Y_2O_3 and Zr_2O_3) is very small. This result indicates that the rate of neutron escaping from the core may be varied when the further shielding area is in placed.

4.Conclusion

In this paper, we have shown that GEANT4 simulations of spallation neutron production agree well with experimental data. The QGSP_INCLXX_HP physics list appears to reproduce the experimental results most closely.

Our simulation of a thorium fuelled MYRRHA type reactor show that reflectors have a significant effect reducing the neutrons escaping from the core. However, the number of neutrons per proton escaping is high. This suggests that extra shielding is necessary for increasing neutron flux inside the core which reflects the rate of thorium-uranium conversion.

The inner shielding area composed of three different materials suggested that all three materials had similar rates of reducing neutrons escaping from the core. This suggested that the result may be varied when outer shielding area is in place.

Reference

[1] C. Bungau, R. Cywinski, and R. Barlow, "Neutron spallation studies for an accelerator driven subcritical reactor," in *Particle Accelerator Conference*, 2009.

[2] S. Meigo, H. Takada, S. Chiba, T. Nakamoto, K. Ishibashi, N. Matsufuji, K. Maehata, N. Shigyo, Y. Watanabe, and M. Numajiri, "Measurements of neutron spectra produced from a thick lead target bombarded with 0.5- and 1.5-GeV protons," *Nucl. Instruments Methods Phys. Res. Sect. A Accel. Spectrometers, Detect. Assoc. Equip.*, vol. 431, no. 3, pp. 521–530, Jul. 1999.

[3] M. Sarotto, "MYRRHA-FASTEF FA / core design," in *international Workshop on Innovative Nuclear Reactors cooled by HLM*, 2012.

[4] S. Agostinelli, J. Allison, K. Amako, and Et.al, "GEANT4 - A simulation toolkit," *Nucl. Instruments Methods Phys. Res. Sect. A Accel. Spectrometers, Detect. Assoc. Equip.*, vol. 506, no. 3, pp. 250–303, 2003.

[5] H. Aït Abderrahim, "MYRRHA An innovative and unique irradiation research facility," in *Tenth International Topical Meeting on Nuclear Applications of Accelerators (AccApp'11)*, 2011.

[6] SCK•CEN, "Applications catalogue of MYRRHA." [Online]. Available: http://myrrha.sckcen.be/en/MYRRHA/Applications. [Accessed: 21-Apr-2016].

[7] D. H. Wright, "An Overview of Geant4 Hadronic Physics Improvements," in *Joint International Conference on Supercomputing in Nuclear Applications and Monte Carlo (SNA + MC2010)*, 2010.

[8] J. Yarba, "Recent Developments and Validation of Geant4 Hadronic Physics," *J. Phys. Conf. Ser.*, vol. 396, no. 2, p. 22060, Dec. 2012.

[9] P. Baeten, M. Schyns, R. Fernandez, D. De Bruyn, and G. Van den Eynde, "MYRRHA : A multi-purpose nuclear research facility," *EPJ Web Conf.*, vol. 79, no. 3001, Nov. 2014.

[10] S. C. Lee, C. Bungau, and R. Cywinski, "Geant4 simulations of proton-induced spallation for applications in ADSR systems," in *Proceedings of IPAC 2016, Busan, Korea*, 2016, vol. 08 Applications for Accelerators, pp. 1943–1945.